NTNU

Norwegian University of
Science and Technology

Investigation of submerged maritime target detection using LIDAR

Unai Ayala Fernández
Luis Manuel Hernández

Master of Science in Electronics
Submission date: July 2009
Supervisor: Jens F. Hjelmstad, IET

Norwegian University of Science and Technology
Department of Electronics and Telecommunications

Problem Description

LIDAR combines the 3D surveillance capability of RADR with the high resoloution imaging capabilities of RADAR. LIDAR operating in parts of the visual and nearIR region offers the additional opportunity of being able to image through a water interface and into a water mass. This thesis addresses the design and evaluation of a LIDAR system operating at oblique incidence angles. Vertical looking LIDAR has been used for bathymetri and fish inventory purposes, and imaging LIDAR has also been used for horisontal and above water range gated imaging of surface and aerial targets. The foucs of this thesis is to investigate the intermediate oblique incidence region, and establish performance parameters for the detection of specific targets as a function of range and depth.
The initial part of the work is to establish the theoritical relatonsships in the form of an extended LIDAR equation with appripriate parameters and the inclusion of environmental factors. Then the candidate will participate in a test campaign and will have access to extperimental data to verify his model. The final part of the work is to evaluate the suitability of LIDAR as a system for some ciritcal applications (e g oil spill detection, submerged buoy detection, submerged container detection, forward looking bathymetri, scanning fish inventory from aircraft and ship)

Assignment given: 09. March 2009
Supervisor: Jens F. Hjelmstad, IET

ABSTRACT

Lidar is an optical remote sensing technology which uses the backscattered light to create information profiles of the scanning area. Normally the air is used as propagation medium, but in this work the Lidar's efficiency to detect submerged target in water is discussed.

Following the theories of light propagation in the air and in the water a model to simulate the target detection is created. The values of scattering and absorption of the laser pulse in water are estimated by Morel equations which give accurate values of the sea water properties. Scattering and absorption define the optical properties of the medium, so the attenuation and the backscattering coefficient are calculated. These value will have a strong dependency to the salinity, pressure, temperature, sea water constituents and so on.

After the estimation of the parameters a model based on Lidar Equation, Fresnel Equations and Snell´s law has been developed with the aim of predict the maximum range to detect the sea surface and the maximum depth to detect the sea bottom.

In order to verify the goodness of the model, a prototype 532nm Lidar system has been used to collect experimental data. The Lidar was used from a 50m high building scanning from near vertical incidence to near horizontal incidence.

The extracted data from the simulations have been compared with the data obtained from realized test. This has given us a predicted maximum range to detect the sea surface of 220m and an estimated maximum depth for a reference target of 17m.

ACKNOWLEDGEMENTS

Unai Ayala Fernández

I would like to thank Luis, my partner in this thesis for his work, his mood and his friendship during the last 8 months.

I wish to express my sincere gratitude to my supervisor at NTNU, Associate Professor Jens Hjelmstad , for offering me the opportunity to make the Master Thesis with him, and for his indispensable guide during the execution of the Master Thesis.

I wish to express my sincere gratitude to Eirik Tenningen , for his indispensable guide during the execution of the tests of the Master Thesis and for his indispensable help.

I would also like to thank to the people at NTNU that, in one way or another, make possible the execution of this Thesis; hence, to extend my gratitude to my home university,*Euskal Herriko Unibertsitatea*, for giving me the chance of this wonderful year at NTNU, Trondheim.

I would like to express my sincere gratitude and love to my parents and my sister. Their support and confidence during all my life have made me as I am, and their effort has allowed me to be here completing my degree with the execution of this Master Thesis.

I would like to express my sincere gratitude to all my family, grandparents, uncles and aunts and cousins.

I wish to express my affection to my friends for being always next to me specially to Endika, Asier, Josu, Ruben and Mikel. Thanks to my classmates from the univertsity who have made wonderful the five years spent together at the university, specially to Telle, for helping me and put up me these years.

Finally, I would like to express my affection to all the friends that have made this Erasmus experience as unique and special as it has been. I wish to highlight my sincere gratitude to Rocio for the wonderful months spent here together, and for its support and confidence that have helped me so much during this period.

Luis Hernández Bailón

I would like to say e*skerrik asko* to my partner Unai Ayala. His collaboration, advice, hospitality, and good mood converted this work together into an amazing experience.

I would like to express how important has been for me that my supervisor at NTNU, Associate Professor Jens Hjelmstad, offered to me to collaborate in this Master Thesis. His advice has been really important and the opporunity to go know a new city, Bergen, during the test part was a pleasure.

I would like to thank Eirik Tennineng for his gracious hospitality and collaboration during our stay in Bergen.

I wish to express my gratitude to everybody who helped me to go on erasmus, and to make me able to discover the wonderful society of Norway; from my home university, Universidad de Valladolid (Uva) and from NTNU. Specially to my teachers of electromagnestism that helped me to like it so much.

I cannot forget to express my deep love to my parents and sisters for helping me during my whole life to become the person that I am now. Their advices and gudie was indispensable to finish my studies and to decide to try to improve my skills traveling abroad. *Mil gracias Papá, Mamá, Susana y Anabel.* Hence, to extend my gratitude to my whole family, specially to my cousins Álvaro and Pablo.

I would like to thank also to all my firends for being my second family, and for helping me whenever i needed them: Miguel, Javier, Luiso, Luis, Jaime, Raúl, César y Diego. I want to mention also all my friends from my university, and the important people that I met in Norway, specially Oscar and Kasia. These six months living in Trondheim have been the best in my life.

To my loved grandmothers and grandfathers.

Index of Contents

1. Introduction....1
2. Research question: 5
2.1. Propagation of light: air and water....8
2.2. Discontinuity: the sea surface....8
2.3. Backscatter from targets....8
2.4. Effect of the aperture of the beam....9
2.5. Lidar model for MATLAB....9
3. Analysis of fundamental issues....11
3.1. Transmission of light in the atmosphere....11
3.1.1. Extinction coefficient and transmittance....12
3.1.2. Total and directional elastic scattering....14
3.1.3. Inelastic scattering: Rayleigh and Mie scattering....15
3.1.4. Absorption by molecules and particulates....24
3.2. Transmission of light in water....29
3.2.1. Inherent Optical Properties....29
3.2.2. Optical Signinificant Constituents of Natural Waters....31
3.2.3. Electromagnetic Properties of Water....34
3.2.4. Absorption....38
3.2.4.1. Absorption by pure sea water....39
3.2.4.2. Absorption by dissolved organic matter....40
3.2.4.3. Absorption by phytoplankton....40
3.2.4.5. Absorption by organic detritus....42
3.2.4.6. Bio-optical models for absorption....42
3.2.5. Scattering....44
3.2.5.1. Scattering by pure sea water....45
3.2.5.2. Scattering by particles....46
3.2.5.3. Scattering by turbulence....47
3.2.4.5. Wavelength dependence of scattering: Bio-optical model....49
3.3. Scattering from submerged objects....52
3.3.1. Objects smaller than the beam footprint....52
3.3.3.1. Surface shape and pointing angle. Reflection theory....52
3.3.1.2. Surface roughness....54
3.3.1.3. Surface molecular and electronic structure....57
3.3.2. Objects bigger than the beam footprint....58
3.3.2.1. Object bigger than the wavelength....58
3.3.2.2. Object with a size similar to the wavelength....59
3.3.2.3. Object smaller than the wavelength....59
4. Lidar System Model....61
4.1. Lidar equation....62
4.2. Snell law....66
4.3. Fresnel Equations....67
4.4. Model....68
4.4.1. Air transmission before the discontinuity....69
4.4.2. Air tranmission after the discontinuity....69

4.4.3. Water transmission after the discontinuity....69
4.5. Backscattering and transmission loss coefficients....70
4.5.1.Backscattering in the air....70
4.5.2. Transmission loss coefficients....70
4.5.3. Transmission loss in water....71
4.5.3.1. Absorption coefficient 71
4.5.3.2. Scattering coefficient....72
4.5.4. Backscattering in water....72
4.5.5. Chorophyll concentration profile....72
4.6. The sea surface....73
4.7. Model implementation and Matlab code....79
4.7.1 Analysis of the simulated data and model limitation. 83
5. Test of LIDAR system inaquatic environment....91
5.1. Test objectives and plan....91
5.2. Lidar system description....92
5.3. Test site description....93
5.4. Description of test execution....96
5.5. Lidar test data presentation....104
5.6. Lidar test data analysis....112
5.7. Background data assessments....121
6. Discussion....125
7. Conclusion....129
REFERENCES....131

List of Figures

Figure 1: The red zone is the operational range of lidar.....6
Figure 2: NASA EAARL system.....7
Figure 3: The angular distribution of scattered light intensity for the particles of different size.....20
Figure 4: Different scattering mechanism.....21
Figure 5: Geometry used to define inherent optical properties.....29
Figure 6: The optical constants of pure water. The right axis gives the real part of m, and the left axis gives the imaginary part of m, where m is the complex index of refraction 35
Figure 7: Spectral absorption coefficient of pure water (solid line) and of pure sea water (dotted line) as a function of wavelength.....36
Figure 8: Real index of refraction of water for selected values of pressure, temperature, and salinity.....37
Figure 9: Shows a(λ), solid line, and b(λ), dotted line, of pure sea water.....39
Figure 10: Chlorophyll-specific spectral absorption coefficients for eight species of phytoplankton.....42
Figure 11: Examples of spectral absorption coefficients a(λ) for various waters. Panel (a) shows a(λ) for waters dominated by phytoplankton, panel (b) is for waters with a high concentration of nonpigmented particles, and panel (c) is for waters rich in yellow matter.....43
Figure 12: Total spectral absorption coefficient a(λ) for selected chlorophyll concentrations C.....44
Figure 13: Particle volume scattering functions form various waters.....47
Figure 14: Reflection from a surface.....52
Figure 15: Light reflected from a convex and a diverging mirror.....53
Figure 16: Reflection from different kinds of curvatures.....54
Figure 17: Geometry for derivaton os Kirchoff's law.....55
Figure 18: Different reflection of fish scales.....58
Figure 19: Different values of Reflectance 58
Figure 20: Rayleigh scattering.....60
Figure 21: Geometric factor.....64
Figure 22: Snell Law.....66
Figure 23: Shows how the refracted angle changes in funtion of incident angle.....66
Figure 24: Fresnel equations, angles due to the normal.....68
Figure 25: Fresnel equations, angles due to the horizontal.....68
Figure 26: Shows chlorophyll profile with C0=0.5 s=9 h=50 zmax=15.....73
Figure 27: Different sweeps over plane sea.....74
Figure 28: Zoom of Figure 29.....76
Figure 29: Laser beam with bigger slope and smaller beam width than the wave.....76
Figure 30: Laser beam with slope and beam width bigger than wave.....76
Figure 31: Laser pulse with smaller slope and beam width than the wave.....77
Figure 32: Solution to the slope problem.....78
Figure 33: Main diagram block.....80
Figure 34: Calculation of parameters.....81

Figure 35: Simulation of the sweep....82
Figure 36: Received power from a range between 100 and 400 meters, plot is a scale of grays....84
Figure 37: The received power from a range between 100 and 400 meters, plot in 3-D graph....85
Figure 38: Received power form a sweep between 100 and 400 meters with a width beam....87
Figure 39: Received power form a sweep between 400 and 700 meters with a wide beam....88
Figure 40: Attenuation coefficient of light in water for different round trip times measured in nanoseconds....89
Figure 41: Lidar system out of the cover....93
Figure 42: Map of the measurement place....93
Figure 43: Aereal view of the building....94
Figure 44: Picture from Nordnes....94
Figure 45: Picture from Skuteviken....95
Figure 46: Map of Bergen sea deepness....96
Figure 47: Parts of the Lidar System....97
Figure 48: Fixing lidar system....98
Figure 49: Wood made structure to handle the laser....99
Figure 50: Schema of the main and secondary roof....99
Figure 51: Main view of Lidar setup....100
Figure 52: Field of view and sky conditions....100
Figure 53: Using the lidar from the secondary roof....103
Figure 54: Near limit....105
Figure 55: Far limit....106
Figure 56: Laser shot using the divergence lens....107
Figure 57: Received power 108
Figure 58: Measuring different angles....109
Figure 59: Different scanners....110
Figure 60: First sweep from 31º to 8º....111
Figure 61: Laser off structure and final sweep....112
Figure 62: Schema of range detection with divergent lens....116
Figure 63: Schema of range detection without divergent lens....117
Figure 64: Schema of range detection of the bottom of the sea....118
Figure 65: Comparison between the estimated deepness and a map of the sea bottom. The red point is 235 m far from the laser....119
Figure 66: Volume clutter from sea water....120
Figure 67: Volume clutter from sea water, front view....120
Figure 68: Volume clutter from sea water....121
Figure 69: Picture taken using a 532 nm filter....122
Figure 70: Picture taken using a 532 nm filter....123
Figure 71: Picture taken using a 532 nm filter....124

Index of Tables

Table 1: Index of refraction of sea water for different wavelengths and temperature at atmospheric pressure 38
Table 2: Colour, wavelength, frequency and energy of light.....57
Table 3: Different attenuations depending on the weather.....71
Table 4: The received power at some different round trip times.....86
Table 5: The limits for sea surface detection depending on the noise.....86
Table 6: Laser specifications.....92
Table 7: Parameters used to shoot the laser.....101
Table 8: Operating range of the first day.....113
Table 9: Estimated range for detection.....121
Table 10: Estimated limits for sea surface detection from the simulations.....125
Table 11: Estimated limits from realized tests.....125
Table 12: Spectral absorption coefficient of pure sea water, aw, as determined by Smith and Baker. Values of the molecular scattering coefficient of pure sea water, b, and of the diffuse attenuation coefficients Kd used in their computation of aw are also shown…134
Table 13: Measured absorption coefficient at $\lambda = 440$ nm due to yellow matter, ay(440), for selected waters.....135
Table 14: Absorption by pure sea water, a, and the nondimensional chlorophyll-specific absorption coefficient, ac*'.....135
Table 15: The volume scattering function at $\Psi = 90°$, $\beta(90°;\lambda)$, and the scattering coefficient $b(\lambda)$ for pure water and for pure sea water.....136

Chapter 1

Introduction

Lidar, LIght Detection and Ranging, is an optical remote sensing technology. This technology, uses the scattered light by any material that is on his way to find range and/ or other information of a distant target. For this purpose it uses laser pulses. It operates over the received information that the backscattered light provides. The main parameters are: received power and round-trip-time, that is the elapsed time between the pulse emission and the reception at the original point. It also can use information like phase shift and changes in polarization.

Lidar technology has application in many different fields geography, geology, geomatics, archaeology, geomorphology, seismology, remote sensing and atmospheric physics.

One of the most important applications is terrain scanning. One example of this application is the ALSM (*Airborne Laser Swath Mapping*) and laser altimeter. The light backscattered by the ground gives the information to build a 3D map of the ground surface, for example, a mountain it will backscatter the light faster than the ground that is surrounding it just because it is higher, so the round trip time difference is going to be used to create a profile of the terrain.

High spatial and temporal resolution of the measurements, the possibility of observing the atmosphere at ambient conditions, and the potential of covering the

height range from the ground to more than 100 km altitude make up the attractiveness of lidar instruments (Weitkamp, 2005).

Atmospheric sounding, is the use of lidar to investigate the structure and composition of the atmosphere. These systems are operating from the UV to the IR (0.2 to 10 microns) bands. Using this technology different clouds that are at different altitudes, warm air flowing up in the atmosphere, drops of water and some more atmospheric measure can be made. For this purpose the different backscattering properties of the structures are used to deduce which components are in the atmosphere (Flamant, 1999).

Another application is urban scanning. Drawing a map of a city becomes a difficult work when the altitude of each building has to be considered. Using lidar an easy, fast and accurate profile of the city can be obtained. Because of the precision of the system trees and cars are distinguished. For this mapping the lidar is normally shot from a plane, but also the laser is shot over the top of a building, in this case the field of view is smaller. The basics of this application are the same as for the terrain scanning, a building roof will backscatter faster the light shot from a plane than the ground because it is closer to the laser and the receiver.

Underwater bathymetry , the study of under water depth of lakes or ocean floors, also is made by lidar technology. The laser is shot from a plane or a boat, and the difference between the time that the sea surface and the bottom of the sea backscatter the light is the depth of the sea at this point. The difference with our system is that we do not use a vertical beam. We use a beam with a concrete inclination.

The history of lidar is well explained and resumed in (Weitkamp,2005). Here, an adaptation of this text is presented.

The lidar principles were subject of study before the existence of the laser. At the 1930s there were some attempts to measure air density profiles in the upper atmosphere using the scattering intensity from search light beams.

In 1938, still in the field of the atmosphere study, pulses of light were used. The purpose was to measure cloud base heights. The generation of light pulses by electric sparks and flash lamps allowed to change the system where the emitter and the detector were in different locations to a system where they were in the same place, so the height information is actively deduced from a measurement of the round-trip time between pulse emission and signal detection. In 1953 Middleton and Spilhaus introduced the acronym lidar for this kind of measurement technique.

The development of the lidar has been always linked to the laser technology development. Since, the lidar techniques are much more effective with more efficient lasers devices. So the rapid development of lidar started with the invention of the laser in 1960 and the giant-pulse or Q-switched laser in 1962. In 1963, Fiocco and Smullin published atmospheric observations with a ruby laser.

Since this moment, it took just about 10 years to suggest and demonstrate all basic lidar techniques. Most of them were put together in the first book about lidar, written by E.D. Hinkley in 1976. Since them, lidar successful was following the progress in optical and electronic technology, as said before, in particular laser technology. That also implies that lidar researchers were involved in laser development. Many instruments use lasers specifically designed from lidar to meet the high requirements of certain lidar techniques on laser power, wavelengths, pulse width, beam shape, and spectral purity often not fulfilled by commercial products. But not only the development of the laser has contributed to lidar technology, another technology improvements have also helped a lot, such as: optical filters with narrow bandwidth, high transmissitivity, steep spectral slopes and high out-of-band suppression; data acquisition systems with a dynamic range of several orders of magnitude, efficient detectors for broad wavelength regions, and computers that can process large amounts

of data with high repetition rate belong to devices needed for advanced lidar systems. Lidar has therefore always been both a source and a beneficiary of technological innovation.

Chapter 2

Research question: "What is operational envelope of blue green lidar for subsurface imaging of objects"

The lidar market, as it is shown in (Cary, 2009), can be divided into two segments: lidar sensor, software manufactures and sales, and lidar services provision (including data acquisition, processing and sales). Lidar technology is relatively mature, but the marketplace – i.e. customers – is not. For the first segment of the market, we find that it is stable, the systems have relatively standardized features, and competition is largely based on price. About the services provision there are two primary functions, the first is coordination and sales of lidar flights, and the second is the processing of raw lidar data and subsequent services (i.e. analysis, mapping, data integration).

Lidar data has many potential applications in industries such as forestry, state and local government, emergency response/disaster mitigation and management, natural resources management, mining, oil and gas exploration, urban mapping and development, telecommunications, power supply, etc.

The Current Technology Limitations - Survey results indicate that the lidar technology itself is growing faster than the demands of the market. The improvements still tend to be incremental, such as increased scanning frequency rather than big fundamental technology changes. Cost remains the most significant barrier. Hardware

technology continues to evolve and push the attainable accuracy levels higher – the large problem is still processing and data management of large datasets. Improvements in lasers and the IMU are rapid.

Eventhough, since 2006, the number of airborne lidar data collection systems grew by 64%, but the number of users doubled, resulting in demand growing faster than the supply. The top 3 uses of the data were identified as topographic mapping, flood risk assessments and watershed analysis. One area of note was that 42% of those surveyed reported that they were doing their own data processing. In the 2005 report all post processing was being done by the data acquisition firm. Software firms take note.

Looking out to 2012, the report predicts that the sales of software and data processing services are most likely to grow in the 11 to 20% range and that hardware costs have an equal chance of coming down as remaining flat. Western Europe seems to be the one area where growth is supposed to be slower than the rest of the world, but in general the future for the aerial lidar market looks bright.

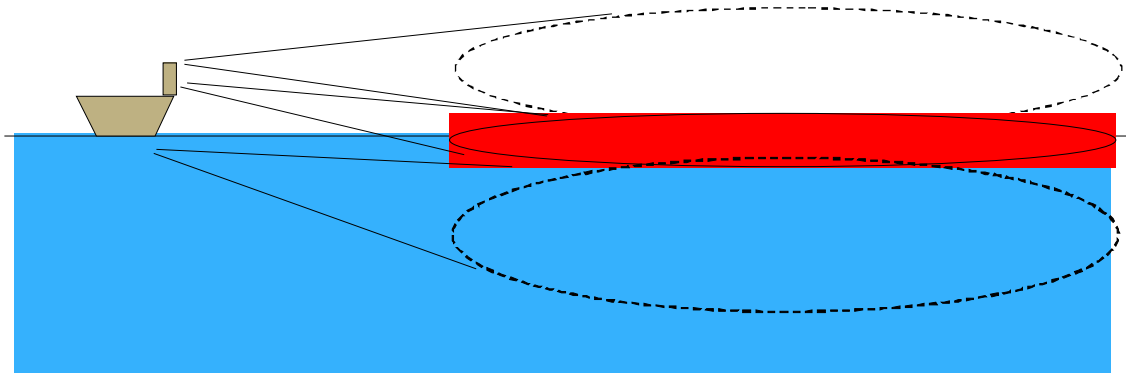

Figure 1: The red zone is the operational range of lidar

More specifically our objective is the investigation of submerged maritime target detection using lidar. The laser systems have been used many times for different

purpose through the air. For example the study of the atmosphere (Weitkamp, 2005) examining the backscattered light from the different particles. In that way is possible to guess, with not so much error, which weather is the most probable. The use of lidar for detecting targets over the ground surface has been developed and used time ago (Klein, 1997). For example, a military aircraft carrying Low-Altitude Navigation and Targeting Infrared System for night (LANTIRN), the information can guide the bullets to this target, also the Ground-based command and control system are using a similar technique.

For this radar the wavelength used is 1.064 nm, that is in the infrared zone. A lot of lidar application work over 1000 nm. In this document, the issue of analysis are the 532 nm lidar systems. Using this laser we are working in the green light zone. There are some applications that use this laser wavelength to measure the ground surface and others for bathymetry, because the smaller attenuation in water than other wavelengths.

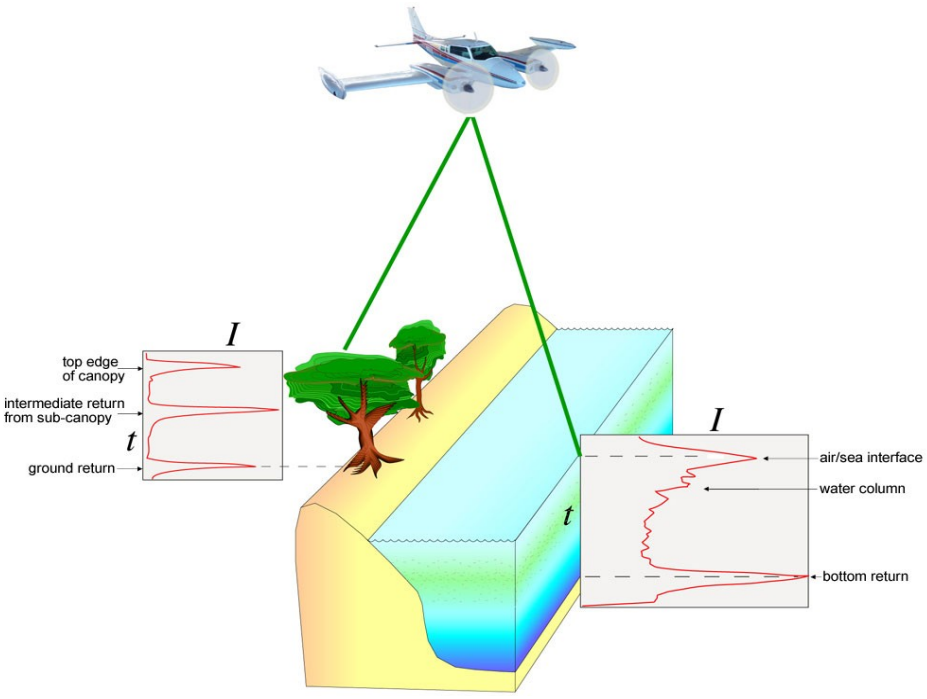

Figure 2: NASA EAARL system

For us the main study case is similar to the part in the right of the picture. There, the received data is obtained when the backscattered light of 532 nm is detected after

shooting it from a plane to the sea. There are two big peaks, the first one correspond to the sea surface, it will be explained later why it scatters more light than the air and the water. The second peak is due to the bottom of the sea. There, a solid material backscatters more light because of its bigger reflectance. Our aim is to stablished where the limits of sea surface detection and sea bottom detection are for the incident beam.

Our research question can be divided in different sub-questions:

2.1. Propagation of light: air and water

The light is affected by the components of the atmosphere, and the received power will depend on this factor. For example, in a cloudy day the attenuation of the light will be higher than a sunny day, because there are no water droplets. Also the propagation trough the air is different than the one trough the water. The Mie and Rayleigh backscattering theory are going to be study. Also how the constituents of water change its optical properties.

2.2. Discontinuity: the sea surface

The sea surface will affect also to our beam. Depending on how big are the waves the refraction of the light will be different. The discontinuity is more important for us because we pretend to shoot the laser not in a vertical way. Otherwise from a big building in a direction between the horizontal and the vertical. So the reflected light is not going directly back to the detector.

2.3. Backscatter from targets

The final purpose is to try to detect submerged targets. For this, a description of how is the behaviour of different kind of targets when being affected by a light beam is going to be done. For doing this, the electromagnetic laws that describe how the light travel through different materials, and how it is backscattered by different surfaces will be used.

2.4. Effect of the aperture of the beam

Every light beam has an aperture that makes the beam becomes bigger while the distance that it covers is increasing. We have to study the different behaviour when the beam is big and when it is small, for this purpose we have a divergence lens that makes the switching from a narrow to a wide beam.

2.5. Lidar model for MATLAB

Once the study about previous section has been done, Lidar model was created to find where the limits were, for that, the model was implemented in Matlab from where the data to take some conclusion was obtained.

We are going to work just modelling the received power, but for further analysis it should be a good idea to try to model an imaging system. For this we will need to consider spatial (transversal) resolution, and we should take care because this will be affected by turbulence and scattering.

Chapter 3

Analysis of fundamental issues

Since the laser is shot from the top of a building and the detected object is under the water surface, is needed to describe the transmission of light through the air and the water, and how it is backscattered from the submerged target. For this purpose we are going to state which effects affect the light in every moment.

3.1. Transmission of light in the atmosphere

All the information used for this section was taken, directly or modified, from (Kovalev, 2004).

To quantify the losses we need a magnitude that characterize the amount of energy in a beam of light. We are going to use the Radiant flux (F). It is defined as the rate at which energy passes a certain location per unit time (J/s, W).

Details of the scattering process depends significantly on the wavelength and the width of the spectral interval of the light. The wider band, more complicated methods have to be used to obtain estimates of the light scattering intensity. But we are working with a laser which band is suppose to be enough narrow so we have not this difficult. The most simple way is to consider the laser as monochromatic source.

3.1.1. Extinction coefficient and transmittance

We have two main effects that attenuate the intensity of the light beam; absorption and scattering. The intensity of light absorption depends on the atmospheric composition, there is more absorption when the amount of absorbers is bigger, such as carbonaceous particles, water vapor, or ozone. The absorption changes the internal energy of the gaseous or particulate absorbers. This does not happen when light scattering occurs. In this case, a portion of the incoming light is dissipated in all directions with an intensity that varies with the angle between the incoming light and the scattered light. The intensity of the scattering in a given angle depends on physical characteristics of the scatterers within the scattering volume, these two effects are included in the transmittance term

$$T(H)=\frac{F_{\lambda}}{F_{0,\lambda}}$$

This equation show how the radiant flux of a monochromatic beam after crossing a scattering or absorbing medium becomes smaller, some energy is lost during the way. T(H)=1 means that the medium is transparent while T(H)=0 means that absorption plus scattering finish with all the energy of the beam.

But if the medium is heterogeneous we need to define a differential element as following

$$dF_{\lambda}(r)=-\kappa_{t,\lambda}(r)F_{\lambda}(r)\,dr$$

Where $\kappa_{t,\lambda}$ is the probability per unit path length that a photon will be removed from the beam. Now, we divide by F_{λ} and then integrating both sides we have the Beer's law. This law describe the total extinction of the collimated light beam in a turbid layer

$$F_{\lambda}(r)=F_{\lambda,0}e^{-\int_{0}^{H}\kappa_{t,\lambda}(r)dr}$$

Comparing this equation with the previous one, the transmittance is

$$T(H)=e^{-\int_0^H \kappa_{t,\lambda}(r)dr}$$

So $\kappa_{t,\lambda}$ is the extinction coefficient of scattering or absorption and it can be written as the sum of two terms (wavelength dependency has been removed)

$$\kappa_t(r)=\beta(r)+\kappa_A(r)$$

Where $\beta(r)$ is the elastic scattering coefficient and $\kappa_A(r)$ is the absorption coefficient.

In the air, the removal of light energy from a beam can take place because of different reasons:

1. Scattering and absorption at the same time. That occurs because aerosol particles, such as water droplets, mist spray, or airborne dust.
2. Scattering of the light energy by molecules of atmospheric gases, such as nitrogen or oxygen.
3. Absorption of energy by molecules of atmospheric gases, such as ozone or water vapor.

The problem is that normally the light is not a perfectly collimated beam and we need to consider the effect of the divergence. For that, is useful the approximation known as the point source of light may generally be used. This approximation needs that the distance between the source and the photoreceiver is much larger that the size of the light source. The Allard's law states that, for a point source of light, the amount of light captured by a remote light detector is inversely proportional to square of the range from the source location to the detector and directly proportional to the total transmittance over the range

$$E(r)=\frac{IT}{r^2}=\frac{I}{r^2}e^{-\int_0^r \kappa_t(r')dr'}$$

Where E(r) is the irradiance (the amount of radiant flux intercepted by a unit area) at range r from the light source, and I is the radiant intensity of the light energy source.

3.1.2. Total and directional elastic scattering

For the scattering taking place only a narrow beam crossing a volume filled by gas molecules or particulates is needed. The reason of the scattering is the difference of refraction indexes between the medium and the molecules or particles. The illuminated particle re-emits some fraction of the incident light energy in all directions, becoming a point source of the re-emitted light.

The intensity of the angular scattering depends on the angle between the incident light and the scattering direction. The radiant spectral intensity of light with wavelength λ scattered per unit volume in the direction of θ relative to the direction of the incident light is proportional to spectral irradiance E_λ and a directional scattering coefficient for scattering angle θ

$$I_{\lambda,\theta} = \beta_{\lambda,\theta} E_\lambda$$

The directional scattering coefficient $\beta_{\lambda,\theta}$ determines the intensity of light scattering in direction θ. The scattered light may have different sources:

1. Molecular and particulate elastic scattering constituents, which have the same wavelength as the incident light.
2. Resonance scattering may occur with no changes in wavelength
3. Additional spectral constituents, such as a Raman or fluorescence constituent, in which wavelengths are shifted relative to that of the incident light λ.

In the following section the points 2 and 3 are considered. If we have an atmosphere with no absorption and only elastic scattering. In that conditions the radiant flux scattered per unit volume over all solid angles can be derived as the integral of the following expression

$$F_{(4\pi)} = \int_0^{4\pi} I_\theta \, d\omega = \beta E$$

where

$$\beta = \int_0^{4\pi} \beta_\theta \, d\omega$$

is the total volume scattering coefficient. The phase function is formally defined as the ratio of energy scattered per unit solid angle in the direction θ to the mean energy per unit solid angle scattered over all directions (Van der Hulst, 1957). If we have not polarized light the phase function is

$$P_\theta^{'}=\frac{\beta_{theta}}{\beta/4\pi}=\frac{4\pi\beta_\theta}{\int_0^{4\pi}\beta_\theta d\omega} \quad \text{and always} \quad \int_0^{4\pi}P_\theta^{'}d\omega=4\pi$$

As the particulate radii become larger, they scatter more total energy and a larger fraction of the total in the forward direction as compared to small particles. For remote sensing the phase function is often normalized to 1, so

$$\int_0^{4\pi}P_\theta d\omega=1$$

And we can describe the phase function as the ratio of light scattered in direction θ to the total scattering:

$$P_\theta=\frac{\beta_\theta}{\beta}$$

3.1.3. Inelastic scattering: Rayleigh and Mie scattering

The different sizes, types, shapes and composition of the atmospheric particles make them scatter the light in different ways. And also due to the wavelength of the light we will have different intensity and angular phase of the scattering phase function. For example the refraction index depends on the wavelength, and the refraction index is an important parameter in any scattering or absorption process.

$$10^8(m_s-1)=8342.13+\frac{2406030}{130-\nu^2}+\frac{15997}{38.9-\nu^2}$$

But for simplicity we are considering the refraction index as a constant value. Perhaps further studies could include this consideration.

Rayleigh Scattering

If we do not consider the depolarization effects and the adjustments for temperature and pressure, the molecular angular scattering coefficient at wavelength λ in the direction θ relative to the direction of the incident light can be shown to be

$$\beta_{\theta,m} = \frac{\pi^2 (m^2-1)^{2N}}{2N_s^2 \lambda^4} (1+\cos^2\theta)$$

where N is the number of molecules per unit volume at the existing pressure and temperature, and N_S is the number density of molecules at standard conditions (N_s=2.547 *10^{19} at T_S=288.15K and P_S=101.325kPa). m is the real part of the index of refraction. Assuming isotropic air molecules. If we assume also symmetry about one axis, a differential solid angle is

$$d\omega = 2\pi \sin\theta \, d\theta$$

$d\theta$ is a differential plane angle. So to obtain the molecular volume scattering we must just integrate in all the possible angles

$$\beta_m = \int_{\phi=0}^{2\pi} \int_{\theta=0}^{\pi} \sin\theta \, d\theta \, d\phi$$

and solving this integral we have

$$\beta_m = \frac{8\pi (m^2-1)^{2N}}{3N_S^2 \lambda^4}$$

the expression of the molecular volume scattering coefficient.

"The intensity of molecular scattering is sensitive to the wavelength of the incident light: the scattering is proportional to λ^{-4}. Therefore, the atmospheric molecular scattering is negligible in the infrared region of the spectrum and dominates scattering in the ultraviolet region. For example, with other conditions being equal, light scattering at wavelength 0,25 μm (the ultraviolet region) differs from that at wavelength 1 μm by a factor of 256!" (Kovalev, 2004)

So now we can state that the molecular phase function normalized to 1, is

$$P_{\theta,m}=\frac{\beta_{\theta,m}}{\beta_m}=\frac{3}{16\pi}(1+\cos^2\theta)$$

This molecular phase function phase function is symmetric, that means that we are backscattering ($\theta=180^{\circ}$) the same light than in the normal direction ($\theta=0^{\circ}$) .

For us, because we are working at sea level, the N factor becomes approximately 2.55×10^{19} molecules/cm^{-3}, the volume backscattering coefficient at the wavelength λ becomes

$$\beta_m=1.39[\frac{550}{\lambda(nm)}]^4\times10^{-8}cm^{-1}\,sr^{-1}$$

Another concept useful is the *cross section.* For molecular scattering, the cross section defines the amount of scattering due to a single molecule

$$\sigma_m=\frac{\beta_m}{N}$$

where N is the molecular density. The molecular cross section specifies how much of the incoming energy that is scattered by one molecule in all directions when that molecule receives some light. Now using the expression of the molecular backscattering coefficient we have that

$$\sigma_m=\frac{8\pi^3(m^2-1)^2}{3N_S^2\lambda^4}$$

Right now we have characterised the molecular scattering. The main basics are the following:

1. The total and angular molecular scattering intensity is proportional to λ^{-4}. Thus, the infrared waves scatter much less light than the ultraviolet part of the spectrum.
2. The light scattered to forward and backward is the same because the molecular phase function is symmetric.

The type of scattering described in this section, commonly known as Rayleigh scattering, is inherent not only to molecules but also to particulates, for which the radius is small relative to the wavelength of incident light.

Mie Scattering

Mie scattering is the one due to light scattering by particles. Because particles are bigger than molecules, their size is comparable to the wavelength and then the effects of the scattering is much more important. Now the scattering can be seen as an interaction between waves that wrap themselves around and through the particle, constructively interfering in some cases, destructively interfering in others.

For spherical and conducting particles we have that if the size of the particle is a multiple of the wavelength the interference is constructive, but if it is a multiple of the wavelength and a half the interference is destructive. In the first case the cross section is big and in the second one is minimum. But real particles are often no ideally spherical or conductors, and the electromagnetic wave travels also trough the particle, no just around it, and then the peaks in the angular scattering are often offset from exact multiples of the wavelength, depending on the magnitude of the index of refraction of the scattering material.

When the size of the particle is much greater than the wavelength, the laws of geometric optics govern.

The laws that govern particulate scattering are much more complex than the ones shown before. Normally they are solved with computer programs or using approximated formulas.

But for the study of the atmosphere there are some methods that try to include different sizes, shapes, refractive index and compositions. We are going to assume that

they are spherical, that the incident light is spectrally narrow, and that multiple scattering is negligible and can be ignored.

Monodisperse Approximation

We start considering every factor as simple as possible. The scattering volume is assumed to be filled uniformly by particles of the same size and composition. These particles each have the same index of refraction and, therefore, scattering properties. So the total particulate scattering coefficient can be written, similarly to molecular scattering as

$$\beta_p = N_p \sigma_p$$

where N_p is the particulate density and σ_p is the single particle cross section. In particulate scattering theory, two additional dimensionless parameters are defined. The scattering efficiency is the ratio of particle scattering cross section σ_p to the geometric cross-sectional are of the scattering particle

$$Q_{SC} = \frac{\sigma_p}{\pi \rho^2}$$

where ρ is the particle radius. To model the particle the size parameter is also needed, it is

$$\phi = \frac{2\pi\rho}{\lambda}$$

so we can rewrite the total particulate scattering coefficient as

$$\beta_p = N_p \pi \rho^2 Q_{SC}$$

the dependence of this coefficient with different values of Q_{SC} is explained as ϕ is getting bigger, the scattering factor increases, reaching values around 4. And then it decreases and oscillates about an asymptotic value of $Q_{SC}=2$. For this parameters the effect of the scattering does not depend on the wavelength of the incident light.

Therefore we can distinguish 3 types of scattering depending on the size parameter:

1. $\phi \ll 1$ Small particles. Normally found in a clear atmosphere.

2. $\phi > 40-50$ Large particles. Those ones are in heavy fogs and clouds.
3. $1 < \phi < 25$ The intermediate type is for particles in the lower part of the atmosphere.

If $\phi < 0.2$ or $(\rho < 0.03\lambda)$ we can considerate the scattering similar to the one for molecules (Rayleigh). It has the same dependence with λ^{-4} (with the correspondent response to ultraviolet and infrared light), and also it is symmetric in the forward and backward hemispheres.

$$\sigma_P = \frac{128\pi^5\rho^6}{3\lambda^4}\left(\frac{m^2-1}{m^2+2}\right)^2$$

The phase function is also similar to the molecular scattering (is symmetric) one while the parameter size stays small. When it increases the fraction of light in the forward direction increases. For large particles the phase distribution varies a lot depending on the size as is shown in the following figure. But when scattering occurs from an ensemble of different size particulates in a real finite volume, the peaks are smoother.

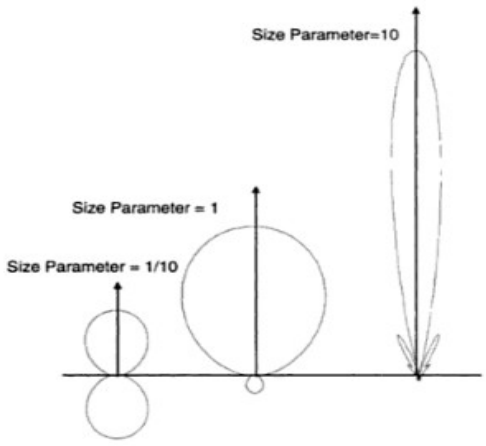

Figure 3: The angular distribution of scattered light intensity for the particles of different size

Summarizing the main topics of scattering for particles where $\phi > 1$ and comparing them with the molecular scattering we have that:

1. The scattering in the forward direction is greater than the one in the backward direction.

2. The directional dependence of the particulate scattering is more complicated. When the size parameter increases some additional lobes appear.
3. Scattering produced by large particles is no sensitive to the wavelength of the incident light.

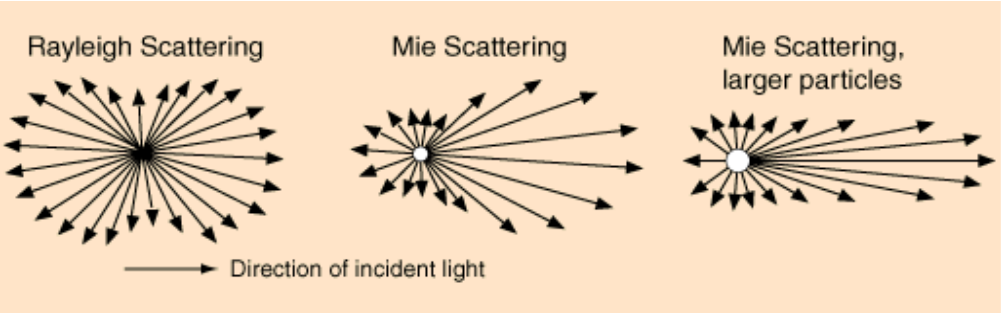

Figure 4: Different scattering mechanism

Polydisperse Scattering systems

Normally the real atmosphere is not composed by particles of the same size, shape and composition. Because there is not a standard distribution for the atmosphere, it is needed to measure for every scenario the total number of scattering particles. In volume we can see that as

$$N = \sum_{i=1}^{k} N(\rho_i)$$

where $N(\rho_i)$ is the number of particles with radius ρ_i. And the total scattering is obtained as

$$\beta_P = \sum_{i=1}^{k} N(\rho_i)\pi\rho_i^2 Q_{SC,i}$$

but we are still considering every particle as spherical scatterers. That is normally true only for water droplets or water-covered particulates. Some different distributions can be used, but the most common are a modified gamma distribution or a variant because of the mathematical simplicity.

The expression of the total scattering has and integral formulation

$$\beta_P = \int_{\rho_1}^{\rho_2} n(\rho)\pi\rho_i^2 Q_{SC}\, d\rho$$

and from this we can obtain the phase function normalized to 1 in the same way that we used in the scattering by molecules

$$P_{\theta,p} = \frac{\beta_{\theta,p}}{\beta_p}$$

In lidar measurements, it is common practice to assume that backscattering ($\theta = 180^{o}$) is related to total scattering or extinction. The commonly used assumption is a linear relationship between the backscattered coefficient and the extinction coefficient, that is more accurate when the medium is more homogeneous. The validity of this approximation was for the relationship between both coefficients shown by calculating these parameters for a wide range of droplet size distribution and in laboratory measurement with a He-Ne laser and polydisperse clouds generated in scattering chambers.

We have to consider that all this expressions are considering the possibility of single scattering, that means that the photons received were scattered only once. The formulas for multiple scattering are too complex. The multiple scattering depends on the divergence and the diameter of the light beam, on the range from the light source to the scattered volume, on the wavelength of the emitted light, and on the field of view of the fotodetector optics.

Inelastic scattering

The scattering process that we have seen until this point produce a photon that is the same incident photon but it changes its direction. That is the predominant effect in the atmosphere, and it is normally known as Rayleigh scattering. But there is another kind of scattering in which one of the result of the interaction between the incident photon and the molecules is another photon or photons whose frequency has been shifted. That type of scattering is known as Raman scattering. The intensity depends on

the polarizability of the molecules. If the molecule which is hit is polarizable, it has some vibrational modes that can be excited by the incident photon, i.e. the molecule reachs a higher level of energy and the amplitude of its vibration is increased. After this point the molecule relax and the result is a photon that has less energy than the difference between the first and the final vibrational states of the molecule.

When any molecule is affected by an external oscillating electric field with a magnitude of $E = E_0 \sin(2\pi \nu_{ext} t)$ (E_0 , ν_{ext} are the amplitude and the frequency of the incident field respectively) a dipole moment is induced in the molecule. This is because the nuclei tend to move in the direction of the applied field and the electrons in the opposite direction. The induced dipole will be proportional to the field amplitude by $p = \alpha E$, and α is the polarizability of the molecule (it is different from zero for every atom and molecule).

$$\alpha = a_0 (\frac{d\alpha}{dr}) \delta r$$

where δr is the separation between nuclei. If the molecule is oscillating harmonically is $\delta r = r_0 \sin(2\pi \nu_v t)$ (r_0 is the amplitude and ν_v the frequency at which the molecule is oscillating before the application of the external field). After if we apply a electromagnetic field and the molecule is linearly polarizable the molecule will have the following dipole moment

$$p = \alpha_0 E_0 \sin(2\pi \nu_{ext}) + E_0 r_0 \frac{d\alpha}{dr} \sin(2\pi \nu_{ext} t) \sin(2\pi \nu_v t)$$

or, written in a different way

$$p = \alpha_0 E_0 \sin(2\pi \nu_{ext}) + E_0 r_0 \frac{d\alpha}{dr} \sin(2\pi \nu_{ext} t) \sin(2\pi \nu_v t)$$

The first term has the same frequency than the incident photon, that is because this term represent the elastic Rayleigh scattering. The second and the third term correspond to the Raman scattering that occur at the Stokes frequency $\nu_{ext} - \nu_{vu}$ and the

anti-Stokes frequency $\nu_{ext}+\nu_{vu}$. So the Raman scattering occur in two frequencies close to the laser frequency.

If the molecule is not aligned with the applied field we have to multiply this expression by $\cos\phi$. And if the molecule is rotating ϕ will change along the time as $\phi=2\pi\nu_{\phi}t$. And then will appear a lot of terms in different frequencies ν_{ext} $\nu_{ext}\mp\nu_{vu}$ $\nu_{ext}\pm\nu_{\phi}$, etc. thus a spectrum of frequencies will occur. The following figure show us this spectrum.

However, vibrationally shifted states beyond the first order are sufficiently weak so that they are seldom used in lidar.

3.1.4. Absorption by molecules and particulates

Particulates and molecules can act as light absorbers and not only as scatterers. Some of this atmospheric light-absorbers are carbon dioxide, water vapor, ozone, and oxygen. However, these particulates are absorbers only for determinate wavelength of the incident beam, they can absorb the energy of the ultraviolet, visual, and infrared spectrum. Also some trace contaminants that are found in the atmosphere are absorbing light from discrete parts of the spectrum, and so, a special kind of lidar, differential lidar or DIAL is used to detect their presence in the atmosphere.

As shown in section 3.1.3 the index of refraction is an important parameter when we are talking about electromagnetic process in the atmosphere. The complex index has a real and an imaginary part. The real part is commonly named index of refraction and it indicates the ratio of the speed light in a vacuum to the speed of light inside the medium, and the imaginary part is related to the absorption properties of the medium. These properties depends of the particulate type and size. Our lidar application is working in the lowest part of the troposphere, there we can find water and water-soluble particulates, and some insoluble particulates that act as absorbers.

For particles of the same type and size the Mie scattering theory gives us a expression for the absorption coefficient

$$\kappa_A = N \pi \rho^2 Q_{abs}$$

where κ_A is the absorption coefficient, Q_{abs} is the absorption efficiency factor, and N is the number of absorbers per unit volume. The absorption cross section is related to the absorption coefficient

$$\kappa_A = N \pi \rho^2 Q_{abs}$$

and we can rewrite the absorption coefficient as

$$\kappa_A = \sigma_A N$$

if the medium analyzed is not homogeneous the integral expression must be used

$$\kappa_{A,p} = \int_{\rho_1}^{\rho_2} \pi \rho^2 Q_{abs}(\rho, m) n_A(\rho, m) d\rho$$

where $n_A(\rho, m)$ is the number density of the absorption particles as a function of radius and complex index of refraction, and $Q_{abs}(\rho, m)$ is the absorption efficiency factor for the complex index of refraction m.

The lidar technology use wavelengths where the absorption occurs in groups or bands of discrete absorption lines. But the lasers are made on purpose to avoid these bands and the attenuation is normally not a big problem. Eventhough, for example the Ho:YAG laser works at 2.1 μm and it must be tuned to use another bands.

A molecule can absorb energy using three different mechanisms: electronic transitions, vibrational transitions and rotational transitions. There are also 3 parameters that characterize the absorption/emission lines: the absorption strength of the lines, S, the central position of the line (the most probable wavelength to be absorbed), ν_0, and the shape/width of the line. The central position of an absorption/emission line is a function of the quantum mechanical states of the particular molecule in question. The strength of the line id the total absorption of the line, it is related with the population density of the beginning and ending states involved in the transition, which is related with the temperature of the molecule.

The width and shape of these bands are function of the lifetime to the excited quantum mechanical state. By Heisenberg uncertainty principle, there is a relationship between the ability to accurately determine both the lifetime and the energy of a given state simultaneously. The product of the uncertainties in time and energy must be greater than than h/2π, so we can write:

$$\Delta t_{lifetime} \Delta E \approx \frac{h}{2\pi} \Rightarrow \Delta = \frac{1}{2\pi\, DELTAt_{lifetime}} \approx \frac{\Delta E}{h}$$

in addition to this effect the lines are wider because of the Doppler shift of the frequency due to the velocity of the molecules. The Maxwell-Boltzmann distribution governs the distribution of the molecular velocities for a given temperature. The probability that a molecule in a gas at temperature T has a given velocity V in a particular direction is proportional to

$$e[\frac{-MV^2}{2\mathrm{kT}}]$$

where k is the Boltzmann constant, $8.617\text{x}10^{-5}$ eV/degree and M is the mass of the molecule. The shift due to the motion of an emitter with velocity, V and emissions with frequency, ν_0, is known as the Doppler shift, whose magnitude is

$$\Delta \nu = \pm(\frac{V}{c})\nu_0$$

and combining the two last formulas we have that the extinction at a given wavelength is related to the peak extinction

$$\kappa_D(\nu) = \kappa_{D_0} \exp[\frac{-Mc^2}{2\mathrm{kT}}(\frac{\nu-\nu_0}{\nu_0})]$$

that is a Gaussian-shaped distribution with a half-width of

$$\Delta \nu = \nu_0 \xi \sqrt{\frac{T}{M}}$$

where the mass of the molecule M is in gram-atoms and the temperature T is in Kelvin; the quantity ν_0 denotes the center line frequency, and ξ is a constant ($3.58\text{x}10^{-7}$ degrees$^{-1/2}$).

But there is still a third mechanism that acts to broaden (apart from the one derived from the lifetime and the Doppler shift), the spectral absorption lines is collisional or pressure broadening. This is the dominant effect in the lower atmosphere. It assumes that the rotational or the vibrational state is interrupted by a collision with another molecule. The frequencies of the oscillation before and after the collision are assumed to have no relationship to each other. The line shape due to collisional broadening is given by the formula (Bohren and Huffman, 1983; Measures, 1984)

$$\kappa_C(\nu) = \kappa_{C_0} \frac{P}{T} \nu^2 \frac{\Delta \nu_c}{(\nu - \nu_0)^2 + (\Delta \nu_c)^2}$$

where the half-width due to molecular collisions, $\Delta \nu_c$, is also a function of temperature and pressure and is given by

$$\Delta \nu_c = \Delta \nu_{c_0} \frac{P}{P_0} \left(\frac{T_0}{T}\right)^n$$

where P_0 and T_0 are the pressures and temperatures for collisions ν_{c_0} .

For visible light, collisional broadening dominates over Doppler broadening, and the ratio of the line width is given approximately by

$$\frac{\Delta \nu_{Doppler}}{\Delta \nu_{collisional}} \approx 10^{-12} \frac{\nu_0}{P}$$

For the region in which the line widths are approximately equal, the total width is given by $\Delta \nu \approx ((\Delta \nu_{Doppler})^2 + (\Delta \nu_{collisional})^2)^2$ and it has the Voight line shape.

For remote sensing measurements, where the concentration of absorbing gases of interest is generally small the dependence of light on the absorption coefficient can be written in a similar way to the scattering

$$\frac{F_\nu}{F_{0,\nu}} = e^{-\kappa_A(\nu) r} = e^{-N \sigma_A(\nu) r}$$

where N is the number density of absorbing n¡molecules and, for simplicity, the dependence is written for a homogeneous absorption medium. This expression is valid

when every molecule absorbs light energy independently from other molecules, i.e. the absorption cross section depends neither on the concentration of the absorbing molecules nor on the intensity of the incident light.

The absorption can change with the pressure, because in the atmosphere, the pressure is caused mainly by nitrogen and oxygen gases, that are absorbers. But in our application the pressure is going to be constant in the atmosphere because we are going to work between 50 meters high and the sea surface.

3.2. Transmission of light in water

The theoretical background of this chapter has been extracted from C.D. Mobley in 1994.

The transmission properties of the light depend on some parameters. These parameters are divided into two mutually exclusive classes: inherent and apparent. Inherent optical properties (IOP's) are those properties that depend only upon the medium and Apparent optical properties (AOP's) are those properties that depend both on the medium (the IOP's) and on the geometric (directional) structure of the ambient light field. We are going to focus in the IOPs. The two fundamental IOP's are the absorption coefficient and the volume scattering function.

3.2.1. Inherent Optical Properties

The inherent optical properties describe the optical properties of natural water based on the radiative transfer theory.

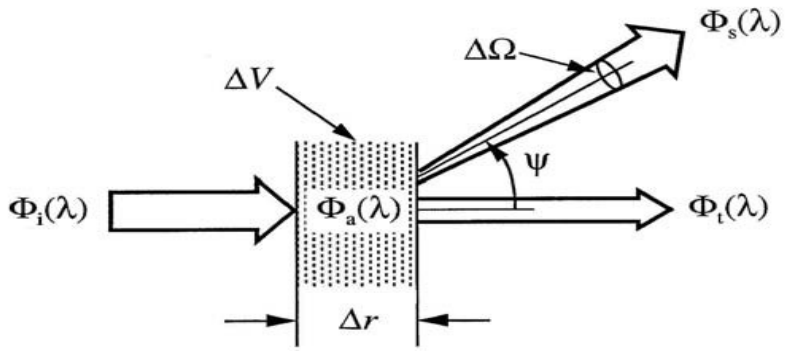

Figure 5: Geometry used to define inherent optical properties

Considering a small volume ΔV of water, of thickness Δr , illuminated by a narrow collimated beam of monochromatic light of spectral radiant flux Φi(λ). Some part of the incident flux Φi(λ) is absorbed within the volume of water, Φa(λ). Some part is scattered out of the beam at an angle Ψ, Φs(λ,Ψ) , and the remaining flux is

transmitted through the volume with no change in direction, Φt(λ). Let Φs(λ) be the total flux that is scattered into all directions. Furthermore, assuming that no inelastic scattering occurs, the conservation of energy would be,

$$\phi_i(\lambda)=\phi_a(\lambda)+\phi_s(\lambda)+\phi_t(\lambda)$$

The spectral absorptance A(λ) is the part of the incident flux that it is absorbed in the volume of water:

$$A(\lambda)=\frac{\phi_a(\lambda)}{\phi_i(\lambda)}$$

The spectral scatterance B(λ) is the part of the incident flux that it is scattered out of the transmited beam,

$$B(\lambda)=\frac{\phi_s(\lambda)}{\phi_i(\lambda)}$$

and the spectral transmitance T(λ) is

$$T(\lambda)=\frac{\phi_t(\lambda)}{\phi_i(\lambda)}$$

Clearly, A(λ) + B(λ) + T(λ) = 1. The spectral values do not have units.

The inherent optical properties usually employed in hydrologic optics are the spectral absorption and scattering coefficients, which are respectively the spectral absorptance and scatterance per unit distance in the medium. In the geometry of Fig.5 the *spectral absorption coefficient a(λ)* is defined as

$$a(\lambda)=\lim_{\Delta r\to 0}\frac{A(\lambda)}{\Delta r}\quad (m^{-1})$$

spectral scattering coefficient b(λ) is

$$b(\lambda)=\lim_{\Delta r\to 0}\frac{B(\lambda)}{\Delta r}\quad (m^{-1})$$

The s*pectral attenuation coefficient c(λ)* is defined as

$$c(\lambda)=a(\lambda)+b(\lambda)\quad (m^{-1})$$

3.2.2. Optical Signinificant Constituents of Natural Waters

In order to estimate the correct values of the absorbing and scattering coefficient of natural waters, we need to have some knowledge of the composition of those waters. Natural waters contain a continuous size distribution of particles ranging from water molecules of size 0.1 nm, to small organic molecules of size 1 nm, to large organic molecules of size 10 nm, to viruses of size 100 nm, to ..., to whales of size 10 m, to submarines of size 100 m. Strickly speaking, natural waters are composed of particles. Traditionally the constituents of natural waters are divided into "dissolved" and "particulate" matters, of organic and inorganic origins, living and nonliving.

Pure sea water consists of pure water plus various dissolved salts, which average about 35 parts per thousand (35%) by weight. These salts increase scattering, and make the scattering from pure sea water 30% bigger than the scattering from pure water. These salts have a negligible effect on absorption at visible wavelengths, so in our case the salt is not going to be one of the limiting factor, but it is likely that they increase absorption somewhat at ultraviolet wavelengths and the increase is bigger while the wavelength is extremely long.

Dissolved organic compounds are produced during the decay of plant matter and consist mostly of various humic and fulvic acids (Kirk, 1983 cited in Mobley,1994). Generally are brown and in sufficient concentrations they colour the water yellowish brown, so they are called yellow matter or colored dissolved organic matter. They have to be taken in care at blue and ultraviolet wavelengths because the absorption increases. In ocean waters, the absorption by yellow matter is usually small compared to absorption by other constituents like phytoplankton.

Particulate matter have two different origins: biological or physical. The organic particles of optical importance are created as bacteria, phytoplankton, and zooplankton grow and reproduce. Inorganic particles are created primarily by weathering of terrestrial rocks and soils. These particles can enter the water as wind-blown dust settles

on the sea surface, or as rivers carry eroded soil to the sea. This particulate matter usually is the major determiner of absorption and scattering properties of natural waters.

Organic particles occur in many forms:

VIRUSES. Natural marine waters contain virus particles in concentrations of 10^{12} to 10^{15} particles m-3 (Suttle, *et al.* 1990 cited in Mobley,1994). These particles are generally much smaller (250 nm) than the wavelength of visible light. In spite of their large numbers they are inefficient absorbers and scatterers on a per-particle basis. However, very small particles can be efficient backscatterers. Viruses sometimes may contribute significantly to the backscatter coefficient, at least at blue wavelengths in very clear waters.

COLLOIDS. Nonliving colloidal particles in the size range 0.4-1.0 μm are found in typical number concentrations of 10^{13} m^{-3}, and colloids of size 0.1 μm are found in abundances of 10^{15} m^{-3} (Koike, *et al.*, 1990; Wells and Goldberg, 1991 cited in Mobley,1994). Part of the absorption traditionally attributed to dissolved matter probably is due to colloids.Modelling results based on Mie scattering theory (e.g. Stramski and Kiefer, 1991 cited in Mobley,1994) suggest that colloids contribute significantly to backscattering.

BACTERIA. Living bacteria in the size range 0.2-1.0 μm occur in typical number concentrations of 10^{11}-10^{13} m^{-3}. Bacteria can be significant scatterers and absorbers of light, especially at blue wavelengths and in clear oceanic waters, where the larger phytoplankton are relatively scarce (Spinrad, *et. al*., 1989; Morel and Ahn, 1990; Stramski and Kiefer, 1991 cited in Mobley,1994). Bacteria are likely the most important microorganisms contributing to particulate backscattering.

PHYTOPLANKTON. These ubiquitous microscopic plants occur with incredible diversity of species, size, shape, and concentration. Phytoplankton are the particles primarily responsible for determining the optical properties of most oceanic waters. Their chlorophyll and related pigments absorb light in the blue and red and thus, when concentrations are high, predominate in determining the spectral absorption of sea water. These particles are generally much larger than the wavelength of visible

light and are efficient scatterers, especially via diffraction, thus strongly influencing the total scattering properties of sea water. Although large particles scatter strongly at small scattering angles, and thus contribute to *b*, they scatter only weakly at large angles. Therefore the larger phytoplankton contribute relatively little to backscattering.

ORGANIC DETRITUS. Nonliving organic particles of various sizes are produced, for example, when phytoplankton die and when zooplankton graze on phytoplankton. Even if these detrital particles contain chlorophyll pigments when they are produced, they can be rapidly photo-oxidized and lose the absorption spectrum characteristic of living phytoplankton. They only have a significant absorption at blue wavelengths. Detrital particles are the major backscatterers in the ocean.

LARGE PARTICLES. Particles larger than 100 μm include zooplankton and fragile amorphous aggregates of smaller particles. Such particles occur in highly variable numbers from almost none to thousands per cubic meter. Large particles can be efficient scatterers of light at all scattering angles. Aggregates therefore may significantly affect the optical properties (especially backscatter) of large volumes of water. (Alldredge and Silver, 1988; Carder and Costello, 1994 cited in Mobley,1994).

Inorganic particles generally consist of finely ground quartz sand, clay minerals, or metal oxides in the size range from much less than 1 μm to several tens of micrometers. Sometimes inorganic particles are optically more important than organic particles, but the attention that have been made to them has been insufficient. Such situations can occur both in turbid coastal waters carrying a heavy sediment load and in very clear oceanic waters that are receiving windblown dust (Carder, *et al*., 1986 cited in Mobley,1994).

The phytoplankton coccolithophore species *Emiliania huxleyi* is a most remarkable biological source of crystalline particles. During blooms they, *E. huxleyi,* produces and sheds enormous numbers of small calcite plates that have a negligible

effect on light absorption but are extremely efficient light scatterers: they have a irradiance reflectances of R = 0.39 at blue wavelengths during blooms (compared with R = 0.02 to 0.05 in the blue for typical ocean waters). Such coccolithophore blooms give the ocean a milky white or turquoise appearance.

3.2.3. Electromagnetic Properties of Water

Electromagnetic wave propagation at the level of Maxwell's equations, it is convenient to specify the electromagnetic properties of the medium via its electrical permittivity ε, the magnetic permeability μ and the electrical conductivity σ. Water does not display significant magnetic properties, so the magnetic permeability can be taken equal to the free space (*in vacuum*) value at all frequencies:$\mu = \mu_0 = 4\pi \times 10^{-7}$ N A^{-2}. The electrical permittivity and conductivity depend on the frequency, f, of the propagating electromagnetic wave, as well as on the water temperature, pressure, and salinity. Low frequency values for the permittivity are of order $\varepsilon = 80\varepsilon_0$, where ε_0 is the free-space value. This value decreases to $\varepsilon = 1.8\varepsilon_0$ at optical frequencies. At sea water the conductivity is of 4.4 Siemen m^{-1} .

The effects ε, μ and σ on electromagnetic plane-wave propagation are compactly summarized in terms of the complex index of refraction, m = n- ik. The real part n of m is usually called "the index of refraction" and k is called "the imaginary part of the complex index of refraction". The complex index of refraction:

$$m^2 = \mu \epsilon c^2 - \frac{i \pi \mu \sigma c^2}{f}$$

$$m^2 = (n - ik)^2 = n^2 + k^2 - 2\text{ink}$$

where $c = (\mu_0 \varepsilon_0)^{-1/2}$, is the speed of the electromagnetic wave in the vacuum.

The n and k parameters will be directly related to the scattering and absorption coefficient values. The real part of the complex index of refraction governs the scattering and the imaginary part governs the absorption, this is the reason to know k also like absorption index.

$$a(\lambda)=\frac{4\pi k(\lambda)}{\lambda}$$

Here λ is the wavelength of the electromagnetic wave in the vacuum depending on the f frequency.

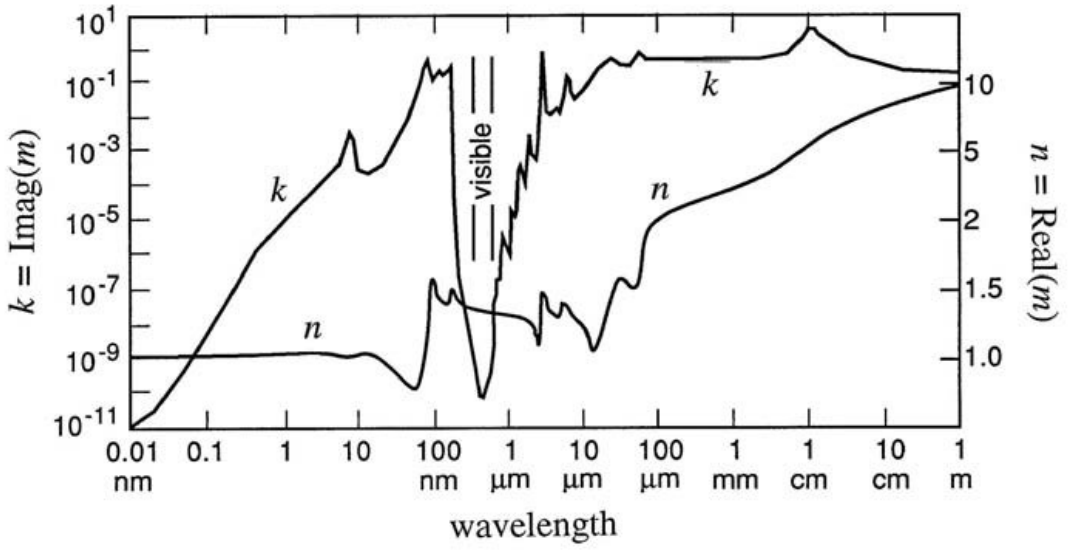

Figure 6: The optical constants of pure water. The right axis gives the real part of m, and the left axis gives the imaginary part of m, where m is the complex index of refraction

The extraordinary characteristic seen in this figure is the narrow "window" in $k(\lambda)$, $k(\lambda)$ decreases by over nine orders of magnitude between the near ultraviolet and the visible bands and then quickly rises again in the near infrared band. This behavior in $k(\lambda)$ gives a corresponding window in the spectral absorption coefficient $a(\lambda)$, as seen in Fig. 7.

The shape of the absorption curve can be explained as follows. At blue wavelengths, photons are barely energetic enough to estimulate electrons into higher energy levels of the water molecule, and the photons do not have the sufficient energy to interact with the molecule as a whole. The photons therefore do not interact strongly with the water molecules, and $a(\lambda)$ is at its minimum. As the wavelength decreases

toward the ultraviolet, the photons become sufficiently energetic to boost atomic transitions, absorption rapidly increases. As the wavelength increases from blue to red and beyond, the photons start having enough energy to boost first the fundamental vibrational and then the rotational modes of the water molecules, and the absorption increases rapidly in the infrared band. At very long wavelengths, the photons are not energetic enough to excite molecular motions, and the absorption decreases.

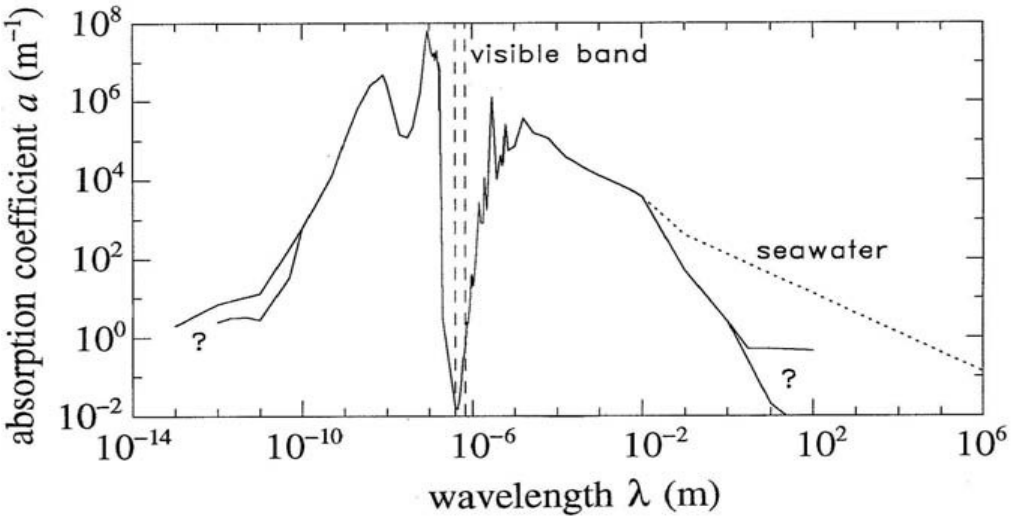

Figure 7: Spectral absorption coefficient of pure water (solid line) and of pure sea water (dotted line) as a function of wavelength.

Ions resulting from the dissolved salts make sea water better conductor of electricity than pure water is , so the behaviour of sea water as a conductor gives it a higher absorption at very long wavelengths, as shown by the dotted line in Fig 7.

The minimum values of $a(\lambda)$ around blue wavelengths is the reason why blue laser are used in water remote sensing.

As we have said, the real part of the index of refraction determines the scattering properties of a medium. If n were constant, there would be no scattering. However,

there are always variations of n in the medium. Even in pure water, random thermal fluctuations vary the numbers of molecules in any given small volume ΔV. These molecule number density fluctuations result in small-scale fluctuations in the index of refraction. In pure sea water, the ions of dissolved salts cause additional molecular-scale fluctuations in n, and hence greater scattering.

Austin and Halikas (1976) made some reports with some tables and interpolating algorithms to determinate the index of refraction, n(λ,S,T,p), as a function of wavelength (λ = 400-700 nm), salinity (S = 0-43%), temperature (T = 0-30°C), and pressure ($p = 10^5$-10^8 Pa, or 1 to 1080 atm). Figure 8 illustrates the general dependence of n on these four parameters: n decreases with increasing wavelength or temperature, and n increases with increasing salinity or pressure.

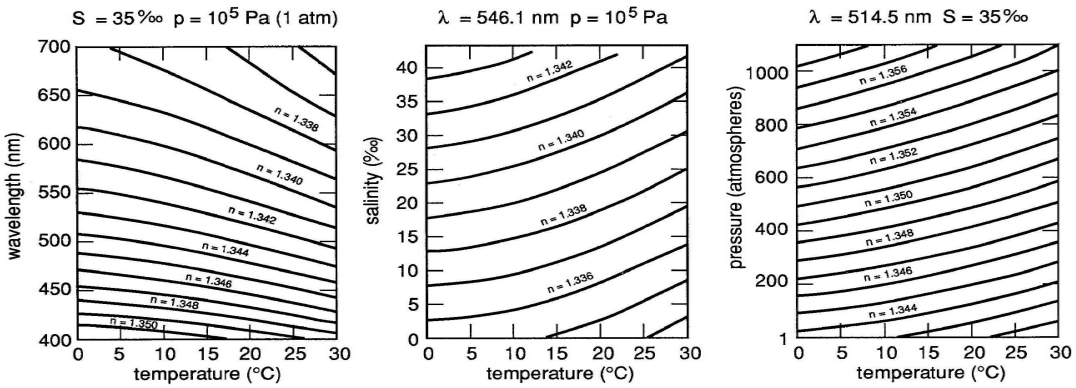

Figure 8: Real index of refraction of water for selected values of pressure, temperature, and salinity.

The extreme values of n obtained from Table.1, 1.329128 and 1.366885, show that n varies by less than 3% over the entire parameter range relevant to hydrologic optics.

The index of refraction of a sample of natural water is also determinated by the presence of particulate matter. The particles found in natural waters often have a

bimodal index of refraction distribution. Living phytoplankton typically have low indices of refraction, in the range 1.01 to 1.09 relative to the index of refraction of pure seawater. Detritus and inorganic particles generally have high indices,1.15 to 1.20 relative to seawater (Jerlov, 1976 cited in Mobley,1994). Typical values are 1.05 for phytoplankton and 1.16 for inorganic particles.

Sea Water (S=35%)

Temp	Wavelength (nm)						
(ºC)	400	450	500	550	600	650	700
0	1.35141	1.34734	1.34442	1.34224	1.34050	1.33911	1.33791
10	1.35084	1.34678	1.34385	1.34167	1.33997	1.33855	1.33738
20	1.34994	1.34586	1.34295	1.34077	1.33904	1.33765	1.33644
30	1.34875	1.34469	1.34179	1.33962	1.33790	1.33649	1.33532

Table 1: Index of refraction of sea water for different wavelengths and temperature at atmospheric pressure

3.2.4. Absorption

Absorption is characterised by the imaginary part of the index of refraction. The spectral absorption coefficient a(λ) is a difficult task to measure in natural waters. Water absorbs only weakly at near-UV and blue wavelengths, so very sensitive instruments are required to measure the real values of the absorption. But the main factor is that the scattering coefficient is never negligible, so the total attenuation value c(λ) is determinated by c(λ)=a(λ) + b(λ). Normally this value is dominated by the scattering coefficient.

The absorption by water itself usually is taken as known, but its value varies with the concentration of different constituents. The highly variable absorption by the constituents of a water body helps connect the optical properties of the water body with its biogeochemical character .

Absorption coefficient is defined as the sum of pure sea water absorption, dissolved yellow matter absorption, phytoplankton absorption and detritus absorption.

3.2.4.1. Absorption by pure sea water.

Smith and Baker (1981) made a careful determination of the upper bound of the a(λ) of pure sea water, $a_w(\lambda)$, in the wavelength range of oceanographic interest, from 200 nm to 800 nm. Their work assumed that for the clearest natural waters, absorption by salt or other dissolved substances was negligible, the only scattering was by water molecules and salt ions, and there was no inelastic scattering. With these assumptions, the inequality (derived from radiative transfer theory)

$$a_w(\lambda) \leqslant K_d(\lambda) - \frac{1}{2} b_{sw}(\lambda)$$

holds. Here $b_{sw}(\lambda)$ is the scattering coefficient of pure sea water and $K_d(\lambda)$ the diffuse

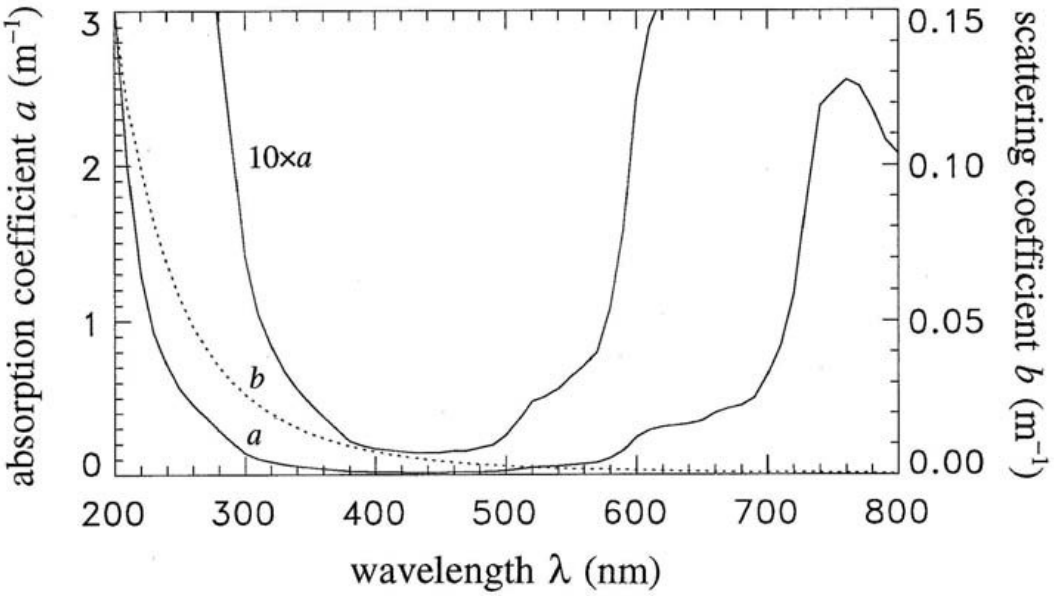

Figure 9: Shows a(λ), solid line, and b(λ), dotted line, of pure sea water.

attenuation function. $b_{sw}(\lambda)$and $K_d(\lambda)$ are taken from the Table.12 from the Appendix A Fig. 9 shows $a_w(\lambda)$ and $b_{sw}(\lambda)$ values.

There is evidence (Pegau and Zaneveld, 1992 cited in Mobley,1994) that absorption by water is weakly dependent on temperature, at least in the red and near infrared and perhaps also slightly dependent on salinity.

3.2.4.2. Absorption by dissolved organic matter

Absorption by yellow matter is modelized by the model (Bricaud, *et al.*, 1981cited in Mobley,1994)

$$a_y(\lambda)=a_y(\lambda_0)\exp(-0.014(\lambda-\lambda_0))$$

over the range 350 nm-700 nm. Here λ_o is a reference wavelength, often chosen to be λ_o=440 nm, and $a_y(\lambda_o)$ is the absorption due to yellow matter at the reference wavelength. The value of $a_y(\lambda)$ of course depends on the concentration of yellow matter in the water. The exponential decay constant depends on the relative proportion of specific types of

Table.13 from the Appendix A gives measured values of $a_y(440)$ for selected waters. Because of the variability in yellow matter concentrations, the values have little general validity even for the particular water bodies sampled, but they do serve to show representative values and the range of influence of yellow matter in determining the total absorption.

3.2.4.3. Absorption by phytoplankton

Phytoplankton cells are strong absorbers of visible light playing a major role in determining the absorption properties of natural waters. Absorption by phytoplankton occurs in various photosynthetic pigments, of which the chlorophylls are best known to nonspecialists. Absorption by chlorophyll itself is characterized by strong absorption bands in the blue and in the red (peaking at λ 430 and 665 nm, respectively, for chlorophyll *a*), with very little absorption in the green. Chlorophyll occurs in all photosynthetic plants, and its concentration in milligrams of chlorophyll per cubic meter of water is commonly used as the relevant optical measure for absorption properties. In practice, the term "chlorophyll concentration" usually refers to the sum of chlorophyll *a*, the main pigment in phytoplankton cells. This sum is often called the "pigment

concentration." Chlorophyll concentrations for various waters range from 0.01 mg m^{-3} in the clearest open ocean waters, to 10 mg m^{-3} in productive coastal upwelling regions, to 100 mg m^{-3} in eutrophic estuaries or lakes. The globally averaged, near-surface, open-ocean value is in the neighborhood of 0.5 mg m^{-3}.

The absorbing pigments are not distributed within phytoplankton cells, they are localized into small "packages", these packages are distributed nonrandomly throughout the cell. This localized distribution of pigments means that the spectral absorption by a phytoplankton cell has less pronounced peaks and so reduced overall absorption than if the pigments were uniformly distributed (Kirk, 1983 cited in Mobley,1994).

A qualitative feel for the nature of phytoplankton absorption can be obtained by measuring some different single-species phytoplankton culture made in laboratoy (Sathyendranath, *et al*., 1987 cited in Mobley,1994). Measured spectral absorption coefficients from different cultures, $a_i(\lambda)$, were first reduced by subtracting $a_i(737)$ to remove the effects of absorption by detritus and cell constituents other than pigments: pigments do not absorb at $\lambda = 737$ nm and that the residual absorption is wavelength independent. The resulting curves were then normalized by the chlorophyll concentrations C_i of the respective cultures to generate the *chlorophyll-specific spectral absorption* curves for phytoplankton, $a_i^*(\lambda)$:

$$a_i^*(\lambda) = \frac{a_i(\lambda) - a_i(737)}{C_i}$$

which are later plotted. One example of this is the Fig.10 where there are 8 different phytoplankton cultures. There are distinct peaks near 440nm and 675nm. There is a little absorption between 550 nm and 600 nm with the minimum near 600 nm 10 % or 30 % of the value at 440nm. There is a considerable variability in the phytoplankton absorption curves, so it is difficult to determinate an exact value for it.

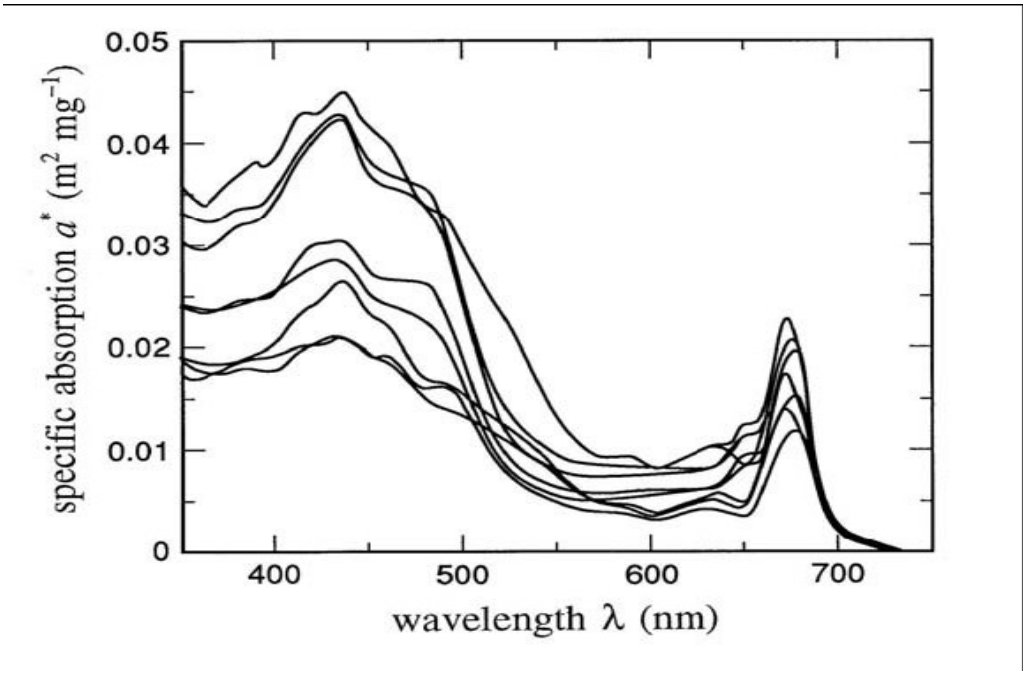

Figure 10: Chlorophyll-specific spectral absorption coefficients for eight species of phytoplankton

3.2.4.5. Absorption by organic detritus.

It is not easy to separate the contributions of living phytoplankton and of the nonliving detritus to the total particulate absorption. To make this some different techniques have been investigated, all of them yield in the same functional form for absorption by detritus, $a_{det}(\lambda)$. Model found by Roesler in 1989:

$$a_{det}(\lambda) = a_{det}(400)\exp(-0.011(\lambda - 400))$$

3.2.4.6. Bio-optical models for absorption

Depending on the concentrations of dissolved substances, phytoplankton, and detritus, the spectral absorption coefficient can range from almost identical to that of pure water to one which shows orders-of-magnitude greater absorption than pure water, especially at blue wavelengths. These great variations can be seen in the Fig. 11

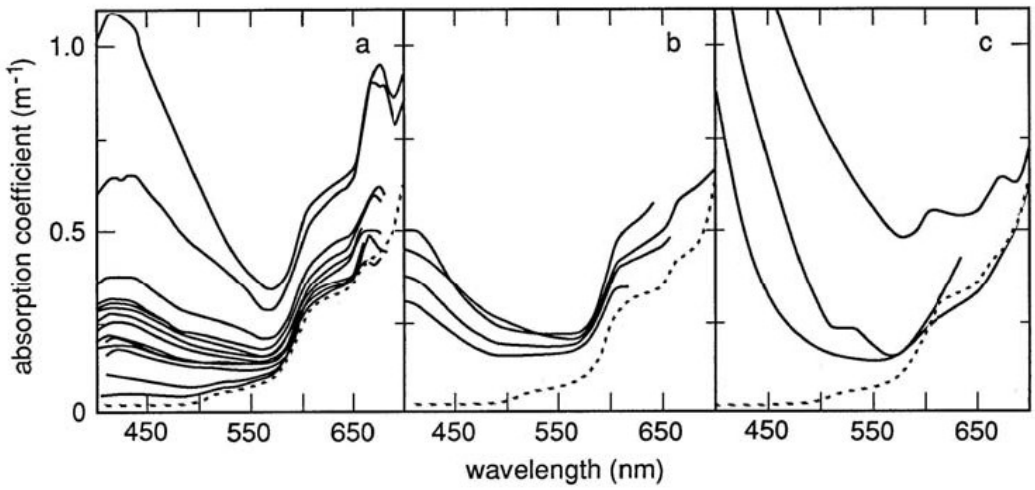

Figure 11: Examples of spectral absorption coefficients a(λ) for various waters. Panel (a) shows a(λ) for waters dominated by phytoplankton, panel (b) is for waters with a high concentration of nonpigmented particles, and panel (c) is for waters rich in yellow matter

Case 1 waters are waters in which the concentration of phytoplankton is high compared to nonbiogenic particles (Morel and Prieur, 1977 cited in Mobley,1994). Absorption by chlorophyll and related pigments therefore plays a major role in determining the total absorption coefficient in such waters,although detritus and dissolved organic matter derived from the phytoplankton also contribute to absorption in case 1 waters. Case 1 water can range from very clear (oligotrophic) water to very turbid (eutrophic) water, depending on the phytoplankton concentration. Case 2 waters are "everything else," namely waters where inorganic particles or dissolved organic matter from land drainage dominate, so that absorption by pigments is relatively less important in determining the total absorption. Roughly 98% of the world's open ocean and coastal waters fall into the case 1 category, so all the bio-optical model are based in this type of waters.

Morel in 1991 based on the bio-optical model for the spectral absorption coefficient of case 1 waters developed by Prieur and Sathyendranath in 1981, made an easier model,

$$a(\lambda)=[a_w(\lambda)+0.06a_c'(\lambda)C^{0.65}][1+0.2\exp(-0.014(\lambda-440))]$$

Here $a_w(\lambda)$ is the absorption coefficient of pure water and $a_c^{*'}(\lambda)$ is a nondimensional, statistically derived chlorophyll-specific absorption coefficient; $a_w(\lambda)$ and $a_c^{*'}(\lambda)$ values are given in Table. 14 from the Appendix A. C is expressed in mg m^{-3} and λ is in nm, the resulting $a(\lambda)$ is in m^{-1}. Figure 12 shows $a(\lambda)$ for various chlorophyll concentrations. The predicted $a(\lambda)$ values are qualitatively similar to the measured $a(\lambda)$ of Fig.11(a), sometimes differ, especially for the higher chlorophyll concentrations.

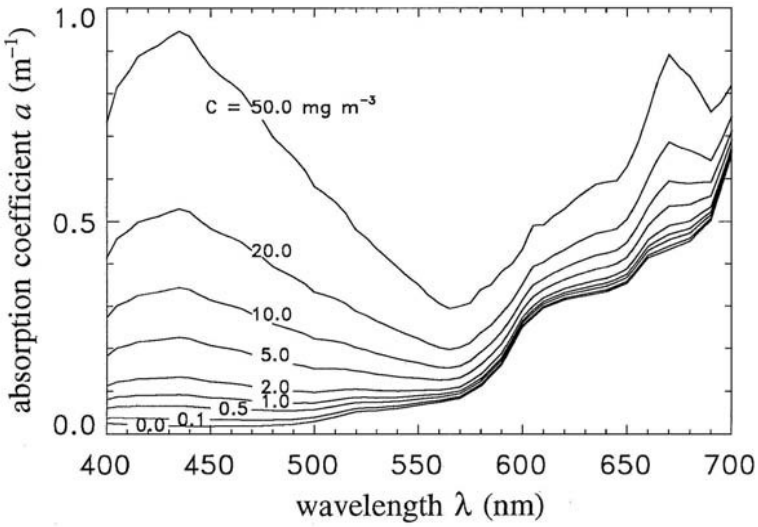

Figure 12: Total spectral absorption coefficient a(λ) for selected chlorophyll concentrations C

3.2.5. Scattering

At the most fundamental all scattering arises from interactions between molecules or atoms and photons. Nevertheless, scattering in natural waters is conveniently viewed as being caused by small-scale ($<<\lambda$) density fluctuations due to random molecular motions, by the ubiquitous large ($>\lambda$) organic and inorganic particles, and by large-scale ($>>\lambda$) turbulence-induced fluctuations in the real index of refraction.

Small-scale scattering determines the minimum values for the scattering, as in the case for absorption, however, the scattering properties of natural waters are greatly modified by the particulate matter that is always present.

3.2.5.1. Scattering by pure sea water

Raman(1922) and Shuleikin (1922) stablished the first fundamental role played by small-scale scattering in natural waters.

Morel in 1974 reviewed the theory about scattering in pure sea water. Random molecular motions give a rise to fluctuations in the number of molecules, changing the scattering effect. In the sea water the basic theory, the random fluctuations in the concentrations of the ions give a change in the index of refraction, so a change in scattering. Based on this assumption Einstein-Smoluchowski theory of scattering gives the following volume scattering function:

$$\beta_w(\psi;\lambda)=\beta_w(90^o;\lambda_0)\left(\frac{\lambda_0}{\lambda}\right)^{4.32}(1+0.835\cos^2\psi)$$

This equation is similar to

$$\beta_{ray}(\psi;\lambda)=\beta_{ray}(90^o;\lambda_0)\left(\frac{\lambda_0}{\lambda}\right)^{4}(1+\cos^2\psi)$$

which is commonly known as Rayleigh scattering. The wavelength dependence $\lambda^{-4.32}$ (rather than λ^4) results from the wavelength dependence of the index of refraction. The 0.835 factor (rather than 1) is attributable to the anisotropy of the water molecules.

The phase function is gives as

$$\beta_w(\psi)=0.06225(1+0.835\cos^2\psi)$$

and the total scattering coefficient is given by

$$b_w(\lambda)=16.06\,\beta_w(90^o;\lambda_0)\left(\frac{\lambda_0}{\lambda}\right)^{4.32}$$

Table 15 from appendix A gives values of $b_w(\lambda)$ and $\beta_w(90^o;\lambda)$. The pure sea water values of scattering are 30% greater than that from pure water, it is because the fluctuations in the concentrations of ions.

The scattering of pure sea water is also called Rayleigh scattering.

3.2.5.2. Scattering by particles

The amount of particles matter in water become the volume scattering function highly peaked in the forward direction and increase the scattering coefficient by at least ten factor.

The contribution of the particulate matter to the total volume scattering function is obtained from

$$\beta_p(\psi;\lambda)=\beta(\psi;\lambda)-\beta_w(\psi;\lambda)$$

where p denotes particles and w water.

Fig. 13 shows several particle volume scattering function determinated in a variety of water type. The particles cause at least four-order-of magnitude increase between $\Psi = 90^o$ and $\Psi = 1^o$. So the main contribution to the scattering from particles is to the forward direction, the rest of scattering angles can be negligible except ar backscattered directions.

Highly peaked forward scattering is characteristic of diffraction-dominated scattering in a polydisperse system. Scattering by refraction and reflection from particle surfaces becomes important at large scattering angles ($\Psi>15^o$).

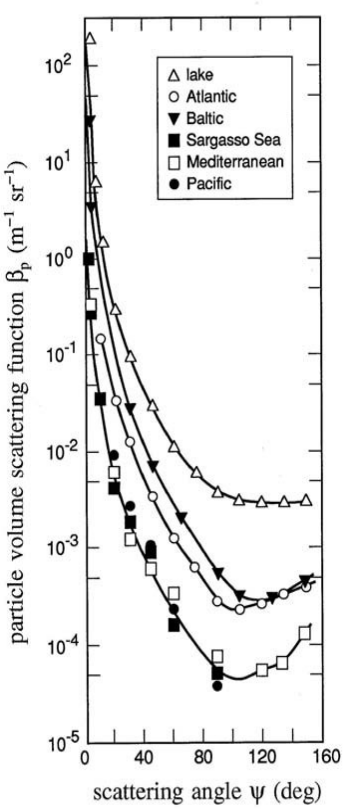

Figure 13: Particle volume scattering functions form various waters

3.2.5.3. Scattering by turbulence

Mie theory predicts that the volume scattering function should flatten out at very small angles. This behavior has been observed for Ψ=1° in laboratory suspensions of polystyrene spheres (Spinrad, *et al*., 1978) but not in natural waters, even for scattering angles less than 0.01°. Evidence indicates that this continued rise in $\beta_w(\Psi)$ Ψ< 1° may be attributed to turbulence. Small temperature and salinity fluctuations occur in natural waters on scales of millimeters and larger. The associated fluctuations in the real index of refraction cause small angular deviations in light rays propagating through the water.

It is possible to know how the size of the turbulence-induced fluctuations in the real index of refraction *n*, as follows. Let us hold pressure *p* and the wavelength λ

constant, so that n is a function only of the temperature T and salinity S. Then taking differentials of $n(T,S)$ gives

$$\Delta n = \left(\frac{\delta n}{\delta T}\right)_S \Delta T + \left(\frac{\delta n}{\delta S}\right)_T \Delta S$$

where ΔT and ΔS are small fluctuations in T and S. If we square the function we will have the average value of the change, if we supposed that they are uncorrelated, S and T, we get

$$\langle (\Delta n)^2 \rangle = \left(\frac{\delta n}{\delta T}\right)^2 \langle (\Delta T)^2 \rangle + \left(\frac{\delta n}{\delta S}\right)^2 \langle (\Delta S)^2 \rangle$$

The root-mean-square value of the index of refraction is $\langle (\Delta n)^2 \rangle^{1/2}$ .The derivatives δn/δT and δn/δS must be evaluated at some particular values, these values are going to be taken from Fig.8. Let us take T=20º and S=35 ‰, lambda=546nm and p=1atm. Then from Fig.8 we will take the corresponding data.

$$\frac{\delta n}{\delta T} \approx \frac{1.3405 - 1.3410}{23ºC - 18ºC} \approx -10^{-4} (ºC)^{-1}$$

and

$$\frac{\delta n}{\delta S} \approx \frac{1.342 - 1.341}{41‰ - 35‰} \approx 2 * 10^{-4} (‰)^{-1}$$

so, supposing that the temperature fluctuations are of magnitude of 0.005ºC and the salinity 0.005 ‰

$$\langle (\Delta n)^2 \rangle^{1/2} = [(10^{-4})^2 (0.005)^2 + (2 * 10^{-4})^2 (0.005)^2]^{1/2} \approx 10^{-6}$$

The turbulence-induced fluctuations in the index of refraction are therefore on the order of parts per million. Such small changes in n are negligible compared to the 5% fluctuation in n when a photon hits a plankton cell with n = 1.05 relative to the water. However, in the case of particle scattering, we envision photons traveling in straight lines between the occasional encounter with a particle, at which time there may be a large change in direction. In the case of turbulence, we envision many turbulent blobs of water, of many sizes, with the photons slightly but continuously changing

direction as they pass through water with a continuously varying index of refraction. It is then possible for the cumulative effect of the turbulent fluctuations to change a photon's direction by a small fraction of a degree. These turbulence-induced deviations manifest themselves in time-averaged scattering measurements as large values at very small scattering angles.

Turbulence-induced scatter can significantly degrade the quality of underwater images. Near the boundary between distinctly different water masses, the fluctuations in *T* and *S* can be much larger than those assumed above, and even still images can be badly degraded. However, turbulence-induced scatter is unimportant in the overall redistribution of radiant energy in lakes and oceans.

3.2.4.5. Wavelength dependence of scattering: Bio-optical model.

The strong $\lambda^{-4.32}$ wavelength dependence seen in point 3.2.5.1 for pure-water scattering is not seen in natural waters. This is because scattering is dominated by diffraction from polydisperse particles which are larger than the wavelength of visible light. Although diffraction depends on the particle size-to-wavelength ratio, the presence of particles of many sizes diminishes the wavelength effects that are seen in diffraction by a single particle. Moreover, diffraction does not depend on particle composition. However, some wavelength dependence is to be expected, especially at backward scattering angles where refraction, and hence particle composition, is important. Molecular scattering also contributes something to the total scattering, and can even dominate the particle contribution at backscatter angles in clear water (Morel and Gentili, 1991 cited in Mobley,1994).

Assuming that $\beta(\psi;\lambda)$ has a wavelength dependence of

$$B_p(\psi;\lambda) = B_p(\psi;546)\left(\frac{546}{\lambda}\right)^n$$

Kopelevich (1983) and Kopelevich and Mezhericher (1983) derived a two parameter model for spectral volume scattering functions. This model separates the contributions by small and large particles to the particulate scattering. Small particles

are taken to be mineral particles less than 1 μm in size and having an index of refraction 1.15 relative to water; large particles are biological particles larger than 1 μm in size and having an index of refraction of $n = 1.03$.

$$B(\psi;\lambda) = B_w(\psi;\lambda) + v_s B_s(\psi)\left(\frac{550}{\lambda}\right)^{1.7} + v_l B_l(\psi)\left(\frac{550}{\lambda}\right)^{0.3}$$

where v_s and v_l are the volume concentrations of small and large particle and $\beta(\psi;\lambda)$ and $\beta(\psi;\lambda)$ the small-particle and large-particle volume scattering function per unit volume concentration of small or large particles.

Integration over ψ of the Kopelevich $\beta(\psi;\lambda)$ model yields a really complex model for $b(\lambda)$:

$$b(\lambda) = 0.0017\left(\frac{550}{\lambda}\right)^{4.3} + 1.34 v_s\left(\frac{550}{\lambda}\right)^{1.7} + 0.312 v_l\left(\frac{550}{\lambda}\right)^{0.3}$$

More easy model have been used than this from Kopelevich. A commonly employed bio-optical model for $b(\lambda)$ is that of Gordon and Morel (1983)

$$b(\lambda) = \left(\frac{550}{\lambda}\right) 0.30 C^{0.62}$$

Here λ is in nm, and C is the chlorophyll concentration in mg m^{-3}. This model includes the contribution of pure water to the total scattering; this contribution is negligible except at very low chlorophyll values. Morel (1991) adds a pure-water term, $b_w(\lambda)$, to the right-hand side of the equation, so that the model gives the correct value at $C = 0$

A related bio-optical model for the total backscattering coefficient $b_b(\lambda)$ is found in Morel (1988):

$$b_b(\lambda) = 1/2 b_w(\lambda)[0.002 + 0.02(1/2 - 1/4 \log C)\left(\frac{550}{\lambda}\right)][0.30 C^{0.62} - b_w(550)]$$

This model explicitly shows the contributions by pure water and by particles. The first factor in brackets in the second term on the right-hand side of the equation

represents the probability of backscatter by a particle; the second factor in brackets is the total scattering by particles. The (½ - ¼log$C$) factor gives the particle contribution a wavelength dependence in very clear (C = 0.01 mg m^{-3}) water and no wavelength dependence in very turbid (C = 100 mg m^{-3}) water.

3.3. Scattering from submerged objects

For submerged targets we have to distinguish between two kind of targets, bigger than the laser beam or smaller than the beam. After this consideration we should bear in mind different parameters from the object that will determine the value of the scattering coefficient, for example shape and composition.

3.3.1. Objects smaller than the beam footprint

3.3.3.1. Surface shape and pointing angle. Reflection theory

When the light hits a target a portion light is reflected with a change in the direction of the beam. The basics of this theory are well known and they are explained in (Tsang el la, 2000). Reflection of light is either specular (mirror-like) or diffuse (retaining the energy) depending on the nature of the interface. The reflected direction is directly related with the surface shape. To illustrate this we are going to use different mirrors (high reflectance) as examples.

When the surface is flat the incident and the reflected angle are the same. We can appreciate this in the following picture.

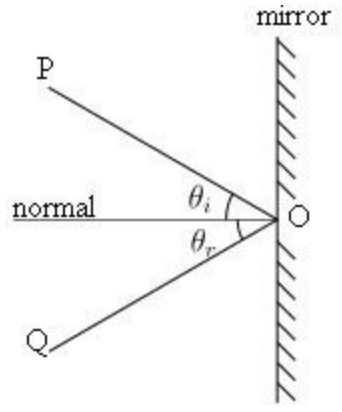

Figure 14: Reflection from a surface

When the surface is curved the situation of the emitter is more important because depending on the reflected angle would be different. We have to compare it with the focus of the curve that the surface describes.

In the following figure we can see some examples. On this figure the light comes from different points and it reachs surfaces with different curvatures.

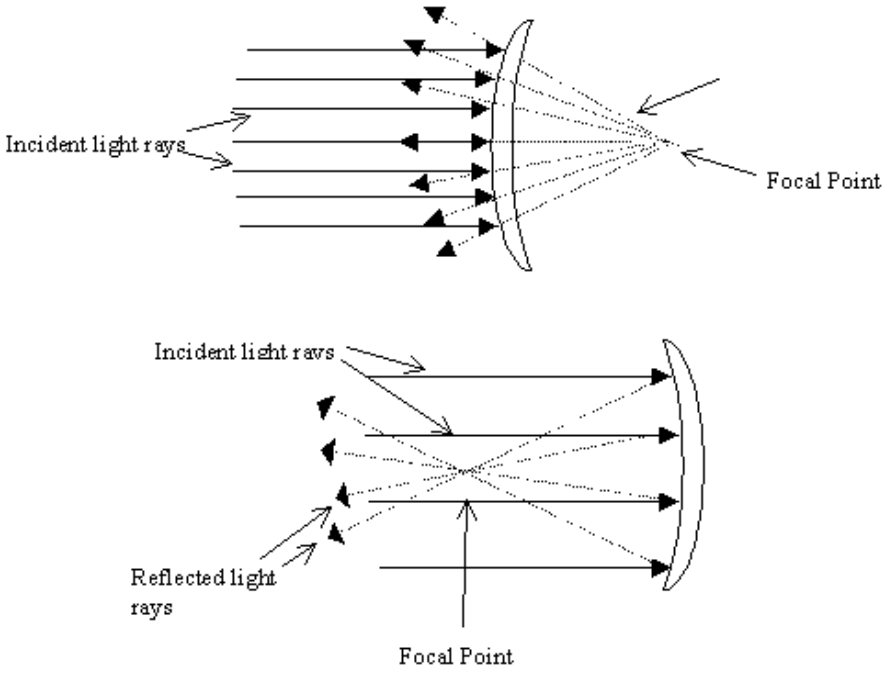

Figure 15: Light reflected from a convex and a diverging mirror

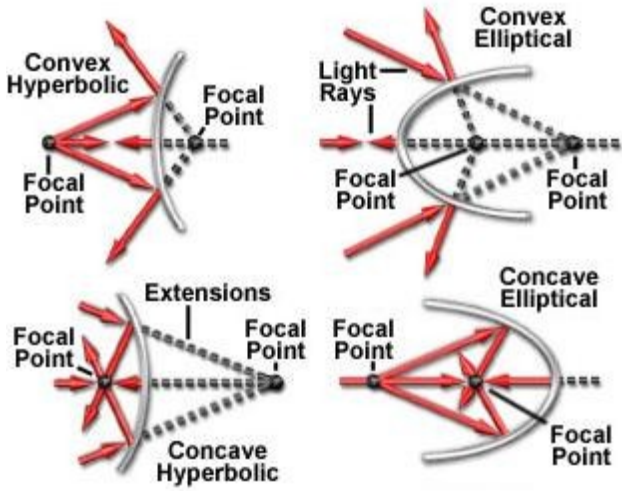

Figure 16: Reflection from different kinds of curvatures

3.3.1.2. Surface roughness

When the surface of the object is not smooth we have to consider the roughness because the scattered light should follow, different directions depending on which part of the rough surface it is the impact. To measure this effect we can use the Kirchoff's law(Tsang et la, 2000).

It generalizes the concept of emissivity. To the case where due to a rough surface and volume inhomogeneities bistatic scattering appears.

If we have a plane wave with polarization α and the scattering medium has an area A. The power scattered into the upper hemisphere is equal to

$$\sum_{\beta=v,h} \int_{upper\ hemisphere} r^2 \frac{1}{2\eta} \left| E_{\beta_s}{}^2 \right| d\,\Omega_S$$

and the absorbed power by the surface is: one minus the power backscattered into the upper hemisphere. This is the absorptivity of the surface.

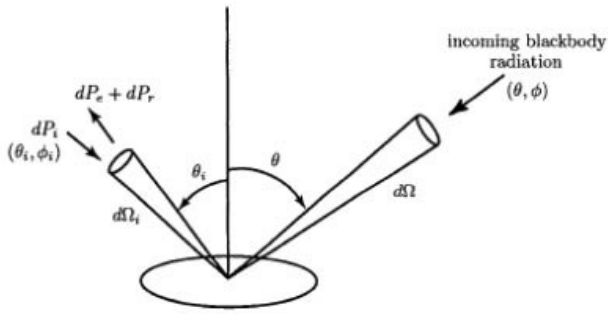

Figure 17: Geometry for derivaton os Kirchoff's law.

This law describes the relation between the emissivity and the absorptivity of the body. The body must be in temperature equilibrium with the blackbody as shown in Fig.17.

$$a_\alpha(\theta_i, \phi_i) = 1 - \frac{\sum_{\beta=v,h} \int_0^{\pi/2} d\theta_s \sin\theta_s \int_0^{2\pi} d\phi_s \, r^2 |E_{\beta s}|^2}{|E_\alpha^i|^2 A \cos\theta_i}$$

$$= 1 - \frac{1}{4\pi} \sum_{\beta=v,h} \int_0^{\pi/2} d\theta_s \sin\theta_s \int_0^{2\pi} d\phi_s \, \gamma_{\beta\alpha}(\theta_s, \phi_s; \theta_i, \phi_i)$$

The power incident on the surface with polarization β is

$$dP_i = \frac{KT}{\lambda^2} d\Omega_i \, A \cos\theta_i \, d\nu$$

The power that leaves the surface is the sum of the following two terms

$$dP_e = e_\beta(\theta_i, \phi_i) \frac{KT}{\lambda^2} \cos\theta_i \, A \, d\Omega_i \, d\nu$$

that is the thermal emission from the surface, and the second one is the radiation that arrives from all directions and is described by the bistatic scattering coefficients coefficients. Thus, the power scattered into solid angle $d\,\Omega_i$ with polarization β is

$$dP_r = \int_{\substack{\text{upper}\\ \text{hemisphere}}} \frac{KT}{\lambda^2} d\Omega \cos\theta A \left\{ \gamma_{\beta v}(\theta_i, \phi_i; \theta, \phi) + \gamma_{\beta h}(\theta_i, \phi_i; \theta, \phi) \right\} \frac{1}{4\pi} d\Omega_i \, d\nu$$

Since the body is in thermodynamic equilibrium with the half-space above, we have

$$dP_i = dP_e + dP_r$$

So we have

$$1 = e_\beta(\theta_i, \phi_i) + \frac{1}{4\pi} \int_{2\pi^+} d\Omega \frac{\cos\theta}{\cos\theta_i} \left[\gamma_{\beta v}(\theta_i, \phi_i, \theta, \phi) + \gamma_{\beta h}(\theta_i, \phi_i, \theta, \phi) \right]$$

and using a reciprocity relation we get

$$e_\beta(\theta_i, \phi_i) = 1 - \frac{1}{4\pi} \sum_\alpha \int_0^{\pi/2} d\theta \, \sin\theta \int_0^{2\pi} d\phi \, \gamma_{\alpha\beta}(\theta, \phi; \theta_i, \phi_i)$$

this expression calculates the emissivity from the bistatic scattering coefficient γ. Finally we can state some conclusions that are extracted from this formula.

1. In the absence of rough surface and volume inhomogeneities, there is no backscattering. Thus monostatic measurements in active remote sensing directly measures the effects of the scattering by random media. For passive remote sensing, one measures the emissivity which has a finite result even when there is no rough surface or no volume scattering. Thus rough surface and volume scattering gives a differential change (which can be small) from the flat surface homogeneous medium emissivity.
2. Active remote sensing often measures only the backscattered light. That requires a good solution of $\gamma_{\alpha\beta}$ for 2π solid angle scattering directions with a further stringent requirement of deriving a net difference from the reflectivity of a flat surface.
3. The derivation of the last expression requires reciprocity and energy conservation. Thus when this expression is used to get emissivity, the solution of

$\gamma_{\alpha\beta}$ should obey energy conservation and reciprocity. This is important when $\gamma_{\alpha\beta}$ is only an approximate solution to the scattering problem.

3.3.1.3. Surface molecular and electronic structure

Another parameter that determines the portion of backscattered light is the composition of the object. More specifically composition of the surface. A surface will scatter more or less light depending on the colour of the surface (this can be seen in the section 5 when the colour of the houses is analysed). The extreme cases are the colours black and white. The white one reflects every wavelength of the visual spectrum, while the black one absorbs all the wavelengths of the same spectrum. In the following table the wavelengths that reflects each colour are shown.

Color	λ/nm	$\nu/10^{14}$ Hz	$\nu_b/10^4$ cm^{-1}	E /eV	E/kJ mol^{-1}
Infrared	>1000	<3.00	<1.00	<1.24	<120
Red	700	4.28	1.43	1.77	171
Orange	620	4.84	1.61	2.00	193
Yellow	580	5.17	1.72	2.14	206
Green	530	5.66	1.89	2.34	226
Blue	470	6.38	2.13	2.64	254
Violet	420	7.14	2.38	2.95	285
Near ultraviolet	300	10.0	3.33	4.15	400
Far ultraviolet	<200	>15.0	>5.00	>6.20	>598

Table 2: Colour, wavelength, frequency and energy of light

Independently of the colour, there is another important factor that determines how much light is backscattered. For example the fish scales reflect the light in a peculiar way due to the electronic proccess that take place over the surface between the incident light and the scales.(Hjelmstad, 2009).

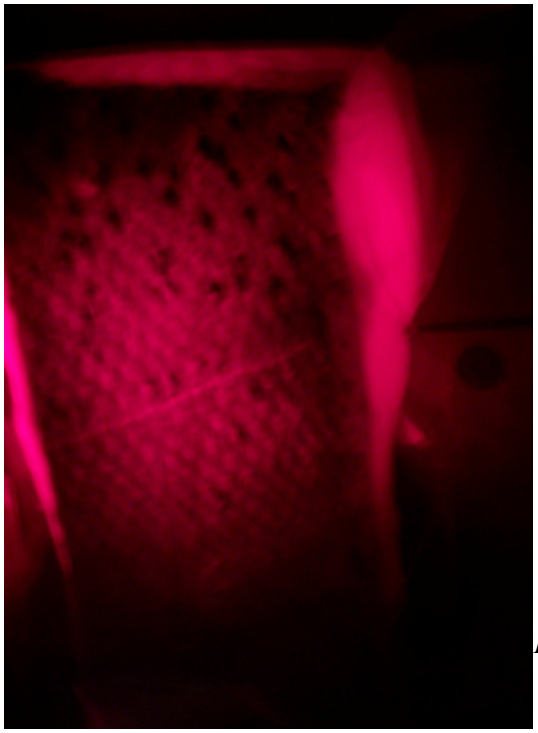

Figure 18: Different reflection of fish scales

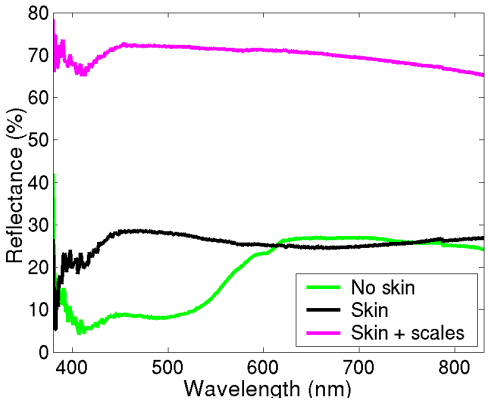

Figure 19: Different values of Reflectance for fish surface

3.3.2. Objects bigger than the beam footprint

For this kind of objects we need to make considerations about comparing the wavelength with the size of the object. We are going to distinguish between sizes bigger, equal or smaller than the wavelength.

3.3.2.1. Object bigger than the wavelength

If the object is too big the geometric optic about ray trajectory is predominant. So the behaviour is basically the one described in 3.3.1.

3.3.2.2. Object with a size similar to the wavelength

When the object has a size similar to the wavelength the Mie scattering is predominant. This scattering produces a pattern like an antenna lobe, with a sharper and more intense forward lobe for larger particles.

Mie scattering is not strongly wavelength dependent and produces the almost white glare around the sun when a lot of particulate material is present in the air. It also gives us the the white light from mist and fog.

We are not going to explain so much about this scattering because, due to the presence of molecules in the air that are in this range of size this scattering was already explained in section 3.1.

3.3.2.3. Object smaller than the wavelength

When the object is quite small we are in the Rayleigh scattering zone. This scattering was also explained before in the section about the light propagation in the air. Because of this we are just going to remember the main characteristics (Hjelmstad, 2009).

It is Rayleigh scattering of the molecules of the air which gives us the blue sky. Lord Rayleigh calculated the scattered intensity from dipole scatterers much smaller than the wavelength to be:

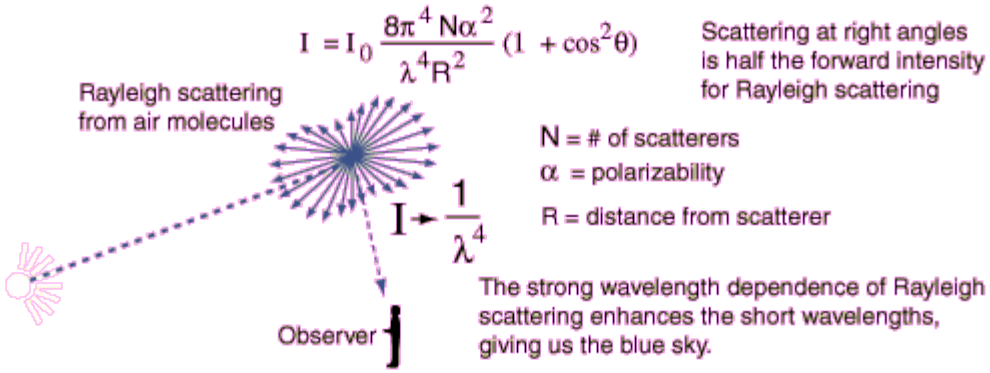

Figure 20: Rayleigh scattering

Rayleigh scattering can be considered to be elastic scattering since the photon energies of the scattered photons is not changed.

Chapter 4

Lidar System Model

The lidar system model will be a mix between some different theories and each equations and models. The core of our model is going to be the Lidar Equation, it is used to measure the received power from a scatter at distance R, the received strength depends on the target characteristics; shape, reflectivity and dimensions, on the lidar setup values and on the absorption and scattering from our transmission medium. These values will be calculated using the theory of Chaper 3. There are different values for water and air, so different models are used.

Our aim is to know how long and how deep the lidar can detect a target using oblique incident beams. Between the sea surface and air, there is a discontinuity, therefore one part of the incident power is going to be reflected again to the air and other part is going to be transmited to the water. To modelize this problem Fresnel´s equation and Snell´s law will be used.

Lidar Equation, Fresnel´equation and Snell´s law are described in the following section, which will summarize our model.

4.1. Lidar equation

Lidar equation and its definition has been extracted from Weitkamp in 2005.

The simplest form to define lidar equation is given by:

$$P(R) = KG(R)\beta(R)T(R),$$

P(R), the power P received from a distance R is made up of four factors. The first factor, *K* describes the performance of the lidar system, the second, *G(R)*, summarizes the range-dependent measurement geometry. These two factors are completely determined and controlled by the user. The transmission properties and backscattering coefficients on the air and on the sea water are contained in the last two factors . The term β (R) is the backscattering coefficient at distance *R*. *T (R)* is the transmission term and describes how much light gets lost on the way from the lidar to distance *R* and back.

The performance of the system can be defined like,

$$K = P_0 \frac{c\tau}{2} A\eta$$

P_0 is the average power of a single laser pulse, and τ is the pulse length. Hence $E_0 = P_0\tau$ is the pulse energy. The term cτ is the length of the volume illuminated by the laser pulse at a fixed time. The factor 1/2 appears because of an apparent folding of the laser pulse through the backscatter process. When the lidar signal is detected at an instant time *t* after the leading edge of the pulse was emitted, backscattered light from the leading edge of the pulse comes from the distance $R_1=ct/2$**.** at the same time, light produced by the trailing edge arrives from distance $R_2=C(t-\tau)/2$**.** Thus $\Delta R= R_1 - R_2= ct/2$ is the length of the volume from which backscattered light is received at an instant time and is called the effective pulse length. *A* is the area of the primary receiver optics responsible for the collection of backscattered light, and η is the overall system efficiency. It includes the optical efficiency of all elements the transmitted and received light has to pass and the detection efficiency. The telescope area *A* and the laser energy E_0, or, rather, the average laser power $P = E_0\ PRF$**,** with the pulse repetition frequency PRF, are primary design parameters of a lidar system. The users will also try to optimize

the overall system efficiency η to obtain the best possible lidar signal. The aim of the experimentalist is to achieve a system efficiency of one, so no losses will be

The geometric factor

$$G(R) = \frac{O(R)}{R^2}$$

includes the laser-beam receiver-field of view overlap function *O(R)* described before and the term R^{-2} . The quadratic decrease of the signal intensity with distance is due to the fact that the receiver telescope area makes up a part of a sphere's surface with radius *R* that encloses the scattering volume . If we imagine an isotropic scatterer at distance *R*, the telescope area *A* will collect the fraction of the overall intensity I_S

$$\frac{I_C}{I_S} = \frac{A}{4\pi R^2}$$

Scattered into the solid angle 4π. In other words, the solid angle A/R^2 is the perception angle of the lidar for light scattered at distance *R*. The factor 4π does not appear explicitly in the lidar equation because it is canceled out by the definition of the backscatter coefficient. It is primarily the R^{-2} dependence that is responsible for the large dynamic range of the lidar signal. If we start detecting a signal with *O(R)*=1 at a distance of 100m. the signal will be 6 orders of magnitude lower at 100km distance just because of the geometry effect. So lidar is a *range-resolving and remote* measurement technique. Geometrical signal compression at short distances is one possibility as can be seen from Fig.21 in which an arbitrary, but realistic overlap function is shown, multiplied with the function R^{-2} . The strong signal in the near field is suppressed by several orders of magnitude. On a few occasions the atmosphere will help in compressing the signal by an increase of the backscattering at larger distances as we will see below. In most cases, however, the atmosphere causes an additional decrease of the signal with range.

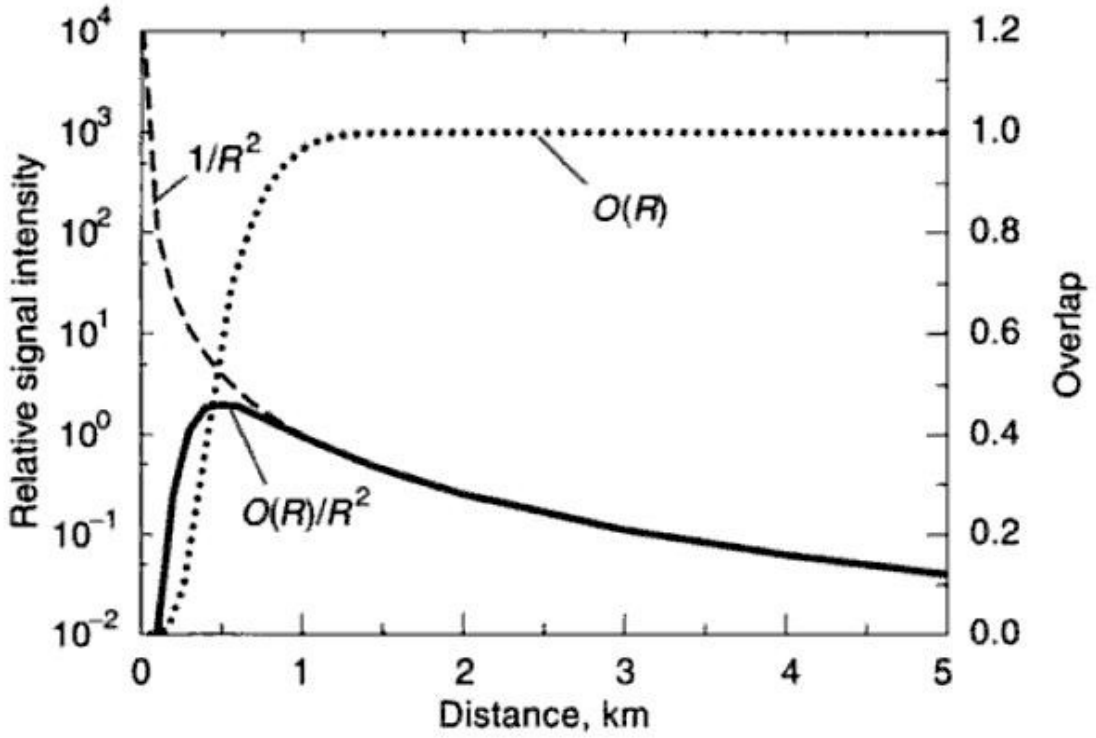

Figure 21: Geometric factor

The backscatter coefficient β (*R,λ*) is the primary parameter that determines the strength of the lidar signal, so the attenuation. It describes how much light is scattered into the backward direction. The backscatter coefficient is the specific value of the scattering coefficient for the scattering angle θ = 180º.

The final part of the lidar equation, we have to consider the fraction of light that gets lost on the way from the lidar to the target and later coming back to the detector. The transmission term *T(R)* can take values between 0 and 1 and is given by this term results

$$T(R,\lambda) = \exp\left[-2\cdot\int_0^R \alpha(r,\lambda)\cdot dr\right]$$

From the specific form of the Lambert-Beer-Bouguer law for lidar. The integral considers the path from the lidar to distance *R*. The factor 2 is the two-way transmission path. The sum of all transmission losses is called light extinction, and α(R,λ) is the

extinction coefficient or attenuation coefficient. It is defined as the product of number concentration and extinction cross section $\sigma_{j,ext}$ for each type of scatterer j, extinction can occur because of scattering and absorpion of light

$$\alpha(r,\lambda) = \sum_j N_j(R)\sigma_{j,ext}(\lambda)$$

By molecules and particles. The extinction coefficient therefore can be written as the

$$\alpha(R,\lambda) = \alpha_{mol,sea}(R,\lambda) + \alpha_{mol,abs}(R,\lambda) + \alpha_{aer,sea}(R,\lambda) + \alpha_{aer,abs}(R,\lambda)$$

of four components, where the indices sca and abs stand for scattering and absorption, respectively. Because scattering into all directions contributes to light extinction, the (integral) scattering cross section α_{abs}, both in m^2, make up the extinction cross section,

$$\sigma_{ext}(\lambda) = \sigma_{sea}(\lambda) + \sigma_{abs}(\lambda)$$

Consequently, the extinction coefficient has the unit m^{-1}.

As indicated in the equations above, both β and α depend on the wavelength of the laser light. This wavelength dependence is determined by the size, the refractive index, and the shape of the scattering particles.

Summarizing the discussion of the individual terms, we can write the lidar equation as

$$P(R,\lambda) = P_o \frac{c\tau}{2} A\eta \frac{O(R)}{R^2} \beta(R,\lambda) \exp\left[-2\int_0^R \alpha(r,\lambda)dr\right]$$

This equation will be the core of our model. Apart from the signal detected from the target, we should mention that the detected signal will always consist of a background contribution P_{bg} in addition to the lidar signal described above. At daytime, the background signal is dominated by direct or scattered sunlight, whereas at nighttime the moon and the stars as well as artificial light sources contribute to the background light. Detector noise is another source of undesired signal. The background must be subtracted before a lidar signal can be evaluated further.

4.2. Snell´s law

Snell's law is a equation used to describe the relationship between the angles of incidence and refraction when an electromagnetic wave, such light, passes through a boundary between two different isotropic media, i.e water and air. The law says that the ratio of the sines of the angles of incidence and of the refraction is a constant that depends on the media.

Snell's law states that the ratio of the sines of the angles is equivalent to the ratio of speed in the two media, or equivalent to the opposite ratio of the indices of refraction:

Supposing that we have two different medium with two different refraction index, like n_1 and n_2, which will have two different electromagnetic speed v_1 and v_2, the relationship between sines can be defined like this,

$$\frac{\sin(\theta_1)}{\sin(\theta_2)} = \frac{v_1}{v_2} = \frac{n_2}{n_1}$$

where θ_1 and θ_2 are the different angles of the media.

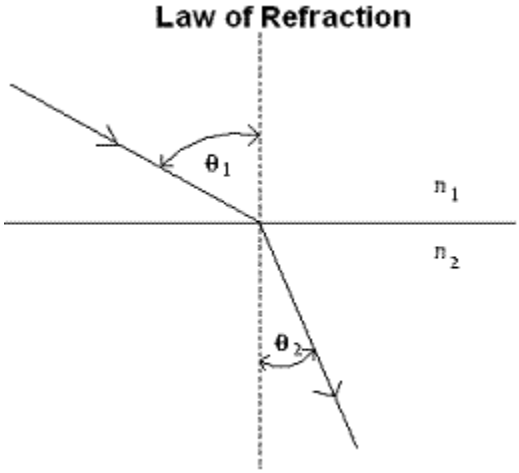

Figure 22: Snell Law

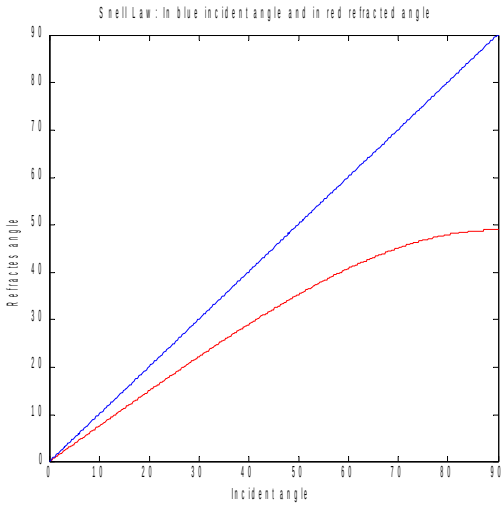

Figure 23: Shows how the refracted angle changes in funtion of incident angle

Some parts of the incident power is refracted to the second media, but the other part is going to be reflected. The reflected angle is the same that incident angle.

$$\theta_{reflected} = \theta_{incident}$$

4.3. Fresnel Equations

In the previous section we have explained that when an electromagnetic wave passes a boundary layer between two different medium, some part of the incident power is refracted and other part is reflected. Snell´s law calculates the reflected and refracted angle depending on the incident angle. Now with Fresnel equation we are going to calculate how much power of the incident wave is going to be reflected and how much is going to be refracted or transmitted to the second medium.

The fraction of the incident power that is reflected from the interface is given by R, reflectance and the fraction that is refracted or transmitted is given by transmittance T. The calculations of R and T depend on the polarisation of the incident ray. If the light is polarised perpendicular to the incident plane, the reflection coefficient is:

$$R_{perpendicular} = \left[\frac{\sin(\theta_t - \theta_i)}{\sin(\theta_t + \theta_i)}\right]^2 = \left(\frac{n_1 \cos\theta_i - n2cos\,\theta_t}{n_1 \cos\theta_i + n2cos\,\theta_t}\right)^2$$

If the incident light is polarised parallel to the incident plane, the reflection coefficient is

$$R_{paralel} = \left[\frac{\tan(\theta_t - \theta_i)}{\tan(\theta_t + \theta_i)}\right]^2 = \left(\frac{n_1 \cos\theta_t - n2cos\,\theta_i}{n_1 \cos\theta_t + n2cos\,\theta_i}\right)^2$$

The transmission coefficien in each case is given by $T_{perpendicular}=1-R_{perpendicular}$ and $T_{parallel}=1-R_{parallel}$.

If the incident light is unpolarised (containing an equal mix of parallel and perpendicular polarisations), the reflection coefficient is $R=(R_{parallel}+R_{perpendicular})/2$.

In our case, the polarization is parallel to the incident plane so, we are going to use $T_{parallel}$ and $R_{parallel}$. Fig.24 shows the values of reflectance and tranmistance for the possible incident angles.

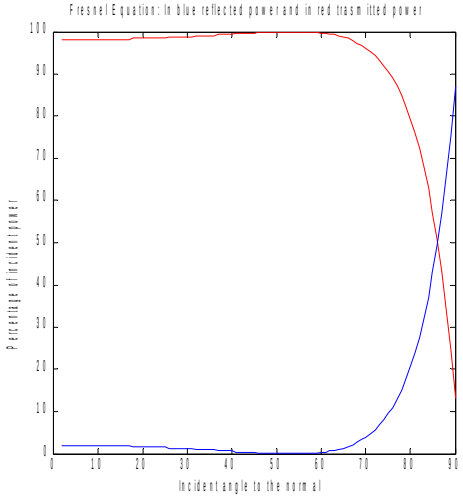

Figure 24: Fresnel equations, angles due to the normal

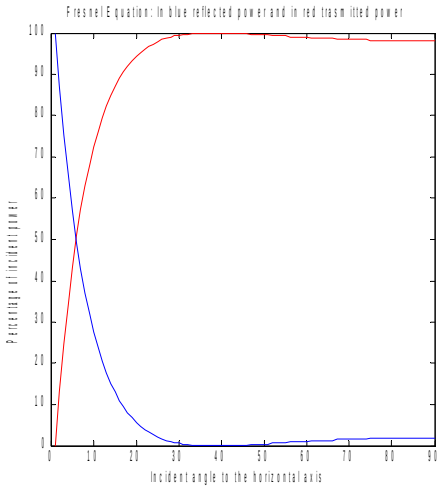

Figure 25: Fresnel equations, angles due to the horizontal

We are going to use the incident angle to the horizontal axis so the Fig.25 is the good one for us.

4.4. Model

As we have mentioned previously our model is based on Lidar Equation, Fresnel Equation and Snell´s Law (to achieve the transmitted and reflected angles). We are going to distinguish the model in two different part depending on the path of the laser pulse. The first part, it goes from the sender until sea surface. The second one, the path from the discotinuity between air and water. This last part will be divided in two different subparts, one where the light is transmitted in the water and the other one the part reflected. In all parts we have to take in care the noise.

4.4.1. Air transmission before the discontinuity

The model in this part is only based on the Lidar Equation, so the power received from a distance R of a scatter is:

$$P(R)=K\ G(R)\,B_{air}(R)\,T_{air}(R)+n(R)$$

Later in this chapter the different especific values will be explained and determinated.

4.4.2. Air tranmission after the discontinuity

Once the light ray arrives to the boundary layer between air and water, one part of the signal will be reflected and the other part is going to be tranmitted to the water. In this point we will focus in the reflected part. The received power also follows the lidar equation theory, but the discontinuity caused that only some of the incident power to be reflected, this quantity is defined by the reflectance term, R, in our model to distinguish from the distance R, it is going to present as Γ_{ref} .As we have seen before, the reflentance is calculated using Fresnel´s equations. The reflected angle is the same one to the incident angle.

$$P(R)=K\ G(R)\,B_{air}(R)\,T_{air}(R)\,\Gamma_{ref}+n(R)$$

4.4.3. Water transmission after the discontinuity.

In the previous point we have said that the incident power is divided when the ray arrives to the boundary layer. For us the most important one is the power transmitted to the water where our target must be detected. In water different values of absorption and different scattering effects appears. These values will limit our model. The power received from a distance R can be defined in the following way:

$$P(R)=K\ G(R)\,B(R)\,T_{air}(R_{air})\,T_{wat}(R_{wat})\,\Gamma_{trx}+n(R)$$

where;

R: The total distance from the sender to the scatter. It is divided in the distance done in the air, and the distance done in the water.

B(R): It is the backscattering value from distance R, if we don´t have an object the value will be the backscattering value of sea water and if we have a target it will be its value.

$T_{air}(R_{air})$: The transmission loss of the air.

$T_{wa}t(R_{wat})$: The transmission loss of the water.

Γ_{trx}: The transmittance value, it is calculated using Fresnel´s equations.

Once the model has been described, we are going to discussed about the especific values of backscattering and tranmission loss of different medium.

4.5. Backscattering and transmission loss coefficients

We are going to divide the scattering and the transmission loss in two different main groups; air and water.

4.5.1. Backscattering in the air.

In our specific case we will be all the time near the sea surface, so it can be done an approximation and say that the backscattering coefficient is going to be equal for all the range from the sender to the sea surface. As we have explained in the section.... this value is going to be defined as:

$$\beta_m = 1.39\left[\frac{550}{\lambda(nm)}\right]^4 \times 10^{-8} cm^{-1} sr^{-1}$$

4.5.2. Transmission loss coefficients.

To modelize the transmission loss of the air, we have taken a table from Laser Radar Systems book where different values are shown depending on the weather conditions. These values are shown in the following table.

Attenuation (dB/km)	Weather conditions
0,2	Extremely clear
0,5	Standard clear
1	Clear
1,7	Light haze
2,8	Medium haze
5,2	Haze
5,5	Medium rain
9	Light fog

Table 3: Different attenuations depending on the weather

4.5.3. Transmission loss in water

In section 3.2 we have described all the parameters that affect the scattering and absorption coefficient. So the transmission loss or the extinction coefficient are estimated with the following expression.

4.5.3.1. Absorption coefficient

So based on the different absorption sources, we have decided to follow the bio-optical model of Morel:

$$a(\lambda)=[a_w(\lambda)+0.06a_c'(\lambda)C^{0.65}][1+0.2\exp(-0.014(\lambda-440))]$$

Here $a_w(\lambda)$ is the absorption coefficient of pure water and $a_c^{*\prime}(\lambda)$ is a nondimensional, statistically derived chlorophyll-specific absorption coefficient; $a_w(\lambda)$ and $a_c^{*\prime}(\lambda)$ values are given in Table.x from the appendix A. C is expressed in mg m^{-3} and λ is in nm, the resulting $a(\lambda)$ is in m^{-1}

For our specific laser, λ is 532nm so the following values are chosen,

$a_w(\lambda)=0.052$.

$a_c^{*\prime}(\lambda)=0.468$.

therefore, the total absorption coefficient depends only on the chlorophyll concentration.

4.5.3.2. Scattering coefficient

In the same way that we have done in the previous section we are going to use the Morel model to define scattering coefficient.

$$b(\lambda)=(\frac{550}{\lambda})0.30C^{0.62}+b_w(\lambda)$$

where $b_w(\lambda)$ is taken from Table x on the appendix A.

The total extinction coefficient is the sum of the both coefficient.

4.5.4. Backscattering in water.

Also Morel distribution is used to calculate its values,

$$b_b(\lambda)=1/2b_w(\lambda)[0.002+0.02(1/2-1/4\log C)(\frac{550}{\lambda})][0.30C^{0.62}-b_w(550)]$$

In the same way that the previous approximation this one is also dependence on the chlorophyll concentration, therefore, in the following section how this profile has been simulated is explained.

4.5.5. Chorophyll concentration profile.

Chlorophyll profiles are often well approximated as a background value plus a Gaussian, so the profile can be defined by (Mobley, 1994)

$$C(z)=C_0+\frac{h}{s\sqrt{2\pi}}\exp(-\frac{1}{2}(\frac{z-z_{max}}{s})^2)$$

The parameters C_0,h,s, and z_{max} vary a lot with time and location. These values will be defined by the user. Example,

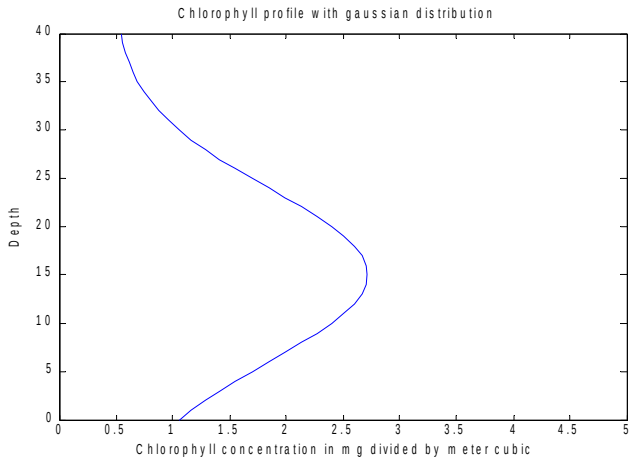

Figure 26: Shows chlorophyll profile with C_0=0.5 s=9 h=50 z_{max}=15

4.6 . The sea surface

The sea surface varies a lot of depending on the weather conditions and enviromental conditions. The sea surface is going to be composed of waves. In our model the waves will be represented by a sine, they are going to be defined by an amplitude and a wavelength. So, the surface will be expressed in the following way:

$$Wave_{value}(x) = A * \sin\left(\frac{2 * pi}{\lambda} * x\right) \quad (m)$$

The value will be the height of the water wave at distance x, measured in meters.

As has been mentioned before the amplitude and the wavelength will define our sea surface, and also they will be the limiting factors for our model.

The laser pulse will be shot with different angles to find which will be the limits for its use to detect the surface, a submerged target and the sea bottom. These limits depend on the sea surface, because with a wave the angle of incident of the ray will

change, so the values for the Snell´s law will change, therefore, the Fresnel equation´s values will change and also the detecting position will change. So how the surface is a really important parameter.

In our theoretical model two different kind of sea have been implemented. The first one and the easiest one, is a plane sea surface, where there are not amplitude variation along the tracking path and as it is possible to see in the following image, for a tracking of different angles, the tracking will be continuous, hence all the sea can be scanned.

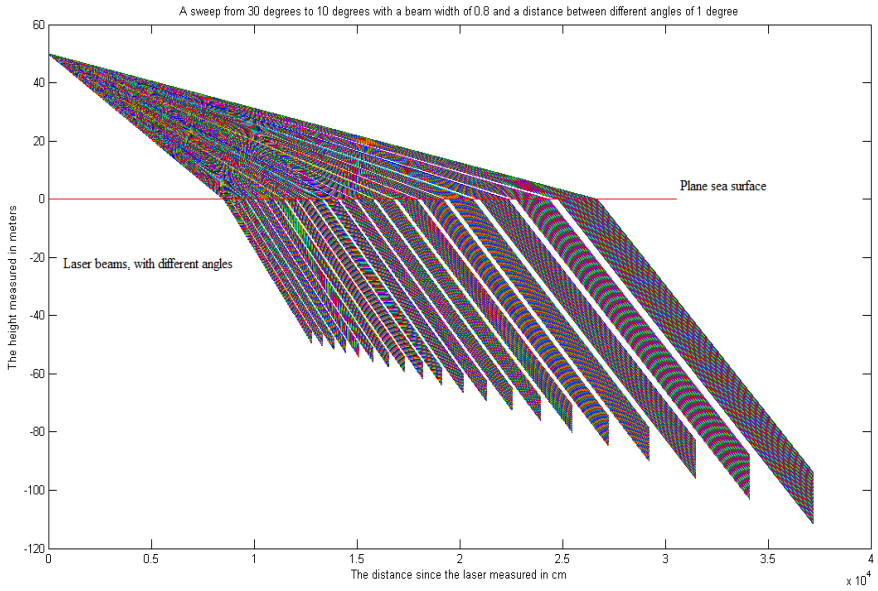

Figure 27: Different sweeps over plane sea

It is possible to see that with a plane sea surface all the area can be scanned and how the beam when the incident angle is increasing the beam width increased and for a single angle more surface is scanned, so our system is less effective.

The second implementation and more realistic one to simulate the real sea is to represent it like a sine. The different conditions for the weather are described by the amplitude and the wavelength. In this kind of sea some problems appears, these problems are connected with the wavelength and its amplitude. The problem appears

when the slope of the wave in modulo is bigger than the slope of the light ray. The slope of the wave is calculated using the derivative of the function, the derivation obtained is,

$$\frac{dWave}{dx} = \frac{A*2*pi}{\lambda} * \cos(\frac{2*pi}{\lambda} * x)$$

The maximum slope is achieved when the cos is in modulo 1, so the maximum slope will be in function of the amplitude and the lambda,

$$\frac{dWave}{dx}_{max} = \frac{A*2*pi}{\lambda}$$

The laser ray´s slope can be calculated with the tangent of the angle,

$$m = \tan(\theta_{inci})$$

As said previously the problem appears when the slope of the wave is bigger than the slope of the laser ray. It is only a problem if the wavelength of the wave is smaller than the laser beam width. Because, the laser width will hit several different points of different waves and there will be parts of the sea that they are not going to be scanned. This assumption is clearly explained in the following figures. In all the figures the used amplitude and wavelength will be the same, in these examples the amplitude chosen is 0.5 meters and the wavelength chosen is 5 meters. So if this values are applied in the derivation of the wave, the maximum slope will be,

$$\frac{dWave}{dx}_{max} = \frac{A*2*\pi}{\lambda} \quad |A = 0.5 \wedge \lambda = 5|$$

$$\frac{dWave}{dx}_{max} = \frac{\pi}{5} = 0.628231$$

As has been mentioned before the slope of the ray must be bigger than once from the wave, therefore, the critical angle will be,

$$(\theta_{cric}) = \arctan(m) \quad |m = 0.628231|$$

$$(\theta_{cric}) = 32.1419^{o}$$

In the first images, it can be seen a ray with a smaller beam width than the wavelength and a slope bigger than once from the wave. For this example they have been used this parameters incident angle of 35º and beam width of 1º, this beam width is smaller than the wavelength.

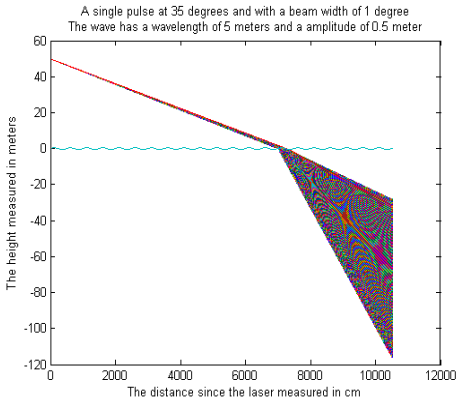

Figure 29: Laser beam with bigger slope and smaller beam width than the wave

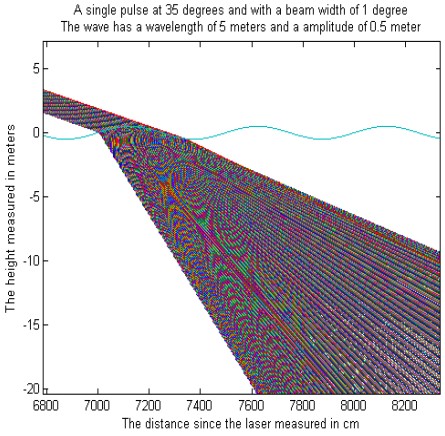

Figure 28: Zoom of Figure 29

While the beam angle is bigger than the critical angle, there is not problem. It does not matter if the beam width is bigger or smaller than the wavelength of the wave as is shown in Fig.30. It will be possible to scan all the sea volume.

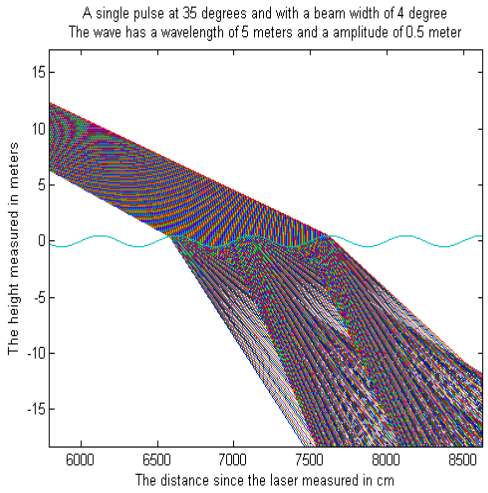

Figure 30: Laser beam with slope and beam width bigger than wave

But once that our angle is smaller to the critical angle, the real problem appears. The whole surface it is not going to be scanned and there will appear some blind zone, so maybe the detection of some target is not going to be possible. In the following figure this effect is going to be clearly understood.

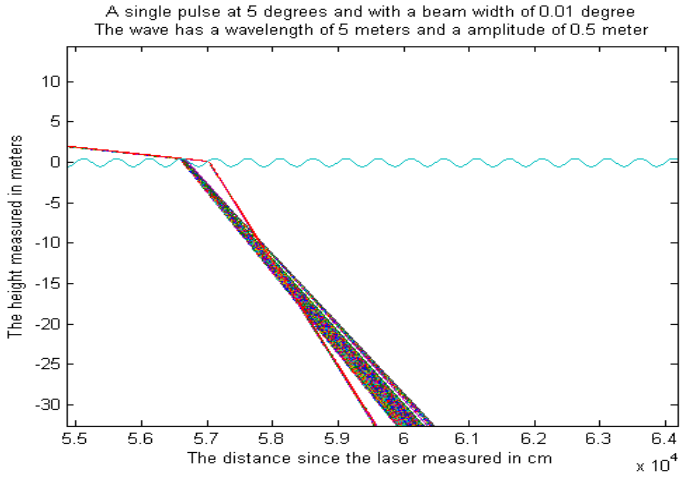

Figure 31: Laser pulse with smaller slope and beam width than the wave

In conclusion the wave form will limit our model, and the accuracy of it. When the sea conditions are making worse, the amplitude will increase and the wavelength will decrease, hence the critical angle will be bigger, so the range of angles where we can insure a good scanning will be smaller and the received images will be worst.

One way to overcome this problem will be to scan during a time longer that the wave needs to cover one wavelength with a same angle, with this solution, it will be possible to detect all the sea volume. This one can be seen in Fig.32, where this solution has been implemented.

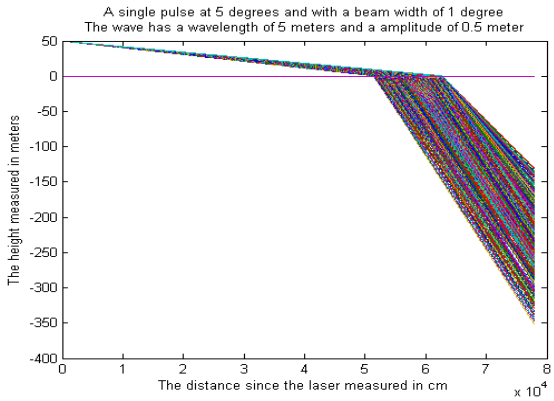

Figure 32: Solution to the slope problem

Apart from the problem of detecting area, another really important problem when the light crosses the water surface is the change in the angle, this angle is measured by Snell´s law. When the sea surface is plane, it is not so difficult to estimate from which area will be our received power, because knowing the incident angle and the beam width, the estimation of the transmitted angles to the sea is possible. But, when the surface is created of waves, this estimation becomes more difficult. Because, the media will be variable and will be really difficult to predict how the beam is being transmitted. Therefore, it is going to be really difficult to have a good accuracy. Apart from the waveform, another limiting factor for the used of Lidar in water, is the scattering of light in this media, as it has been explained in section 3.2.5.2, the scattering will vary a lot depending of a lot of factors. So, finally it is going to be really difficult to predict where the target really is.

In our simulation, to calculate the transmitted angle and the transmitted power in a wavy sea. First, the estimation on where the light and wave cross has been done, later, the slope of the wave has been calculated in this point. Once that this angle has been estimated, the relative angle from the incident ray is calculated and the transmitted angle is obtained, with this angle transmittance and reflectance values are estimated, and finally this transmitted angle is modified to know how the light is going to be transmitted in function of the horizontal axis.

4.7. Model implementation and Matlab code.

In the previous section the created model has been explained, in this part our aim is to described how the different parts of the model have been implemented to create our software. The Matlab code can be found in the Appendix B,.

The main idea of the program is to simulate and collect the different powers received from different round trip times at different angles. First of all some parameters must be specified, these values will be constant, like the height from where the laser is going to be shoot, how much we want to enter the laser in the water and the range that wants to be scanned. Once that these values has been specified, they are converted to angles. In this point we have the maximum and the minimum angles where the sweep will be done. The sweep will be implemented to have in the farthest point a minimum resolution of 1 meter, with this value the decrement between different angles is defined.

The attenuation value of the air is defined by the weather condition, to know the value of attenuation in the water, two different matrix are created, one with the absorption values of each point and another with the scattering value of each point. Once that this is defined the backscattering values is calculated. The values of scattering, backscattering and absorption are calculated by the equations of section 3.2.

Now, we have all the parameters we need to start the simulation. The simulation starts in the maximum angle and will move until arriving to the minimum one. It is going to collect samples of the power each nanosecond, so the time between two different sample is a nanosecond. For each angle, it is going to scan until the maximum round trip time, this time is the amount of nanoseconds our beam at the minimum angle needs to arrive to the maximum deep in water.

The laser beam is implemented like the sum of some different rays, which will cover all our beam width. So once that we have an angle, the following process is going to be repeat until the whole beam width is covered. Once that we have the scanning

angle, Snell´s law and Fresnel equations are calculated. After, the time needed to arrive to the discontinuity is calculated. If the sampled time is smaller than this value, the light is going to be propagated through the air, to calculated the received power from the air, the following file is used, Pulse_air_1.m. But if the sampled time is bigger than that calculated before we will have backscattered light from the air and from the water, for us, the backscattered light from the air will be like noise, because is something that we do not want. To calculate the received power following files are used, for the air, Pulse_air_2.m and for water Pulse_water.m . If the round trip time is the same that the ray needs to arrive to the discontinuity the scatter is going to be the water surface, which will have more backscattering value than air, for this Pulse_Air_3.m is used. This process is repeated for each angle until when the whole beam width is covered.

When the full width is covered the new shooting angle is implemented and the previous process is applied. All the process is graphically explained in the following diagram of blocks.

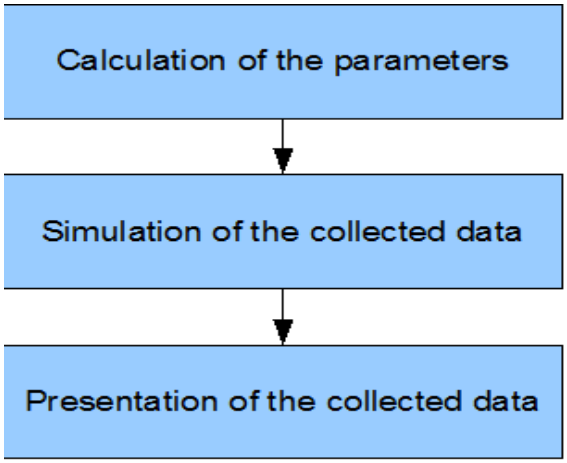

Figure 33: Main diagram block

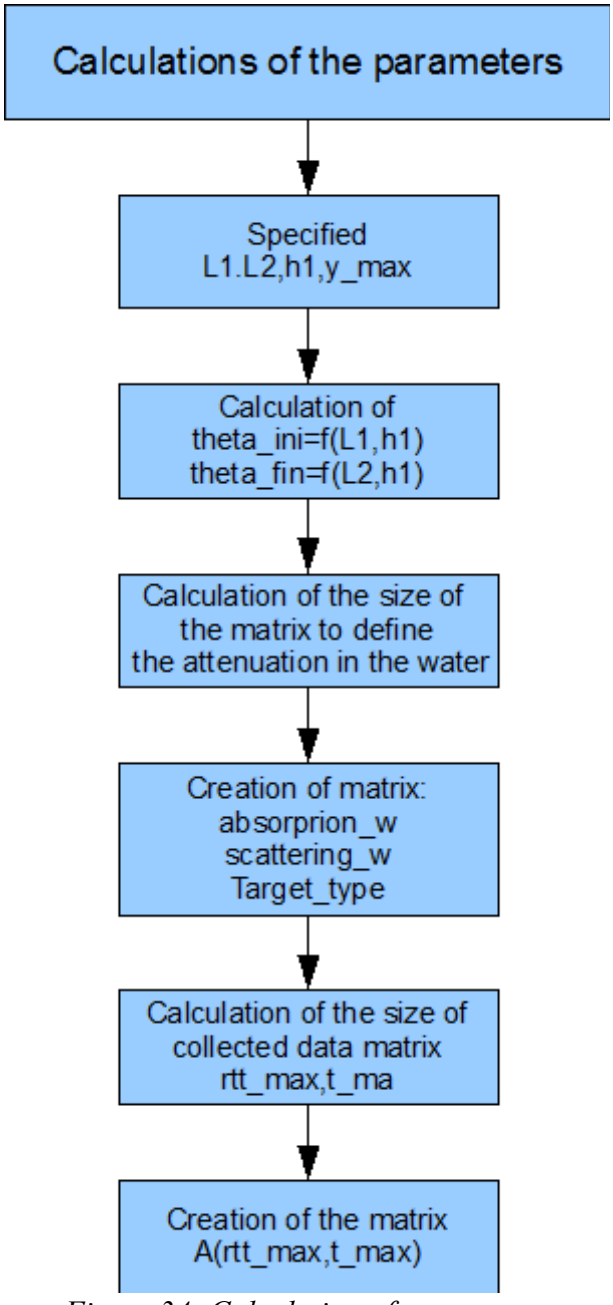

Figure 34: Calculation of parameters

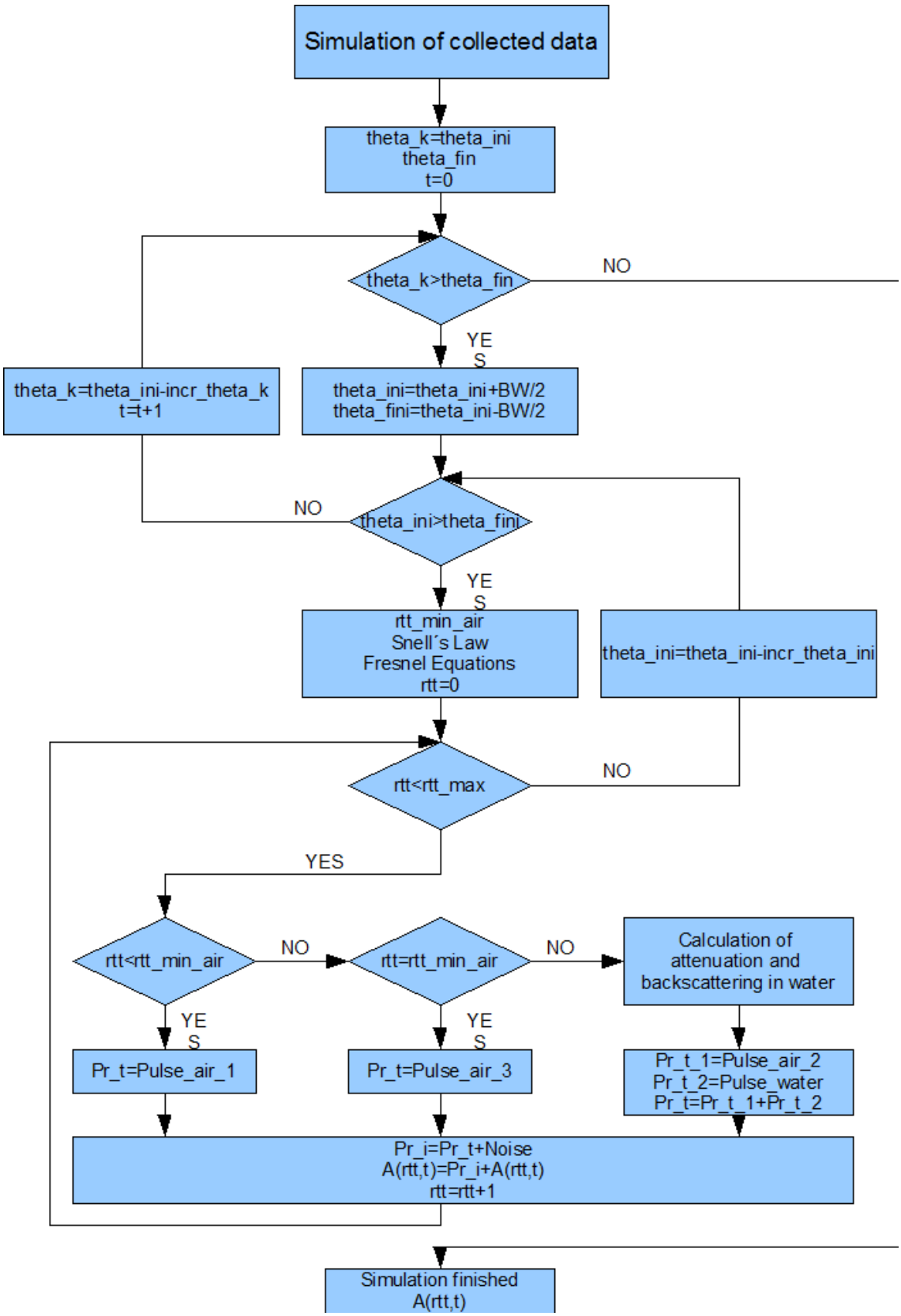

Figure 35: Simulation of the sweep

4.7.1. Analysis of the simulated data and model limitation.

Once that the program has been explained some different test has been realized to find the limits proposed in the 2nd section. Before explaining the extracted data, the limitations of our model have to be described.

The main problem that we have found to create a credible and accurate model has been the real value of the noise of our receiver. According to A.V. Jelalian in 1992, the following sources of noise would be taken in care,

- Background Noise Terms: That reflections from different sources, like the sun or the fog, that contributes undesired signal to the receiver. In our model this will the limiting factor when the detection of the submerged targets want to be done. The amount of signal backscattered from the air will be at one deepness much bigger from the air than from the target behind the water.
- Thermal noise: The thermal noise is expressed by the following equation

  $$Thermal\ Noise = k * T * B * NF$$

  where

  k=Boltzman constant=$1.39*10^{-23}$ J/ºK

  T=300ºK

  B=300 Mhz

  NF=Overall system noise figure of the receiver=10

  these values were given to us by our supervisor.
- Photon Noise: As we are working in the visible band this noise must be taken in care.

Our problem is that the specific value of the parameters that described these noises have been impossible to achieve, because of the military and high technological used of Lidar, so it has been impossible to us to find the real values of them.

So, to solve this big problem we decided to make the simulation with the minimum value given by the thermal noise, we took the value of 10^{-10} Watts

First, the limit value to detect the sea surface is going to be analyzed and later the maximum deepness for a range of .

To find the first limit, one range between 100 meters and 1400 meters have been swept. It has been done in different sweeps of 300 meters, one example of this can be shown in the following figures, where the received power is fewer while the sea surface is further from the shooting point.

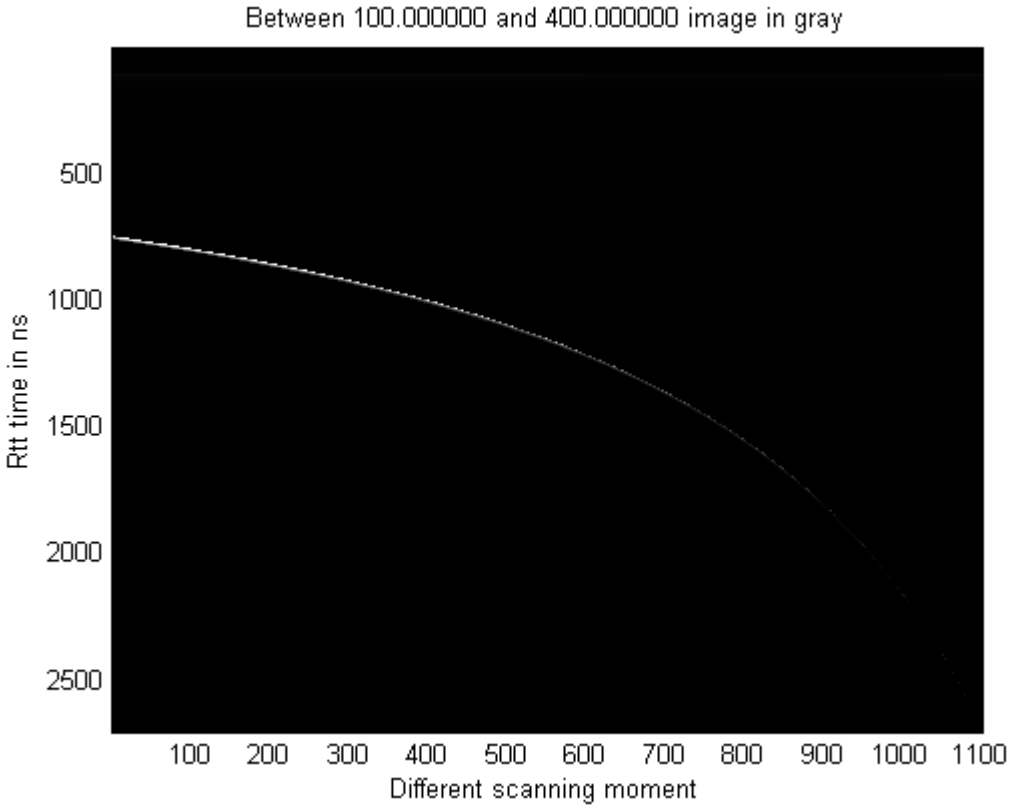

Figure 36: Received power from a range between 100 and 400 meters, plot is a scale of grays

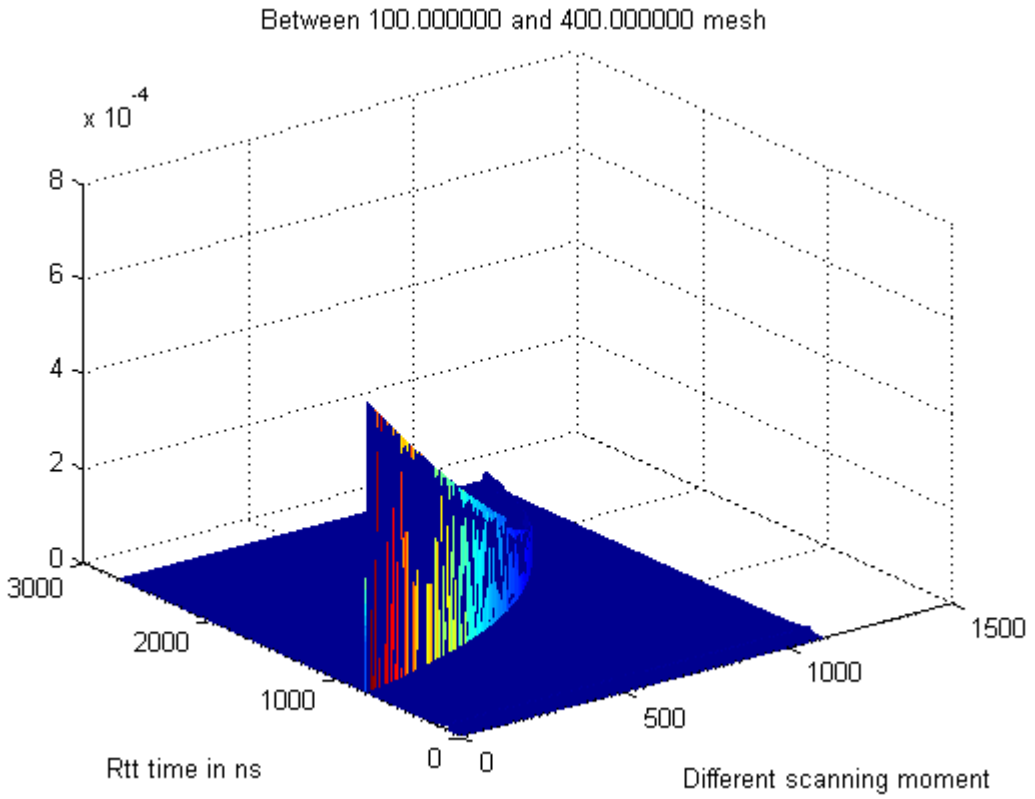

Figure 37: The received power from a range between 100 and 400 meters, plot in 3-D graph

To know where the limit to detect the sea surface is, two parameters are really important, the attenuation of the light in the air and the backscattering value of the sea surface. The first parameter will define how much power will arrive to the sea surface, so will stablish how much light can be backscattered to the receiver. The second one will specify the amount of the incident light is being backscattered to the receiver. Therefore this value will limit the amount of light received from the sea surface. But the most limiting factor is the noise, because if it is bigger than the received power it will be impossible to difference between the noise and the received power.

In our simulations different weather conditions were taken in care, but after checking the result of them, the decision of choosing the best weather condition was taken, this value will define the attenuation of the light in the air.

In the following table the obtained data are shown

Round Trip Time (ns)	Distance to sea surface (m)	Received Power (Watt)
750	100.83	$6.13*10^{-4}$
1250	180.7	$1.67*10^{-4}$
1750	257.7	$7.24*10^{-5}$
2250	333.8	$3.69*10^{-5}$
2750	409.5	$1.25*10^{-5}$
3250	484.9	$8.88*10^{-6}$
3750	560.3	$7.6*10^{-6}$
4250	635.5	$4.7*10^{-6}$
4750	710.7	$2.6*10^{-6}$
5250	785.9	$1.6*10^{-6}$
5750	861	$1*10^{-6}$
6250	936.2	$8*10^{-7}$ - $5.7*10^{-7}$
6750	1011.3	$4*10^{-7}$ - $3*10^{-7}$
7250	1086.3	$2.5*10^{-7}$ - $2*10^{-7}$
7750	1161.4	$1*10^{-7}$ - $1*10^{-8}$

Table 4: The received power at some different round trip times

If the obtained data is analyzed, can be seen that there is not data fewer than the thermal noise that our received has, also can be seen that once that the distance is increasing up the width of our beam is bigger, and the resolution is worse. We decided to make another table where for a more realistic noises these limits will be shown.

Noise	Limit
10^{-5}	Around 180 meters
10^{-6}	Around 400 meters
10^{-7}	Around 930 meters
10^{-8}	Around 1100 meters

Table 5: The limits for sea surface detection depending on the noise

The previous analysis has been done with a narrow beam, the effect of a wider beam can be shown in the following pictures, with a wide beam the amount of signal backscattered from the surface will be smaller, so the limit will be nearer than the limit from a narrow beam.

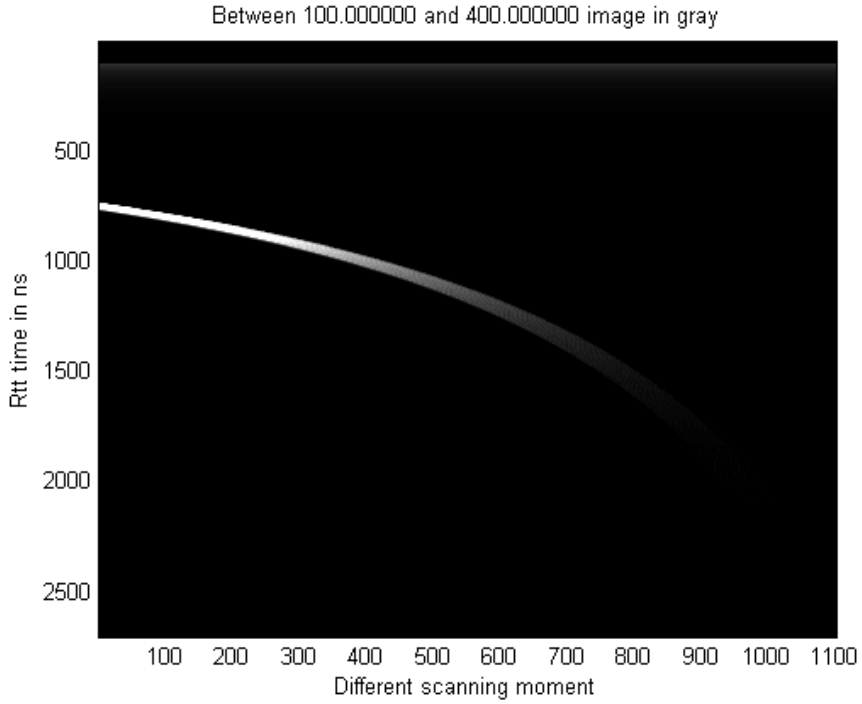

Figure 38: Received power form a sweep between 100 and 400 meters with a width beam

If we compared this figure with the Fig.36, can be seen that a wider area is detected for each angle, and that the power is smaller.

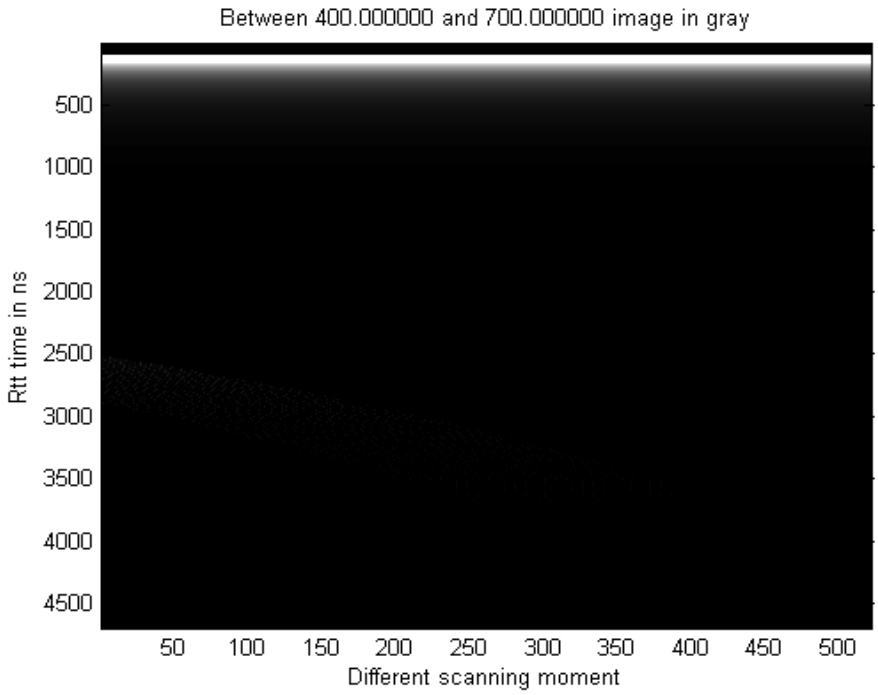

Figure 39: Received power form a sweep between 400 and 700 meters with a wide beam

In this picture is shown a sweep between 400 and 700 meters, where the effect of a wide beam is appreciated. Extracting data from the figure, a detection of a width of 500 ns of sea surface is seen, so, it would be really difficult to decide where the sea surface is, so, the used of wide widths is going to be neglected.

Now the limit of the possible detectable sea bottom is going to be analyzed. As has been previously explained once the light crosses the discontinuity between sea and air, some part of the power will be transmitted to the water and the other will be reflected to the air. The receiver will receive power from the air and from the submerged target or from sea water. The received power from the air will be treat like a external, noise, because it will degrade the received signal.

As it has been explained in the section 3, the transmission of the light in the air and in the water is too different. The attenuation of the light in the water is much bigger than the attenuation of the air. So, the power will decrease really quick and the

backscattered light is going to be really fast smaller than the backscattered one from the reflected part. This limit, it is going to be discussed later, first ,one example of the attenuation of the water is going to be shown.

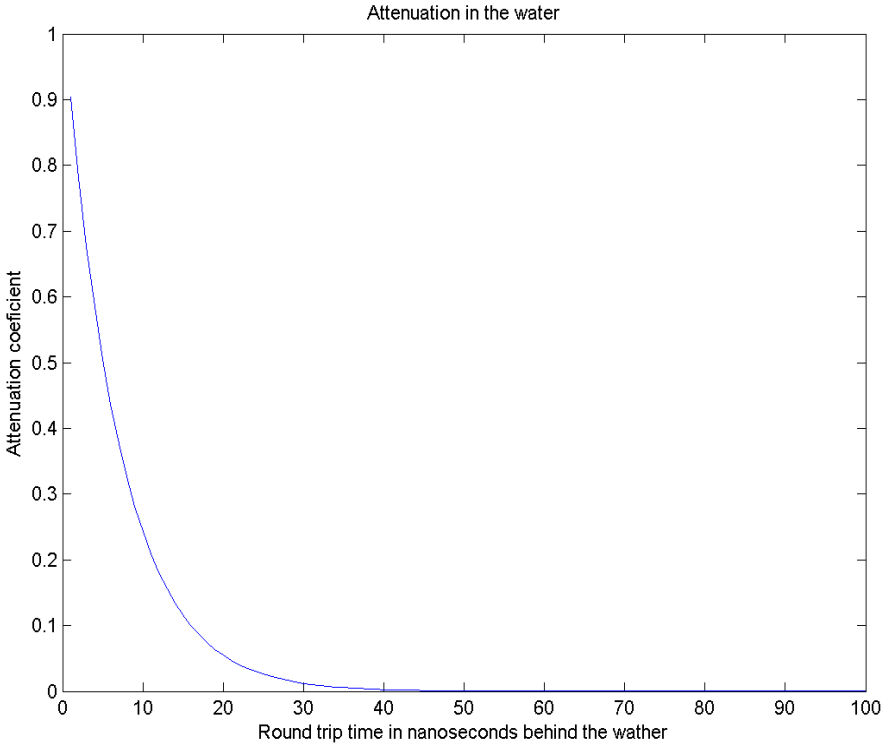

Figure 40: Attenuation coefficient of light in water for different round trip times measured in nanoseconds

For this case the receiver noise should be smaller, because the power will decrease really quick, with a thermal noise of 10^{-10} , the real limiter of the system will be the backscattered power from the reflected part. In this case, after extracting data from the simulations an average depth of 8 meters has been obtained, which will be 75 ns. From this depth the received signal will be too noisy an the detection of any target will be really difficult.

As it has been explained in the previous figure, the attenuation in the water is too big compared with the air one. So, although the backscattering of sea water is 1000

times bigger than the air one, in few meters the received signal from the sea water and from the air are similar, and when the depth is a little bit bigger than that explained before the received power is almost the scattered back from the air.

Chapter 5

Test of LIDAR system in aquatic environment

Once that the physical basics have been stated (section 3) and the Matlab code has been developed and explained (section 4), the final part consist in the practical test. The practical test consist in using a lidar for fish mapping. The laser is shot from the top of a building to a water volume and then the data received are analysed. The most important step is obtain some correlation between the practical data and the data from the simulation, and an explanation for this correlation (sections 5.3, 6, and conclusions).

5.1. Test objectives and plan

The objective of this test is to obtain real data about the research question to compare it with the theoretical results. The research question is detecting submerged target using red/blue lidar to assess the adequacy of those systems for this purpose. Some targets should be dispose in the scanned water volume, and the light backscattered by them should be stored and analysed.

Due to the fact that the students who write this thesis were studying in Trondheim and the laser system is located in Bergen, the supervisor is normally working in Oslo, and the second supervisor was working on his own project, the plan was established to be flexible. Trying to get ready every different point of the plan as soon as possible. The main points of this plan are (estimated time is expressed in parenthesis):

1. Get ready the laser for the testing (5 days):
    1.1Take it out from the previous structure (the laser was previously tested in a boat). (1 day)
    1.2 Set it up in the laboratory and make sure that it is working. (4 days)
2. Build a structure to use the laser over the building. This structure must leave us change the shooting angle easily. (5 days)
3. Move the whole equipment to the top of the building. (1 day)
4. Test the laser over the water volume. (2 days)
5. Test the laser with submerged targets in the water volume. (3 days)

The time to complete all these steps is from February to June of 2009.

5.2. Lidar system description

We are using a LIDAR for fish mapping. The optical system consists on a sender channel and a receiver channel. The system that is copied has realized both a day system and night system in which the sender and receiver channel are mutually adapted.

Laser transmitters are from Big Sky Laser Technologies, Montana USA. The company is a well-established supplier of solid lasers for many years.

Laser is based on a Nd: YAG source which doubles the frequency with a KTP crystal, thus the wavelength is divided from 1064.15 nm to 532,075 nm.

CFR 200 fra Big Sky Laser Technologies		
Parameter	Value	Comments
Energy	130 mJ @ 532 nm	
Pulse length	12-15nS	
PRF	30 Hz	
Beam divergence	< 4 mrad	
Beam diameter	6.3 mm	Record dimension is ¼” dvs 6.35 mm
Energy stability	<	
Line width	< 2 cm^{-1}	Expressed in bandwith
Polarization	Linear	
Line width	< 1 cm^{-1} @ 1064 nm < 2 cm^{-1} @ 532 nm	Equivalent 0.113 nm Equivalent 0.057 nm
Energy density	0.41 J/ cm^{2}	Max. at the end per pulse

Table 6: Laser specifications

Figure 41: Lidar system out of the cover

5.3. Test site description

The building used for placing the laser is normally a grain store where we have rented the roof. The location can be seen in the next map: Hegrenesveien num 39, 5042 Bergen, Norway. (Google maps) The red line represents approximately the trajectory of the laser beam.

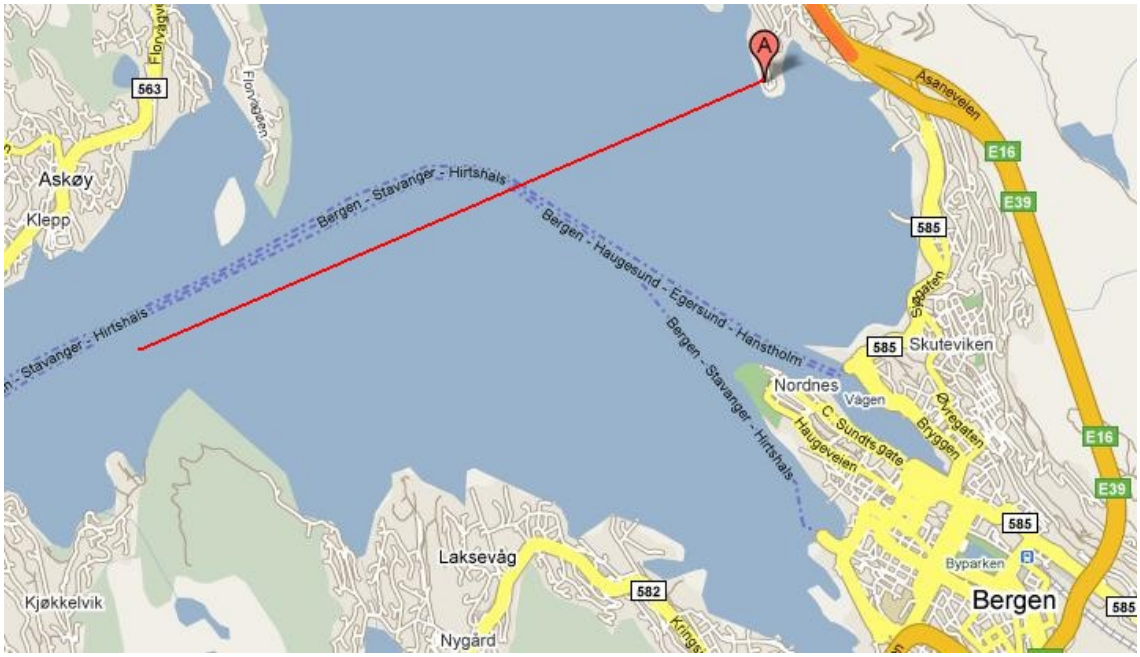

Figure 42: Map of the measurement place

In the following pictures we can appreciate better the shape of the building and where the laser has been placed.

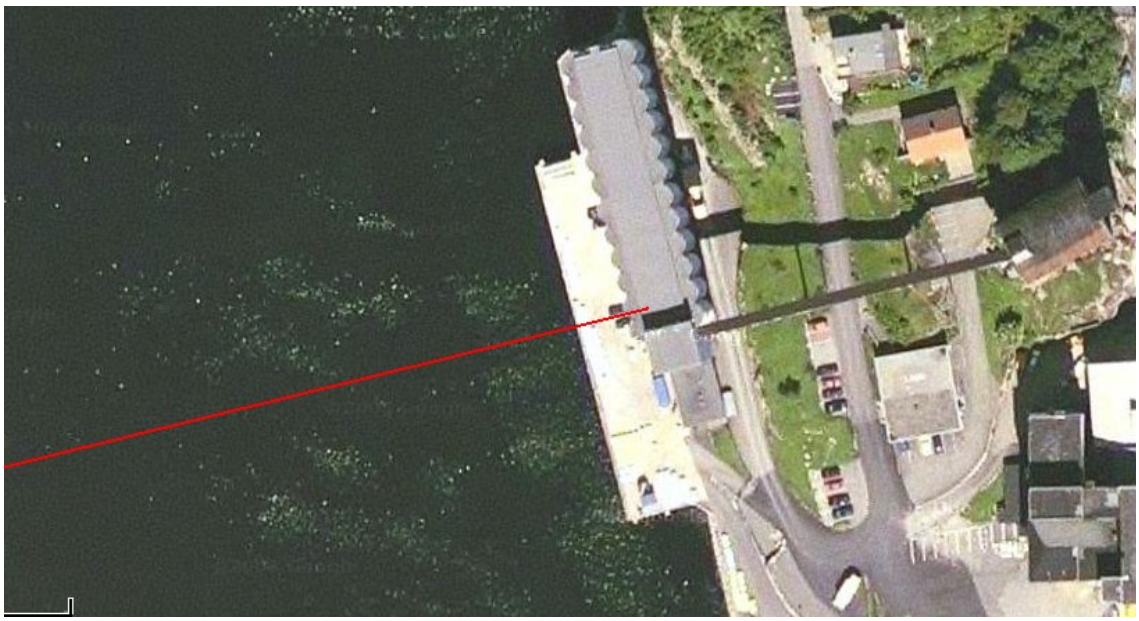

Figure 43: Aereal view of the building

Figure 44: Picture from Nordnes

Figure 45: Picture from Skuteviken

With our lidar system we can measure the deepness of the sea, using the light backscattered from the sea surface and the bottom of the sea. The figure 46 shows us the sea bottom of the fiord of Bergen, the Byfjorden.

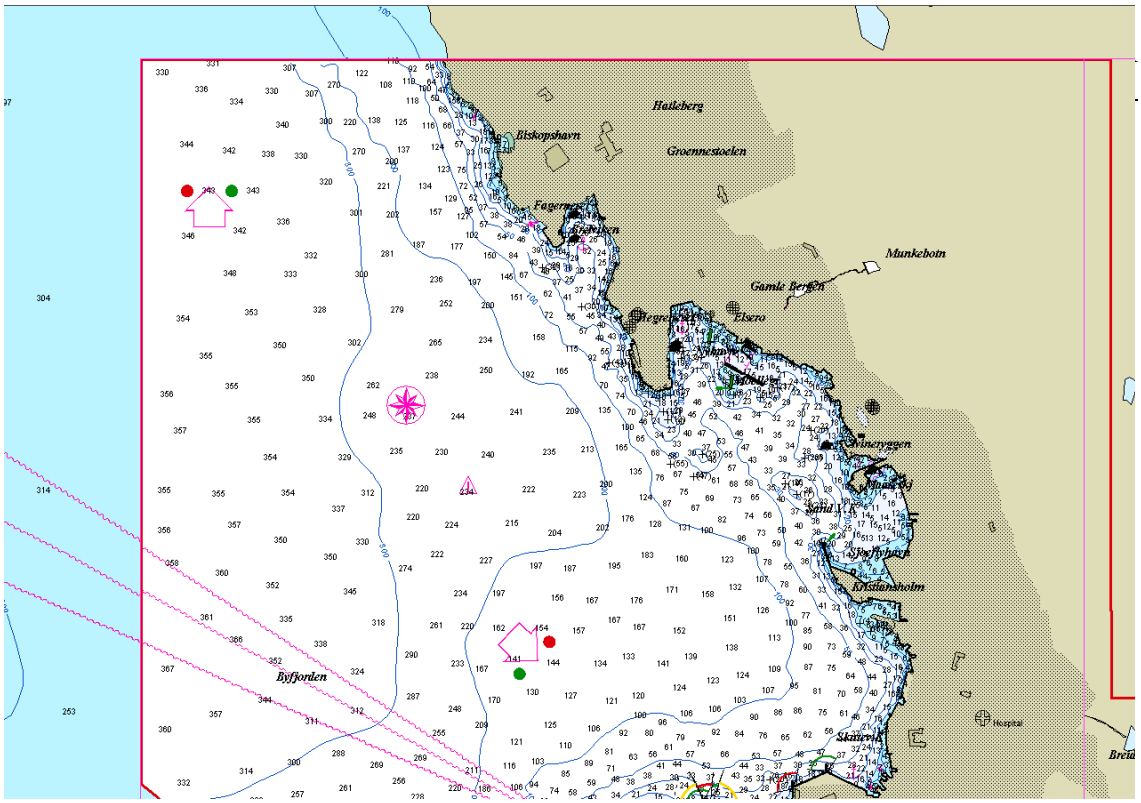

Figure 46: Map of Bergen sea deepness

In the two following sections, 5.4 and 5.5, the whole practical work is described. In the first one the preparations for the test are described, while the second one explains how was the test executed

5.4. Description of test execution

1. Get ready the laser for the testing:

1.1 Take it out from the previous structure

10/02/09 – Because the last time the laser was used in a boat it was inside a big metallic box. The first day we took it out from this box using tools. Inside this box were the power supply, the cooler system, and the data adquisition hardware. At the end of the day we were able to setup the lidar system but when we tried to turn it on we discovered a water leakage and an error message on the display: “Lamp connector optical head”.

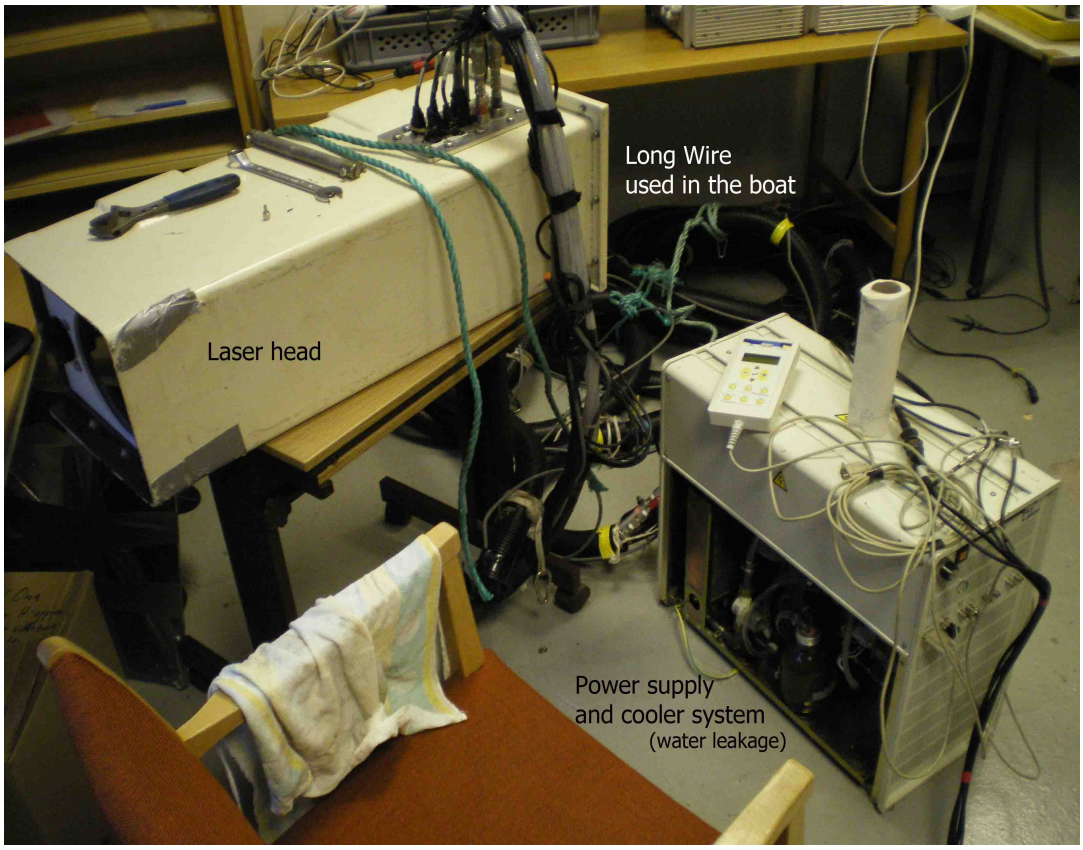

Figure 47: Parts of the Lidar System

1.2 Set it up in the laboratory and make sure that it is working. (4 days)

11/02/09 – Early morning we went to buy some silicone and we fixed the leakage. But the error message did not disappear. After checking every connection we decided to bring a new cable from Trondheim. The cable that was not working can be seen in the picture above. In the following pictures the silicone reparation and the checking of the connections are shown.

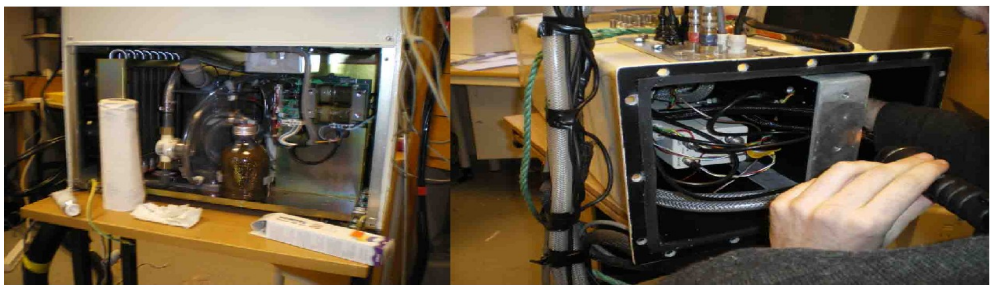

Figure 48: Fixing lidar system

24/03/09 – We arrived to Bergen with the new cable, we changed it for the old one. The error message disappeared. We were able to shoot the laser from the remote control.

2. Build a structure to use the laser over the building.

   25/03/09 – We started to build the structure to handle the laser. We used some tools from the laboratory and we decided to build it using wood because it is the faster way and we had every material already there. The only requirement was that the structure should be able to be stable in different angles along the measurement time.

   26/03/09 – During this day we finished to build the structure. And we checked which different angles we could get using a jack (tool for the car). Also this day we repaired a coaxial wire that communicates the Data acquisition hardware with the computer, and we were able to shoot the laser using the application of the computer.

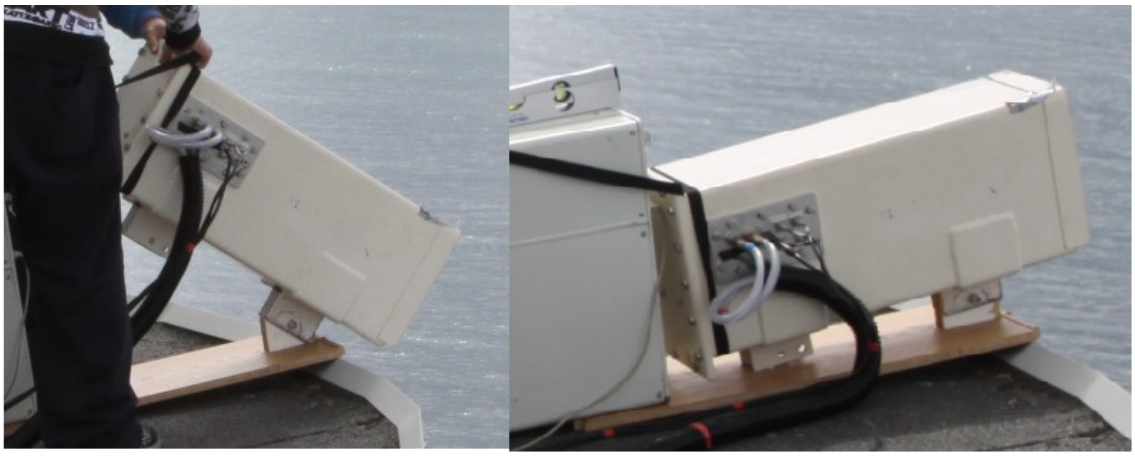

Figure 49: Wood made structure to handle the laser

3. Move the whole equipment to the top of the building.

   12/05/09 – We were testing the laser in the laboratory and we moved it at the end of the day to the measurement place. We also went to buy a long cable for the power supply.

4. Test the laser over the water volume.

   13/05/09 – This day we started the measurements. In the following pictures is shown the LIDAR setup, and the field of view. This day we were using the lidar over the water surface always with the divergence lent for security and using the lidar on the main roof, also for security reasons. A small schema is shown in the following figure.

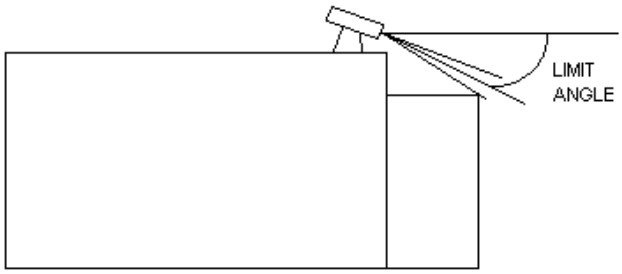

Figure 50: Schema of the main and secondary roof

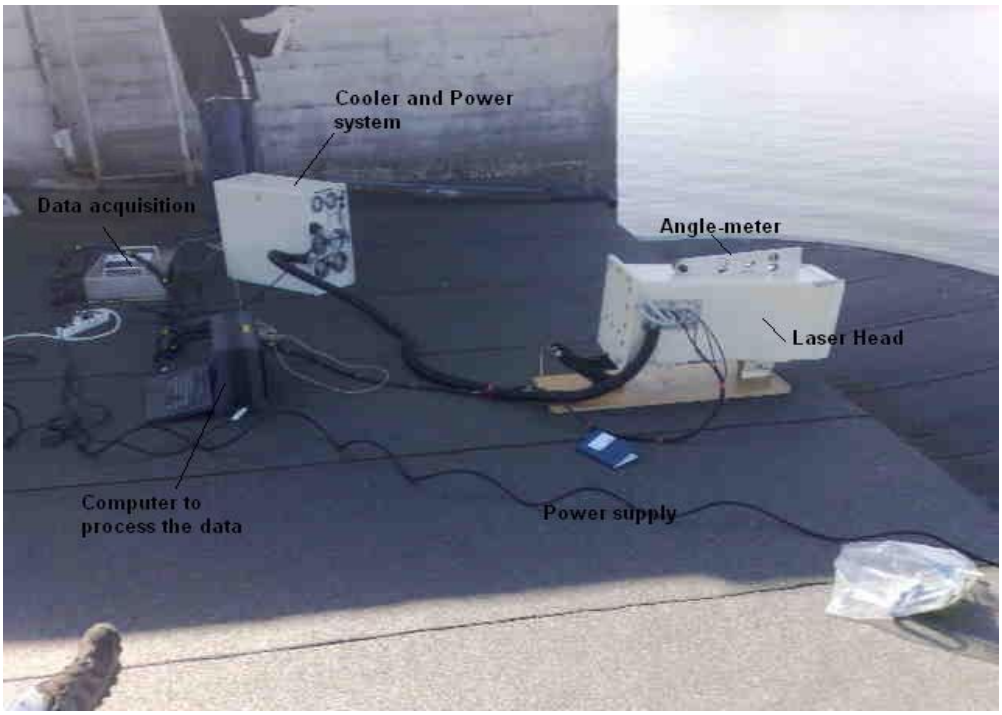

Figure 51: Main view of Lidar setup

Figure 52: Field of view and sky conditions

The sky was clear and there were no clouds. Before 12:36 different measures are made to calibrate properly the laser, the field of view, and the computer software to analyse the received data.
The parameters used to shoot the laser are shown in the table below.

Parameter	Value
Delay	-1 ns
Pulse width	1E-6 ns
Number of samples	1000
Ad delay	0 s
Full-scale range	10 V
Offset	0 V

Table 7: Parameters used to shoot the laser

12:55 – We shot the laser with 18º of inclination and then it reached the surface at 350 ns. After that, we moved the laser to see how the distance to the water surface changes with different angles.

13:07 – With 12º we reach the water at 500 ns. But the peak in the reception is smaller due to the high reflection, that is bigger than the backscattered light. We are in the more noisy zone.

13:12 – We tried to find the limit due to the part of roof that we have under the main roof. This secondary-roof can be seen in the Fig.43. These results are analysed in the next section.

13:23 – We try to accurate the limit of the zone with too much noise, where the reflection is too high.

4. Test the laser with submerged targets in the water volume.

This part of the test was finally discarded. The first reason was the price, it is expensive to bring a submarine or a container just for one day test. That is the most important part that should be issue of study in the future.

09/06/09 - Instead of that, the last day we moved the laser to the secondary roof using a security rope.

The purpose of this day was repeat the measures of the water volume without any target inside it. This time we collected more data from different angles. The previous day we note down the shooting angle. And then we got the .RAW files. But the computer gave us a profile of the intensity of the light received, the difference between this graphic and the .RAW file is that the second one include the analysis of the whole shooting time, i.e. if we shoot the laser during 10 seconds we will collect the data for the 10 seconds, while the first one only represents the light received in a concrete instant.

So this second day we got data from more angles, noting down more data for each angle. Because of the limitation discovered the previous day, we decided to use the laser directly from the secondary roof. That is shown in the following figure.

Figure 53: Using the lidar from the secondary roof

With this new emplacement we had the possibility of shooting with a big angle, that means, shooting to a point closer to the building than the previous day. In the figure we can see Unai fixing a coaxial wire that was in a bad condition, Luis noting down the profile of the data, and Eirik, the second supervisor, checking the work progress. We had some problems with this coaxial wire, we already fixed it at the lab but because of moving it we had to fix it a couple of times at the top of the building.

We were shooting with different inclination angles using the divergence lens. In this way we did not collect all the data that we wanted because the purpose of this lent is to open the light beam to make the light safer to human eye. Because the zone that we were scanning was unoccupied we decided to remove the safety lent and turn off the laser when a boat was crossing close to the beam's footprint.

When we had enough data from different angles we decided to take out the laser of the structure to be able to shoot it using a bigger angle.

Finally we decide that it should be interesting to simulate a sweep covering the whole range. The problem is that to execute this sweep we had to move the laser using our hands and the rate of angle switching was not constant, but anyway, it was a good approximation.

After the first sweep we had a problem with the coaxial wire again. And after we executed the same sweep but using the divergence lens. Because we had reached the limit of the structure turning system we decided to take out the laser from the structure.

In the following sections we are going to analyse the data obtained from this last test.

5.5. Lidar test data presentation

Data resulting from the analysis executed on the 13th of May of 2009.

13: 12 The following figure is a .RAW file generated by the computer that was connected to the LIDAR system. In this kind of figures obtained from the our laser the horizontal axis represent the time. And the vertical axis are the time that needed the light to go to the a point and come back to the receiver, that is just near the emitter. For example the first pixels in the upper left part of the figure represents the backscattered light from the closest part of air close to the laser. The next pixel represents a zone a bit farther. Thus the distance from the the top of the figure until the white/grey horizontal line that is below the words "Sea surface" represents the time that needs the light to cover the distance that is between the laser and the sea surface.

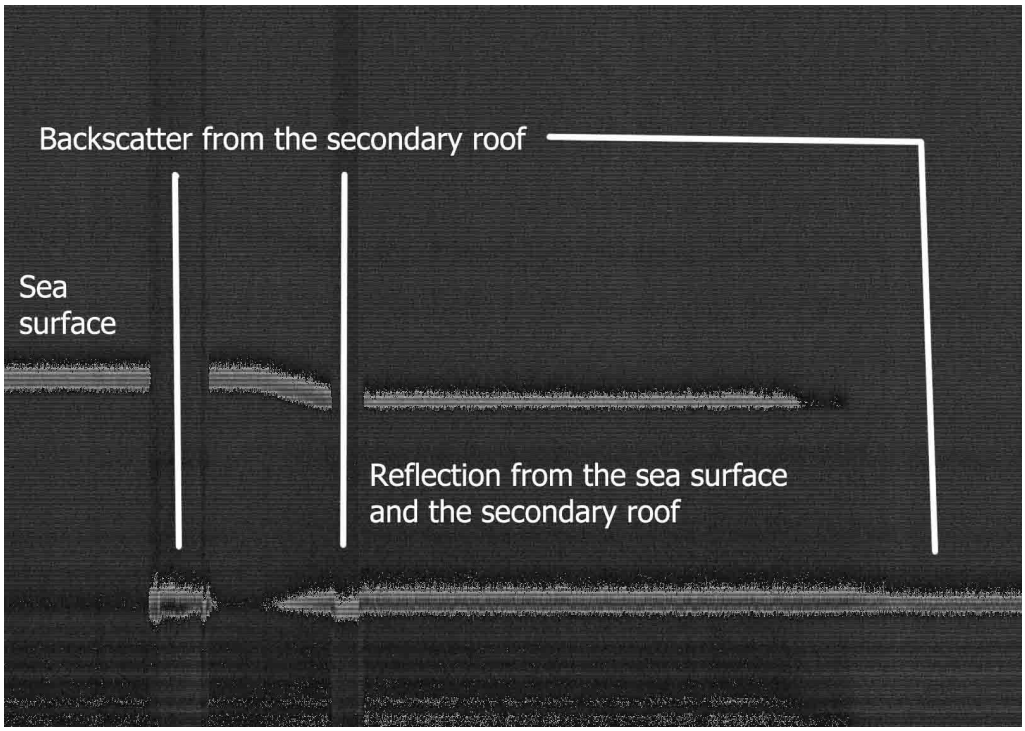

Figure 54: Near limit

12:23 Far limit data presentation

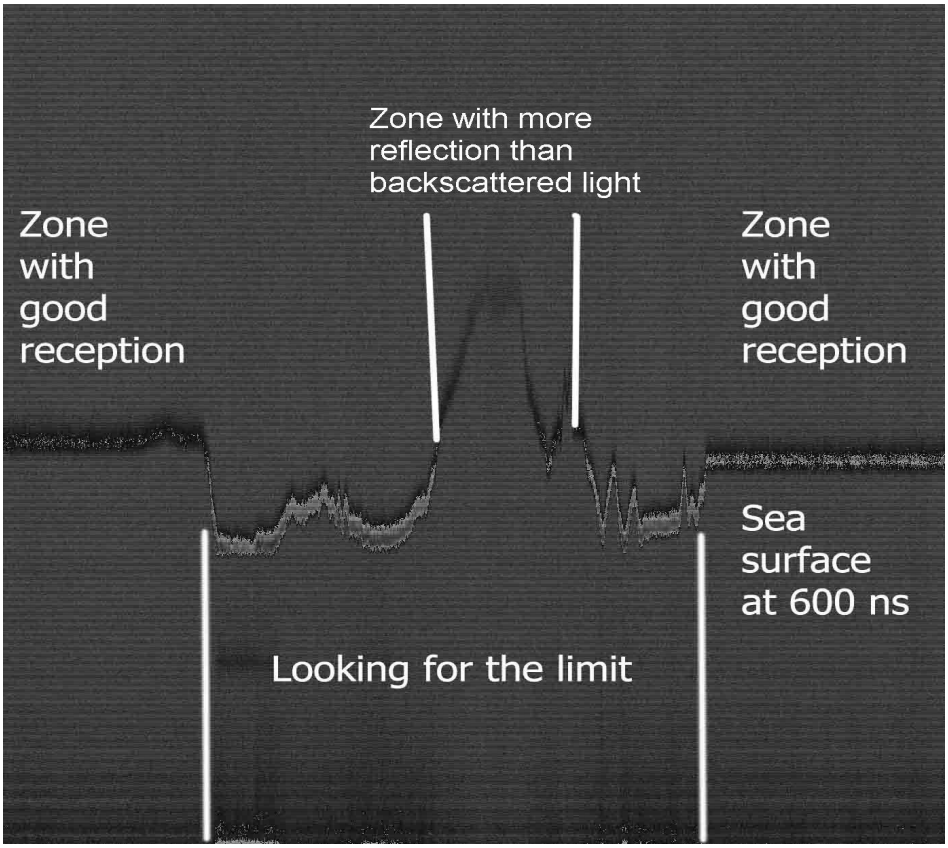

Figure 55: Far limit

Data resulting from the analysis executed on the 9th of July of 2009.

12:10 – We shot the laser using the same configuration as the previous time, the one shown in table7. This first shot was made using the safety lens, with an inclination angle of 17.5º.

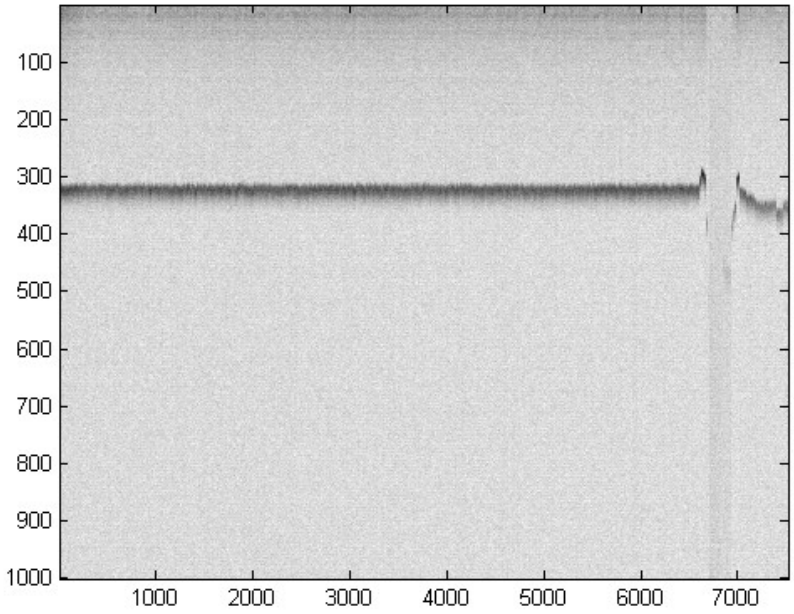

Figure 56: Laser shot using the divergence lens

12:30 – We shot the laser starting with an angle of 9º.

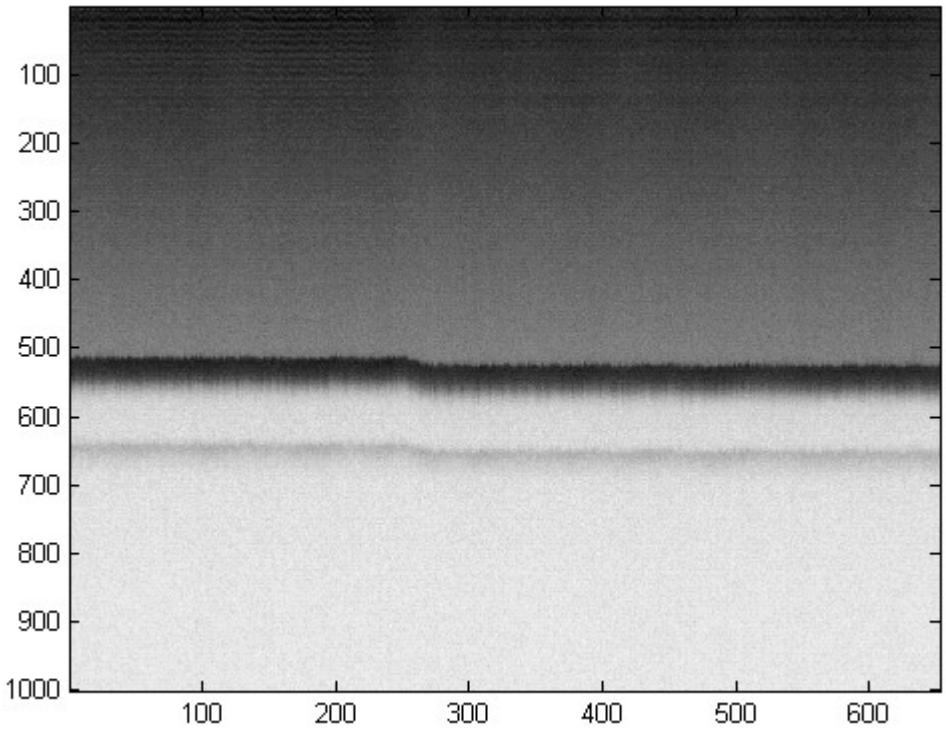

Figure 57: Received power

12:34 – At this point we were measuring different angles without stopping the laser.

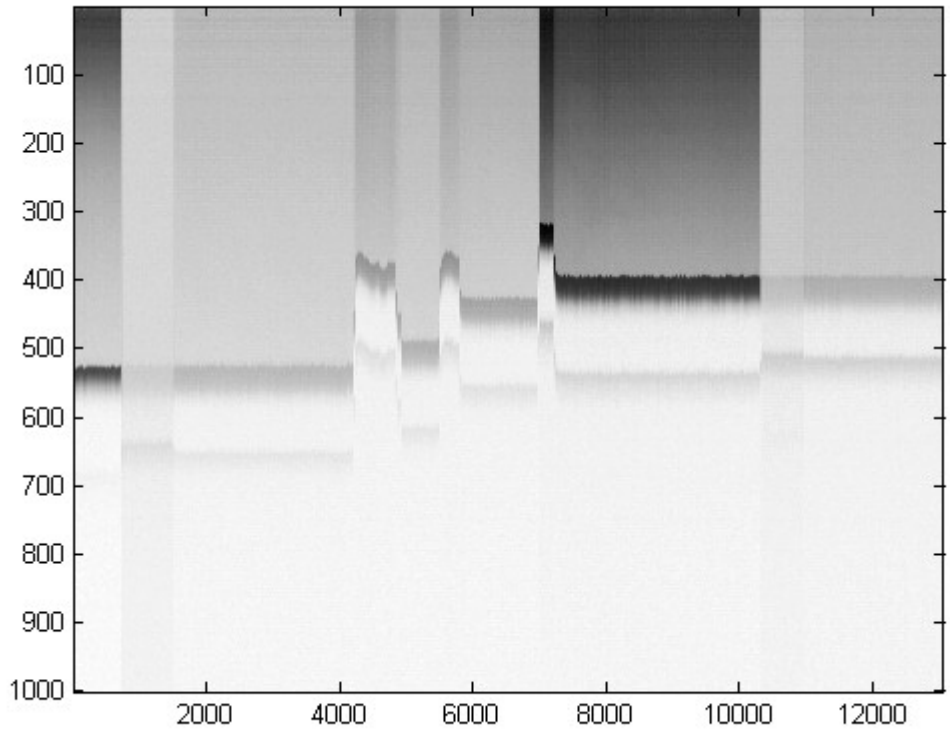

Figure 58: Measuring different angles

12:42 – We were measuring with different angles in a different shot.

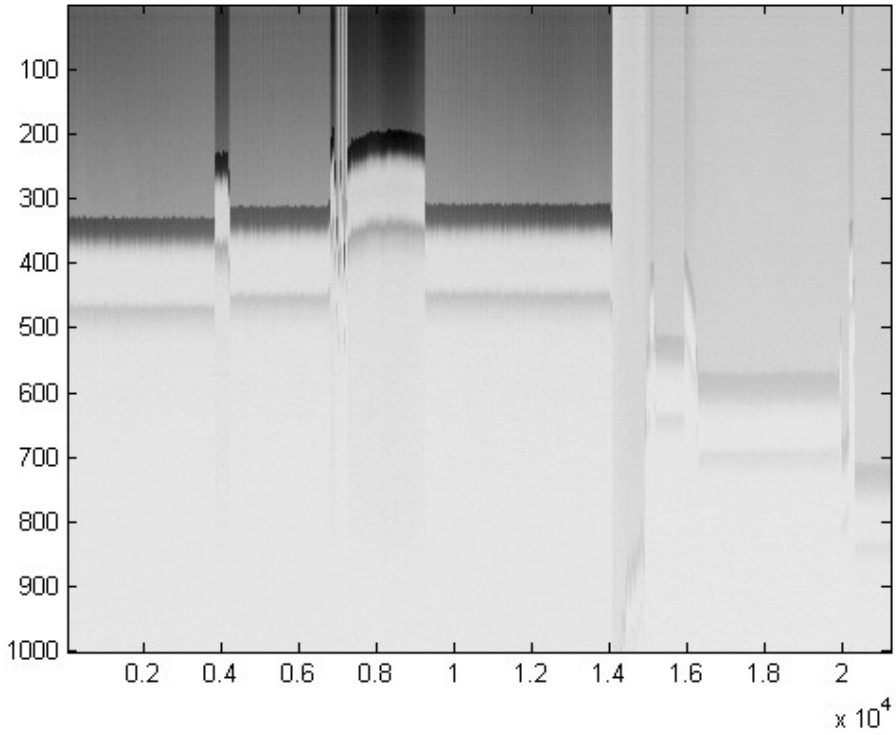

Figure 59: Different scanners

13:08 – At this time we had enough measures from different angles and we started to generate manual sweeps.

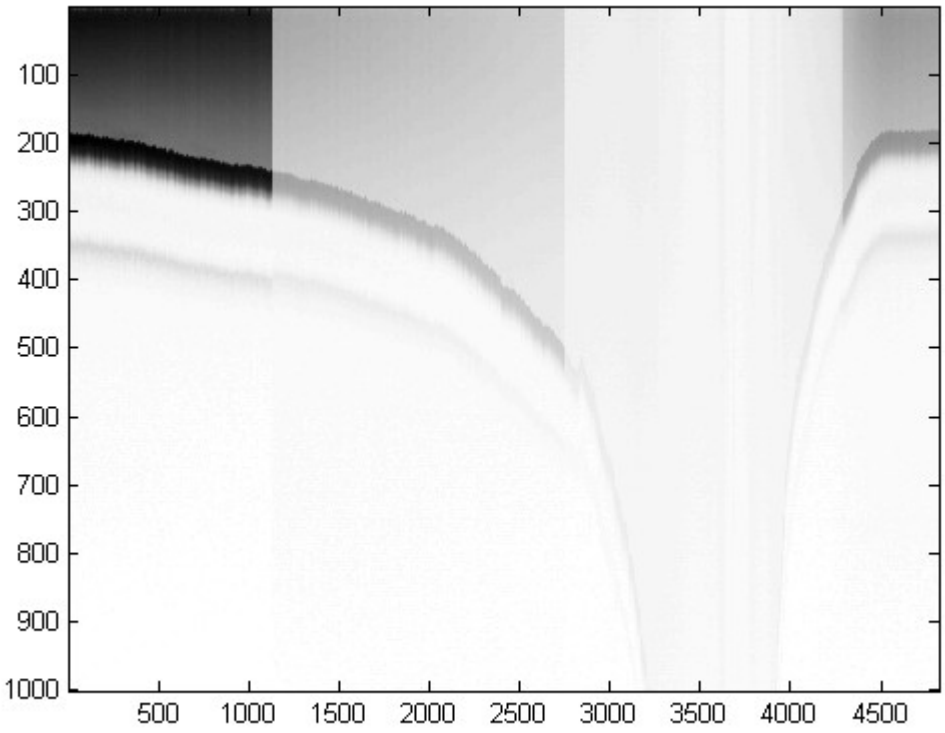

Figure 60: First sweep from 31° to 8°

13:36 – Maximum angle and final sweep

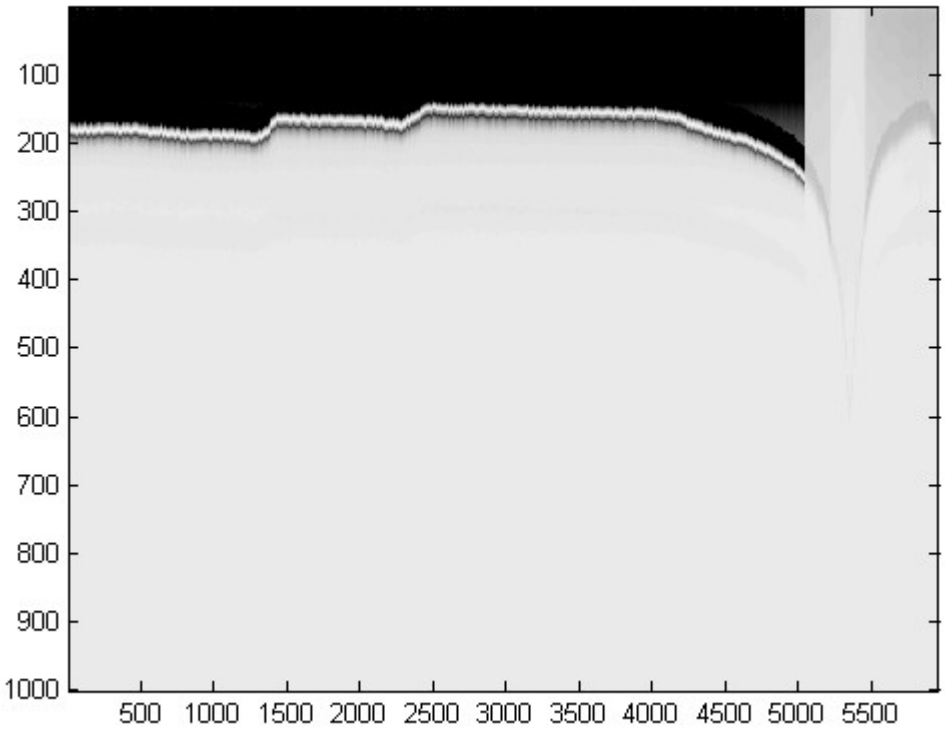

Figure 61: Laser off structure and final sweep

5.6. Lidar test data analysis

13/05/09

13: 12 In figure 55 the limit angle is between 25º-26º. At 23,5º we found the sea surface at 260 ns. This is the nearest distance to the building that we can measure. In the following picture we can see how we were looking for this limit. We were varying the angle. While starting (left part), we had just the reflection of the sea surface, but then we made the angle bigger (so we pointed to a point closer to our building) and the distance to the sea surface decreases

At 16º we have that the measure start to be too noisy, until 14º we have a measure is readable. With this angle we found the sea surface at 600 ns.

13:23, see figure 55. At 14º we have that the measure start to be too noisier, until 10º we have a measure is readable. With this angle we found the sea surface at 600 ns.

Finally our operation range is:

ANGLE (º)	SEA SURFACE (ns)	Distance to the sea surface (m)
23,5	260	78
14	600	180

Table 8: Operating range of the first day

09/06/09

12:10 In figure 56 we can realize that there is only one horizontal line, this one represents the sea surface that is backscattering more light than the air or the water volume because the discontinuity between the air and water. Using the numbers in the vertical axe we can state that the sea surface is at 310 ns far from the laser. That means that the distance to the water surface is 93 meters.

$$distance_{sea\,surface} = time_{stored} * c_{light}$$

The horizontal axis can be read as the time that we were shooting with the same angle. There is shown the numbers of pulses shot. And using the shooting rate of pulses we can know the total shot tim, the pulses rate is 30 Hz, so the are 30 pulses each second and

$$time_{total} = \frac{N_{pulses}}{30\ pulses/s}$$

This file is 250 seconds long, this measure was so long because we were adjusting different elements.

After we decided to remove the divergence lens to had better measures.

12:30 Figure 57. The big difference between this figure and the previous one is that in this one, because the divergence lens was removed the intensity of the light was bigger, i.e., the energy was more concentrated and it could reach the

bottom of the sea and come back. That is why we have this second line at 645 ns. After approximately 250 pulses, 8,3 seconds we turned the laser until 11º degrees.

At 9º we found the sea surface at 510 ns that is 153m, and the bottom of the sea at 650 ns, 195 m. Considering that the beam is turned when it goes inside the water it gets more vertical and we can say that the deepness of the sea should be smaller than 195-153=42m. This result can be compared with the deepness map of the fiord of Bergen, figure 56.

12:34 – Each time the angle is bigger and thus the distance to the sea is smaller, see figure 58. The intervals with non-stable measures were produced because between one measure and the following one to move the angle we had to handle the laser with the hands pointing to a place close to the building.

From 0 to 4100 pulses we were measuring 11º. After we turned the laser and from 4900 to 5600 pulses we measured 13º. Finding the sea surface at 490 ns (147 m). The next angle was 15º, from 5800 to 6900 pulses. The last angle, from 7200 pulses until the end, was 17º

12:42 - The following measures (figure 59) correspond to angles 17º (from the start until 3900 pulses) and 18º (from 4100 to 6900). After this measure the following one, that is quite unstable, correspond to an angle that was obtained. handling the laser using our hands. That angle was, in average, 31º

The last measures that are not easily readable, correspond to the angle 10º, 8º and 3º. When we were shooting with 3 degrees the backscattered light was too low because the reflection over the sea surface was going almost directly in the opposite direction.

13:08 – At this time, figure 60, we had enough measures from different angles and we started to generate manual sweeps. The first one, that correspond with the first figure, was done without the divergence lent from 31º to 8º and come back. We can use the temporal axis to now the variation of angle speed.

The start angle is 31º and the last one is 8º. And the total time is 3200 pulses. The sweep speed was, 0.216 º/second.

13:36 – After the first sweep we had a problem with the coaxial wire again. And after we executed the same sweep but using the divergence lens (figure 61). Because of we had reach the limit of the structure turning system we decided to take out the laser from the structure. From 0 to 150 pulses we were measuring 43º. Until 2300 pulses the angle was 50 degrees. And after this we continue the sweep in the same way as before but without the lens. That is why in this last figure we can not see the reflection from the sea bottom.

Once we have analysed each diagram obtained from the lidar system, we are going to summarize the most important conclusion about the range of detection.

Using the security lens we have a **wide beam** whose light is less concentrate

- Estimated maximum range for detecting sea surface

  The data obtained from the day 13/05/09 were obtained using the divergent lens. The wide beam is able to reach a point nearer to the emitter because the energy is distributed in a bigger beam shape, because it has more aperture than using directly the laser. To find the upper limit of the detection range we have to see the figure 55. In this moment we were using an angle bigger in the part with more noise. The physical limitation that we have is related with the portion of light reflected in the discontinuity between the air and the water. When the light reflected to the air is smaller than the one that is crossing the discontinuity and going into the water we have a good level of light backscattered light. But when

the light reflected is increasing the light backscattered in the direction of the receiver is decreasing. Finally we found that in the last good reception was using an angle of 14º. In this case we found the sea surface at 600 ns. That means that the distance to the sea surface was 178 m. far from the laser. Using this we are able to deduce the altitude of the building that is 43,06 m. and the distance from the bottom part of the building to the point were the laser hit the water, 172, 71 m. These results are shown in the following figure.

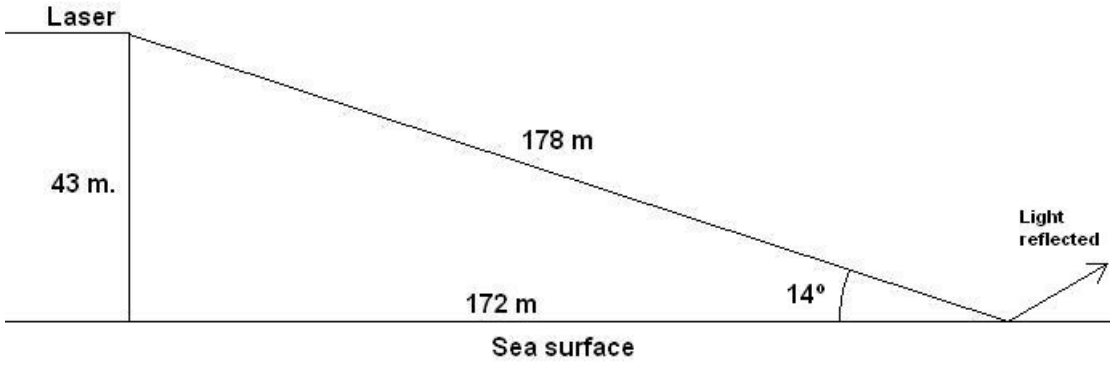

Figure 62: Schema of range detection with divergent lens

- Estimated maximum range for detecting sea bottom.

  Using the wide beam the light backscattered from the sea surface plus the light reflected is so high that the bottom cannot backscatter light until the receiver. Thus the range for detecting the sea bottom using this lens is 0 m.

- Estimated volume clutter from sea water

  To estimate the volume clutter from sea water we need to know the deepness of the sea. But using the divergent lens we cannot detect the bottom and we cannot estimate the volume clutter.

When removing the security lens we have a **narrow beam**. Now the light has less space and the energy flux is higher.

- Estimated maximum range for detecting sea surface

  The day 09/06/09 we were shooting the narrow beam. Using this beam the light can reach farther points and come back to the receiver because of it is more focused, and that makes that the light scattered in the backwards direction is bigger.

  Thus, in the part more in the right of the figure 59 it is shown the measure obtained while shooting with 8º. The highest peak of this measure was at 730ns. But the spectrum was a bit noisy, with 3ºthe noise was to high compare with the signal power. Using this result we arrive to the conclusion that the sea surface was 219 m far from the laser and

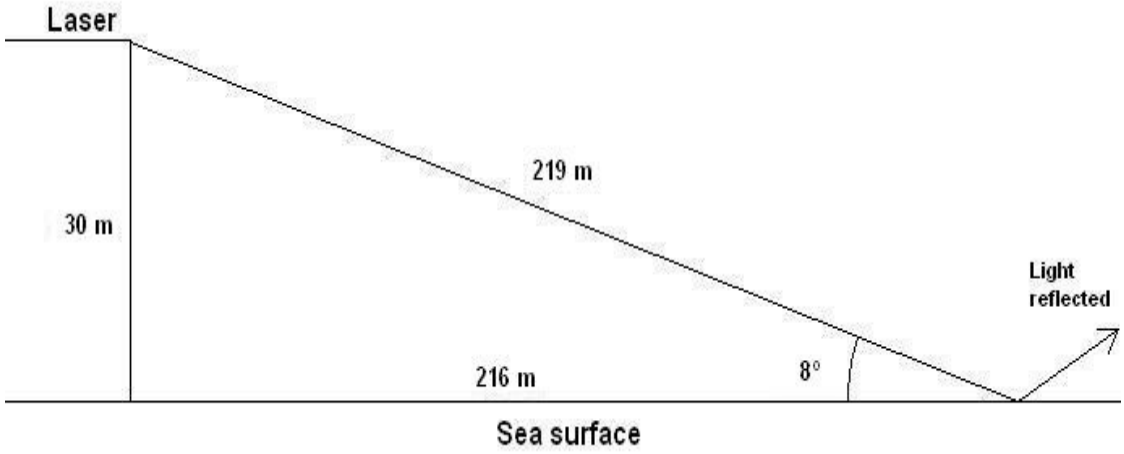

Figure 63: Schema of range detection without divergent lens

- Estimated maximum range for detecting sea bottom.

  Now the beam is more narrow and the light can go inside the water, reach the bottom of the sea and be backscattered until the receiver. The theoretic lowest point were we can measure the distance is the vertical, but we were limited because of the building and the size of the laser. The farthest distance that we can shot is using again 8º. Having a look, we can see that the reflection from the bottom is at 840 ns. But the light covered 730 ns through the air, so it was in the water during 110 ns. During this time it covered 24,739 m. And using the Snell law again we have that

$$\Theta_t = arcsen\left(\frac{n_1}{n_2} sen(\Theta_i)\right) = 48{,}12^{o}$$

  So the deepness of the sea is 16,68 m and the distance to the vertical projection of this point from the point where the beam go inside the water is 18,61 m as it is shown in the following figure

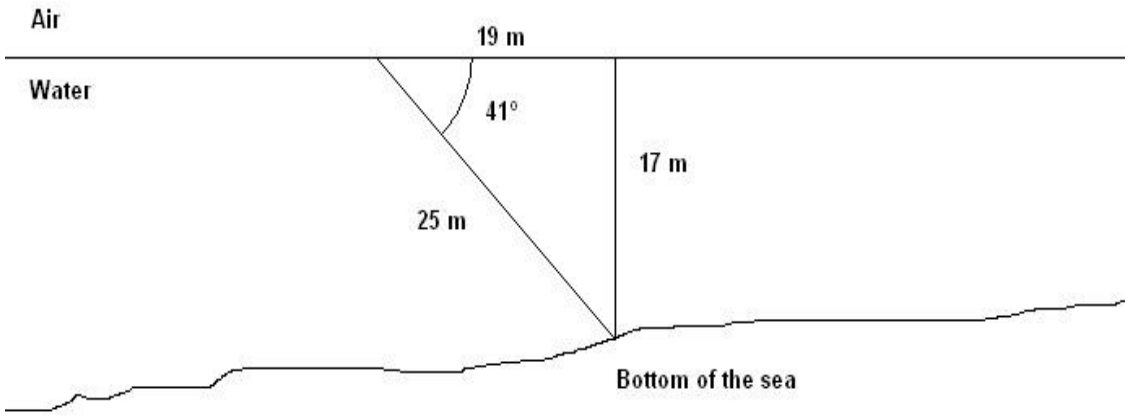

Figure 64: Schema of range detection of the bottom of the sea

Using the map of the bottom surface and a map with a proper scale we can see that there is a difference between the deepness calculated from the lidar test and the one shown on the map, that one is around 180 m. There are two possibilities, or there is a mistake, in the map or in our experiment, or this reflection is due to a phytoplankton mass that is 17 m under the water surface, as it was shown in section 3.2.2 that kind of

components can reflect a big amount of light. In the following figure the calculated deepness is compare with the map.

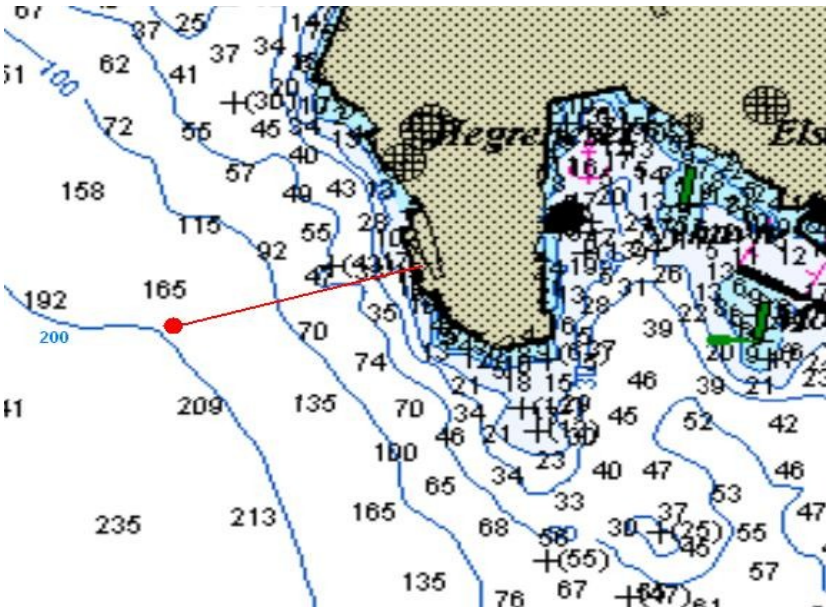

Figure 65: Comparison between the estimated deepness and a map of the sea bottom. The red point is 235 m far from the laser

- Estimated volume clutter from sea water

  Now we know the deepness and we can calculate the volume clutter from water sea. Our down limit is 90º while the upper limit is 8º. We are going to suppose that the deepness of the sea is the same from the last point until the building. After comparing the different figures obtained from the shots that were made without the divergent lens, we can say that this approximation is enough accurate.

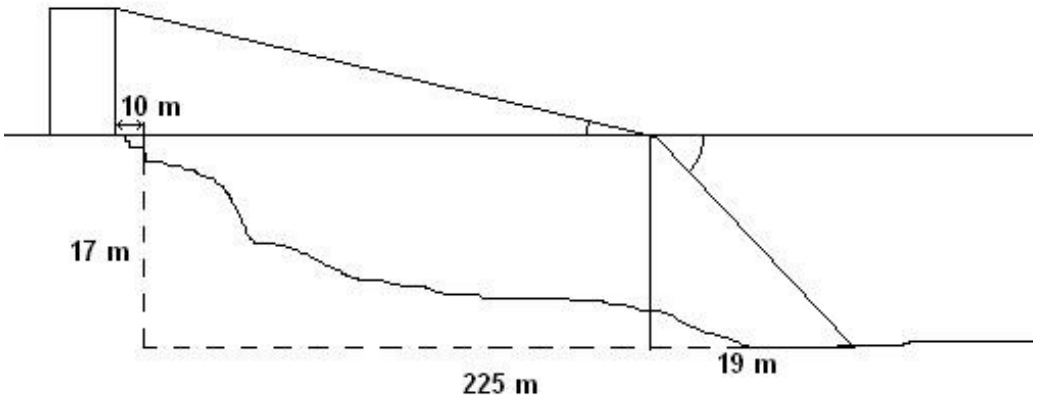

Figure 66: Volume clutter from sea water

So we have an area that is

$$(225-19)\times 17+\frac{(19\times 17)}{2}=3663.5\,m^2$$

And now we new to know how wide is the beam at this point and then know how it is opening under the water. In the specifications we can see that the aperture is 4 mrad, or 0.229 º. Using the Snell law we can create the front view of water that is backscattering light. The following fiugre show us a schema of this situation.

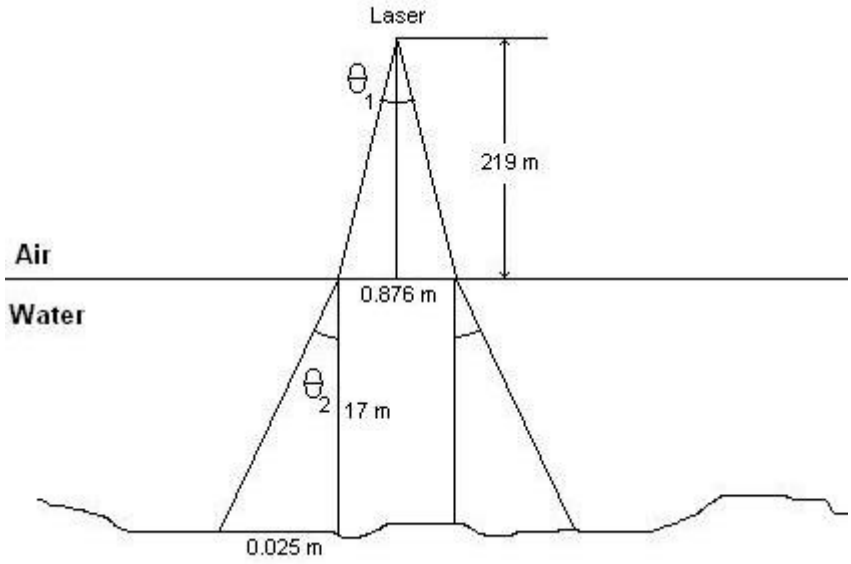

Figure 67: Volume clutter from sea water, front view

The area of the profile covered by light and that is iluminated is

$$s_{front} = \frac{2 \times (0.025 \times 17)}{2} + 0.876 \times 17 = 15.317\, m^2$$

The estimated volume clutter from sea water is 3446,32 m^3, that is the volume of water that can be iluminated.

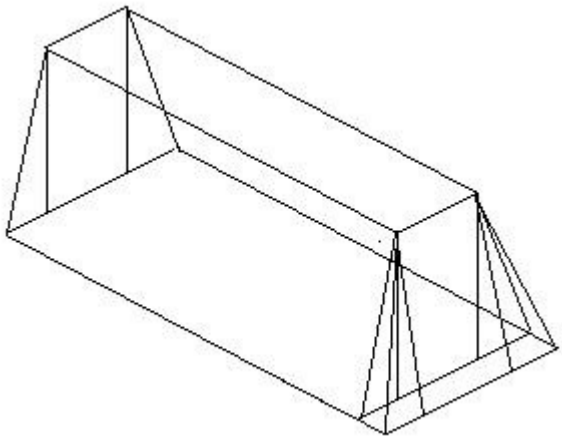

Figure 68: Volume clutter from sea water

The following table put all this values together. The range values are expressed using the distance from the building until the desired point (sea surface or sea bottom)

	Wide beam	Narrow beam
Sea surface (m)	172	216
Sea bottom (m)		235
Volume sea water (m^3)		3446,5

Table 9: Estimated range for detection

5.7. Background data assessments

In addition to the data obtained from the lidar system we had a camera that was able to take pictures using a filter of the same wavelength as the laser beam. We were trying to photograph the beam, but finally the exposition time was too short and we

could not obtain good pictures. But, with this pictures we can analyse the different reflection coefficients of the different elements in the picture.

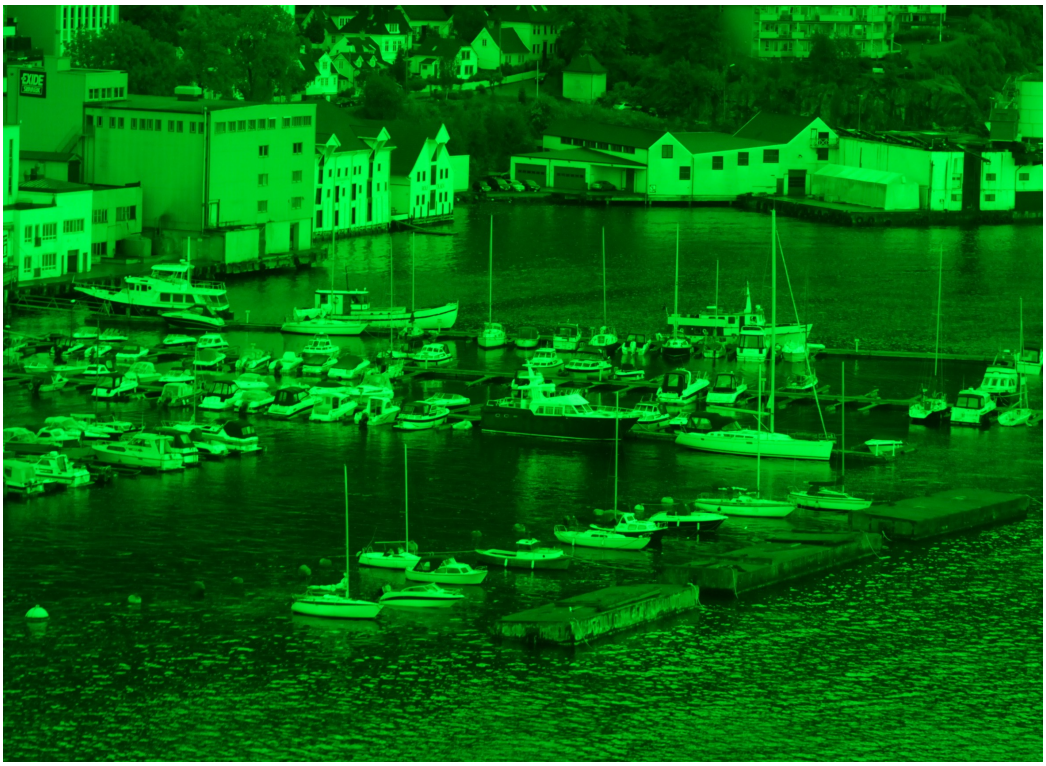

Figure 69: Picture taken using a 532 nm filter

In figure 69 the reflectance of the building is bigger that the one from a tree. That is because the house is painted with white paint. That was explained in section 3.3.4 also the surface is important to establish the reflection coefficient. The sea surface is more reflecting to us when the sea is smooth, in this way the light coming from the sun is reflected in a constant way over the surface, but when there are some waves the trajectory of the light changes and they do not arrive to the camera.

In figure 70, the intensity of the green light coming from the sky is higher because the light is coming directly to the camera while to go to the sea and come back the is a reflectance over the sea surface. The color of the trees is dark green because they are already green and the light coming from them is not so much affected by the 532 nm filter.

Figure 70: Picture taken using a 532 nm filter

In figure 71, we can appreciate how important is the sea surface for the reflectance. We have two main waves forming this sea surface, one going from the up left part to the down right part. The period of this one is much bigger than the second one that is going from the up right part to the down left part. This one has a smaller period, the reflectivity of the different parts of the surface is due to the combination of these two waves. Modelling a more realistic sea surface should be include in the simulation in future works.

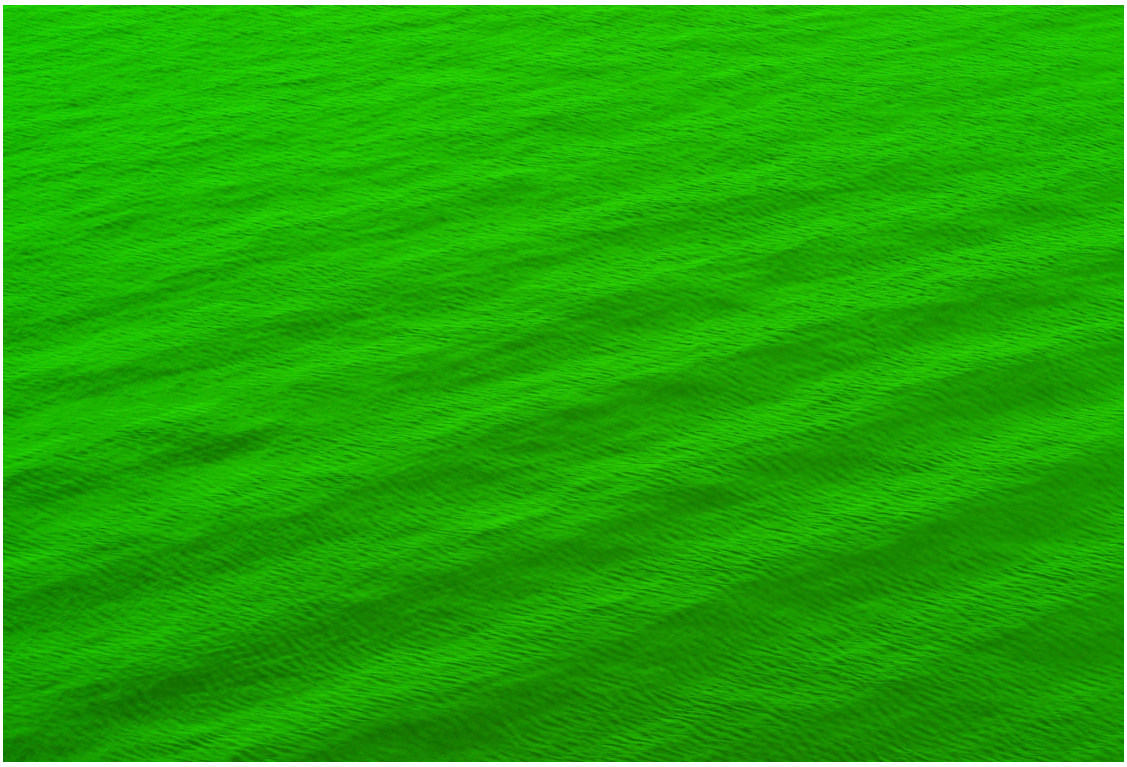

Figure 71: Picture taken using a 532 nm filter

Chapter 6

Discussion

In this chapter the differences between the results obtained in the section 4 and section 5 are going to be explained.

From section 4, the following table has been obtained

Noise	Limit
10^{-5}	Around 180 meters
10^{-6}	Around 400 meters
10^{-7}	Around 930 meters
10^{-8}	Around 1100 meters

Table 10: Estimated limits for sea surface detection from the simulations

The maximum depth estimated from our simulation will be, 8 meters.

From section 5, different values have been obtained, they are shown in the next table.

Sea surface	216 meters
Sea bottom	17 meters

Table 11: Estimated limits from realized tests

It can be seen that the obtained values from our model and obtained one from the tests are a little bit different. The used equipment to make the test, is a commercial system, which has been fabricated with a high accuracy. Apart from that, the weather conditions of our test and once from the simulated ones have been tried to be the most similar possible, but it is really difficult to create the same conditions. As has been previously explained, the attenuation of the light in the air and in the water will have a big dependency to the weather conditions, as example, the attenuation coefficient of the air can vary between 0.1 dB/km to 9dB/Km depending on the weather. So one of the factors to have different results is the simulation of the weather.

Another point to create this difference is the values used to modelize the sea, to achieve it, a model based on Morel has been used. This model is a simple model, which gives general estimated scattering and absorption values of the sea water. The parameters of this model vary a lot from one sea to another, as can be shown in section 3.2. Therefore the characteristic of the sea vary a lot the results of the simulations.

Apart from that, other factor to take in care, is that the properties of salinity, of temperature and pressure are not constant. Their variations will change the index of refraction, which will finally change the total amount of the attenuation coefficient and backscattering coefficient. These values change a lot depending on the weather, on the season of the year and on the situations of the sea, so to have a global model is really difficult.

Once, the reasons to have different results in the simulated model and in the realized test have been explained, can be said a general range and depth is not so realistic.

After comparing the simulated data and the ones from the test, a maximum range of 220 meters for the sea surface detection have been obtained. For a sea depth

scanning more difficult estimation is going to be made. As, we have explained before, there are a lot parameters which will limit our model and that will change our maximum depth. From the extracted data a maximum depth around 17 meters has been estimated. The received power from a deepness bigger than this value will be so small that it is not going to be possible to decide if it is a target or a source of noise.

Chapter 7

Conclusion

The work developed in this Master Thesis consists of the creation of a model to simulate Lidar efficiency in oblique incident detection. The created model is compared with a real system to check the efficiency of it.

The first part of the implementation work consisted of analyzing the transmission of light in the water and in the air. From this analysis an estimated values of scattering and absorption were obtained, so how the sea water and the air affect to the laser beam was stablished.

The properties of scattering and absorption from the water were stablished by Morel equations which give specific value to this parameters depending on the concentration of chorophyll. The characteristic will vary depending on the salinity concentration, temperature and pressure, which will make the model variable and unstable.

Simulated model is based on Lidar Equation, Fresnel Equations and the characteristics obtained from the transmission of the light in the previous analysis. The data extracted from the simulated model show that the sea surface detection range will depend primarily on the receiver noise and on the background noise, although when the detection of the submerged target or sea bottom want to be done, the main limiter factor will be the light backscattered from the reflection.

So, after comparing realized test and simulated data a maximum range of use in sea surface detecion of 230 meters and a maximum deepness of 17 meters have been obtained. These values will vary a little bit depending on the salinity, temperature, pressure, weather conditions, chorophyll concentation and so on. Therefore, more than a general limits for the use of Lidar, they are a guide for use of Lidar, because depending on several parameters they can vary really easy.

Finally, The estimation from where the backscattered signal is coming is very difficult task. The prediction of the beam deviation after crossing the sea surface is not exact because of the wave height and wavelength, and the beam aperture increases a lot after passing the sea surface, so the scanning area is too big. Therefore the obtained data do not have the accuracy needed to decide where really the target is.

Therefore, the use of Lidar is limited to short distance and to short deepness because of the extincion coefficient of light in the water and the resolution problems that will appear at big deepness.

REFERENCES

Cary, T (2009), *Lidar Market: Status and Growth Trends*, Retrieved May 25, 2009, from http://www.caryandassociates.com/downloads/cary_lidar_market_status_and_growth_trends.pdf

Flamant, C & Richard, E. (1999), *ARAT Missions Summary: IOP 02,* Retrieved June 17, 2009, from http://www.aero.jussieu.fr/equipe/MAE/IOP_02.19990918.ARAT_sci_sum.html

Hjelmstad, J. (2009) *Use of LIDAR for maritime applications*. Presentation for NTNU courses

Jelalian, A.V. (1992), *Laser Radar Systems*, Artech House, London

Jensen, J.R. (2007), *Remote Sensing of the Environment*, 2nd ed., Prentice Hall

Klein, L.A (1997), *Millimeter Wave and Infrared Multisensor Design and Signal Processing*, Artech House Publishers.

Kovalev, V.A. & Eichinger, W.E. (2004), *Elastic Lidar: Theory, Practice and Analysis Methods*, Wiley, John & Sons, Incorporated .

Mobley, C. (1994), *Light and Water: Radiative Transfer in Natural Waters*, Harcourt Publishers Ltd.

Waser, R. (2003), *Nanoelectronics and Information Technology*, 2nd ed., WILLEY-VCH Verlag GmbH & Co. KgaA, Weinheim.

Weitkamp, C. (2005), *Lidar, Range-Resolved Remote Sensing of the Atmosphere*, Springer.

Tsang, L., Kong, J. & Ding, K. (2000), *Scattering of Electromagnetic Waves, Volume 1 Theories and Applications* , Wiley-VCH

Appendix

The tables from this appendix has been extracted from (Mobley,1994).

λ (nm)	a_w (m^{-1})	b_{sw} (m^{-1})	K_d (m^{-1})	λ (nm)	a_w (m^{-1})	b_{sw} (m^{-1})	K_d (m^{-1})
200	3.07	0.151	3.14	500	0.0257	0.0029	0.0271
210	1.99	0.119	2.05	510	0.0357	0.0026	0.0370
220	1.31	0.0995	1.36	520	0.0477	0.0024	0.0489
230	0.927	0.0820	0.968	530	0.0507	0.0022	0.0519
240	0.720	0.0685	0.754	540	0.0558	0.0021	0.0568
250	0.559	0.0575	0.588	550	0.0638	0.0019	0.0648
260	0.457	0.0485	0.481	560	0.0708	0.0018	0.0717
270	0.373	0.0415	0.394	570	0.0799	0.0017	0.0807
280	0.288	0.0353	0.306	580	0.108	0.0016	0.109
290	0.215	0.0305	0.230	590	0.157	0.0015	0.158
300	0.141	0.0262	0.154	600	0.244	0.0014	0.245
310	0.105	0.0229	0.116	610	0.289	0.0013	0.290
320	0.0844	0.0200	0.0944	620	0.309	0.0012	0.310
330	0.0678	0.0175	0.0765	630	0.319	0.0011	0.320
340	0.0561	0.0153	0.0637	640	0.329	0.0010	0.330
350	0.0463	0.0134	0.0530	650	0.349	0.0010	0.350
360	0.0379	0.0120	0.0439	660	0.400	0.0008	0.400
370	0.0300	0.0106	0.0353	670	0.430	0.0008	0.430
380	0.0220	0.0094	0.0267	680	0.450	0.0007	0.450
390	0.0191	0.0084	0.0233	690	0.500	0.0007	0.500
400	0.0171	0.0076	0.0209	700	0.650	0.0007	0.650
410	0.0162	0.0068	0.0196	710	0.839	0.0007	0.834
420	0.0153	0.0061	0.0184	720	1.169	0.0006	1.170
430	0.0144	0.0055	0.0172	730	1.799	0.0006	1.800
440	0.0145	0.0049	0.0170	740	2.38	0.0006	2.380
450	0.0145	0.0045	0.0168	750	2.47	0.0005	2.47
460	0.0156	0.0041	0.0176	760	2.55	0.0005	2.55
470	0.0156	0.0037	0.0175	770	2.51	0.0005	2.51
480	0.0176	0.0034	0.0194	780	2.36	0.0004	2.36
490	0.0196	0.0031	0.0212	790	2.16	0.0004	2.16
				800	2.07	0.0004	2.07

Table 12: Spectral absorption coefficient of pure sea water, a_w, as determined by Smith and Baker. Values of the molecular scattering coefficient of pure sea water, b, and of the diffuse attenuation coefficients K_d used in their computation of a_w are also shown

Water body	$a_y(440)$ (m^{-1})
Oceanic waters	
Sargasso Sea	= .0
off Bermuda	0.01
Gulf of Guinea	0.024-0.113
oligotrophic Indian Ocean	0.02
mesotrophic Indian Ocean	0.03
eutrophic Indian Ocean	0.09
Coastal and estuarine waters	
North Sea	0.07
Baltic Sea	0.24
Rhone River mouth, France	0.086-0.572
Clyde River estuary, Australia	0.64
Lakes and rivers	
Crystal Lake, Wisconsin, USA	0.16
Lake George, Australia	0.69-3.04
Lake George, Uganda	3.7
Carrao River, Venezuela	12.44
Lough Napeast, Ireland	19.1

Table 13: Measured absorption coefficient at λ = 440 nm due to yellow matter, $a_y(440)$, for selected waters

λ (nm)	a_w (m^{-1})	$a_c^{*\prime}$	λ (nm)	a_w (m^{-1})	$a_c^{*\prime}$	λ (nm)	a_w (m^{-1})	$a_c^{*\prime}$
400	0.018	0.687	500	0.026	0.668	600	0.245	0.236
410	0.017	0.828	510	0.036	0.618	610	0.290	0.252
420	0.016	0.913	520	0.048	0.528	620	0.310	0.276
430	0.015	0.973	530	0.051	0.474	630	0.320	0.317
440	0.015	1.000	540	0.056	0.416	640	0.330	0.334
450	0.015	0.944	550	0.064	0.357	650	0.350	0.356
460	0.016	0.917	560	0.071	0.294	660	0.410	0.441
470	0.016	0.870	570	0.080	0.276	670	0.430	0.595
480	0.018	0.798	580	0.108	0.291	680	0.450	0.502
490	0.020	0.750	590	0.157	0.282	690	0.500	0.329
						700	0.650	0.215

Table 14: Absorption by pure sea water, a, and the nondimensional chlorophyll-specific absorption coefficient, $a_c^{*\prime}$.

	pure water		pure sea water	
λ (nm)	$\beta_w(90°)$ ($m^{-1} sr^{-1}$)	b_w (m^{-1})	$\beta_{sw}(90°)$ ($m^{-1} sr^{-1}$)	b_{sw} (m^{-1})
350	6.47×10^{-4}	103.5×10^{-4}	8.41×10^{-4}	$134.5\times10-4$
375	4.80	76.8	6.24	99.8
400	3.63	58.1	4.72	75.5
425	2.80	44.7	3.63	58.1
450	2.18	34.9	2.84	45.4
475	1.73	27.6	2.25	35.9
500	1.38	22.2	1.80	28.8
525	1.12	17.9	1.46	23.3
550	0.93	14.9	1.21	19.3
575	0.78	12.5	1.01	16.2
600	0.68	10.9	0.88	14.1

Table 15: The volume scattering function at Ψ = 90°, β(90°;λ), and the scattering coefficient b(λ) for pure water and for pure sea water

```
function Main_plane

%-------------------------------------------------------------------
%Name: Main_plane.m
%Authors: Unai Ayala and Luis Hernández
%
%Description: Simulation of the desired sweep
%-------------------------------------------------------------------

format long

% DEFINITION OF CONSTANTS

% The values of index of refraction and speed in the two media.

c_w=224748825; % Speed of light in the water
c_a=299705543; % Speed of light in the air
na=1.00029;    % Index of refraction of the air
nw=1.33;       % Index of refraction of the water

% INTRODUCTION OF PARAMETERS
% Angle of the LIDAR with ground reference (°, degrees). This is the
angle
% used for the first shot. We are going to scan a part of the sea
surface
% increasing the angle inc_theta degrees.

% Scanning a whole area.First we ask for the limits, for the height
and for
% the resolution in meters over the sea surface

L1=input('The first limit you want to scan (meters), L1=');
L2=input('The last limit you want to scan (meters), L2=');
h1=input('Throwing height(meters)=');
Res=input('The resolution in meters=');
y_max_water=input('Maximum in water(meters)=');
BW=(18*10^(-6))*180/pi;
P=10^6;

% Finding the angles to cover the whole area

theta_in=atand(h1/L1);
theta_fin=atand(h1/L2);

% We have to ensure the resolution at the farthest point

alfa=atand(h1/(L2-Res));

% Angular resolution: we will send pulses each inc_theta degrees
% Lower values give us better resolution

inc_theta_k=alfa-theta_fin;
display(sprintf('We will shoot from %f° to %f°. One shot each %f
degrees\n', theta_in, theta_fin, inc_theta_k));
```

```
% DEFINITION OF MATRIX

% We are using matrix to store the information of each point.
% 3-Storing the sea description with the object
% 1-Storing the data received

% Values to know our limits of the matrix

% Round trip time. With this value we can follow the pulse along its
whole
% way, higher rtt means that we are measuring the backscattering in a
% deeper part of the sea.
% To know the maximum rtt we have that

R_air_max_max=h1/sind(theta_fin); %Maximum distance covered in the air
rtt_min_airmax_airmax=2*R_air_max_max/c_a; %Rtt to cover the previous
one
theta_t_k=asind(na*sind(90-theta_fin)/nw);
R_max_water=y_max_water/cosd(theta_t_k); %Distance covered in water at
farthest
rtt_max_w=2*R_max_water/c_w; %Rtt to cover the maximum distance in
water
rtt_max=rtt_min_airmax_airmax+rtt_max_w; %Maximum rtt

% To know the x and y values of the matrix

R_air_max_min=h1/sind(theta_in); %Minimum distance covered in the air.
rtt_min_airmax_airmin=2*R_air_max_min/c_a; %Rtt needed to cover it
rtt_wat_airmin=rtt_max-rtt_min_airmax_airmin;%Maximum time in water
R_wat_max=rtt_wat_airmin*c_w/2;%Maximum distance covered in water
theta_t_min=asind(na*sind(90-theta_in)/nw);
y_max_wat=R_wat_max*cosd(theta_t_min); %Maximum depth
x_mat_max=L2+y_max_water/tand(theta_t_k);%Maximum distance in
horizontal

% Our matrix in going to be defined in dm, this one will be our
resolution.

error_margin=5;
x_max_mat=(round(x_mat_max)+error_margin)*10;
y_max_mat=(round(y_max_wat)+error_margin)*10;
y_max_water_r=y_max_water*10;


% ATTENUATION IN THE AIR
% We call the function Attenuation where the user choose the
climatology
% and it will determine a value for attenuation in the air

alpha_dB=Attenuation;

%ATTENUATION IN THE WATER

a=zeros(y_max_mat,x_max_mat); %Creation of a matrix for the absorption
b=zeros(y_max_mat,x_max_mat); %Creation of a matrix for the scattering
```

```
a=absorption_w(y_max_mat,x_max_mat);
b=scattering_w(y_max_mat,x_max_mat);
Backscat=zeros(y_max_mat,x_max_mat);%Creation of a matrix for the
backscattering
[Backscat,b_1]=Target_type(y_max_mat,x_max_mat,L1,L2,y_max_water_r,b);

% Total attenuation in water.
c=zeros(y_max_mat,x_max_mat); %Creation of the attenuation matrix
c=a+b_1; %Sum of scattering and absorption


% GENERATE A SWEEP

%To know the maximum rtt value
rtt_max=round(rtt_max*10^9)+1; % Convert to nanoseconds
t_max=round((theta_in-theta_fin)/inc_theta_k)+1; % Number of samples

% The noise that our receiver will have
Noise=10^-10;

% This one will be where we are going to collect our data
A=zeros(rtt_max,t_max);
A=ones(rtt_max,t_max)*Noise;

% Our beam is going to have a footprint, with this parameter we will
try to
% take in care all point of the footprint

incr_theta_ini=BW/25;
theta_k=theta_in;
t=1;
Po=P/25;

% The sweep will start in the first point of the range and will arrive
% until the last point. From L1 to L2
% All time values we have, they are in nanoseconds.

while theta_k>theta_fin
  theta_ini=theta_k+(BW/2);
  theta_fini=theta_k-(BW/2);
  Pr_i=0; % Will be the sum of the different aperture width

  while theta_ini>theta_fini
    % We have to know where our pulse is, if it is in the air or in
    % both of them.

    R_ini=h1/sind(theta_ini);
    rtt_min_airmax=(2*R_ini/c_a)*10^9; % To convert to nanoseconds
    rtt=100;

    %We are going to calculate some parameters of our beam.

    % SNELL

    % Angle of incidice over the normal direction (°)
```

```
theta_i=90-theta_ini;
% Transmitted angle
theta_t=asind(na*sind(theta_i)/nw);

% FRESNEL
%Reflectance
Rs=((tand(theta_t-theta_i))/(tand(theta_t+theta_i)));
gamma=1-Rs; % Transmittance

    while rtt < rtt_max

        if (rtt<round(rtt_min_airmax))
            Po=P/25;
            Pr_t=Pulse_air_1(rtt,Po,alpha_dB);
        else

           % Once the ligth hits the water surface one part of it
           % is going to be transmitted and the other  part
           % is going to be reflected to the air

            if rtt==round(rtt_min_airmax)
             R_hip=(rtt_min_airmax*c_a*10^(-9))/2;
             x=R_hip*cosd(theta_ini);
             Surface=Backscat(1,round(x));
             Pr_t=Pulse_air_3(rtt_min_airmax,Po,alpha_dB,Surface);
            else



           % BACKSCATTER MEASUREMENT
           % Distance covered by the light in the air (m)

            rtt_1=rtt*10^(-9);%To convert in nanoseconds
            R1=h1/sind(theta_ini);%Distance in meters

            %Horizontal distance to the crossing point
            L=sqrt(R1^2-h1^2);
            R2=(rtt_1-2*R1/c_a)*c_w/2;

            % Distance done behind the water in x axis
            L2_sub=R2*sind(theta_t);

            %The exact point in x axis
            x=(L+L2_sub)*10;

            %The distance done behind the water in y axis
            h2=sqrt(R2^2-L2_sub^2);
            y=h2*10;


            x_t=round(x)+1;
            y_t=round(y)+1;

            % The backscatter value from x_t,y_t
            sigma=Backscat(y_t,x_t); %Backscattering matrix.
```

```
                %ATTENUATION IN THE WATER

                 rtt_min_1=rtt_min_airmax+0.1;
                 alpha_wat=0;

                     while rtt_min_1<rtt
                         rtt_water=rtt_min_1-rtt_min_airmax;
                         R_wat=(c_w/2)*rtt_water*10^-9;
                         x_wat_at_1=(L+R_wat*sind(theta_t))*10;
                         y_wat_at_1=R_wat*cosd(theta_t)*10;
                         x_wat_at=round(x_wat_at_1)+1;
                         y_wat_at=round(y_wat_at_1)+1;
                         alpha_wat_1=c(y_wat_at,x_wat_at);
                         R_wat_2=0.1*10^-9*c_w/2;
                         alpha_wat_2=alpha_wat_1*R_wat_2;
                         alpha_wat=alpha_wat+alpha_wat_2;
                         rtt_min_1=rtt_min_1+0.1;
                     end
            Pr_t_1=Pulse_water(Po,R1,R2,alpha_dB,alpha_wat,gamma,sigma);
            Pr_t_2=Pulse_air_2(rtt,Po,alpha_dB,Rs);
            Pr_t=(Pr_t_1+Pr_t_2);
              end
              end

              Pr_i=(Pr_t+Noise); % We add the different powers
              A(rtt,t)=A(rtt,t)+Pr_i;
              rtt=rtt+1;


          end
          theta_ini=theta_ini-incr_theta_ini; % To cover the whole
                                              aperture range of the beam

    end

    theta_k=theta_k-inc_theta_k;
    t=t+1
end

% PRESENTATION OF THE SIMULATED DATA

contour(A)
title(sprintf('Between %f and %f contour',L1,L2));
xlabel('Different scanning moment')
ylabel('Rtt time in ns')
figure

mesh(A)
title(sprintf('Between %f and %f mesh',L1,L2));
xlabel('Different scanning moment')
ylabel('Rtt time in ns')
figure

Image_1=A;
```

```
maxi=max(max(Image_1));
Image=Image_1*(255/maxi);
image(Image)
colormap(gray(100))
title(sprintf('Between %f and %f image in gray',L1,L2));
xlabel('Different scanning moment')
ylabel('Rtt time in ns')
figure
save('matrix','A')
```

```
function Main_wave

%-------------------------------------------------------------------
%Name: Main_wave.m
%Authors: Unai Ayala and Luis Hernández
%
%Description: Simulation of a sweep in a wavy sea
%-------------------------------------------------------------------

format long

% CONSTANT PARAMETERS

c_w=224748825; % Speed of light in the water
c_a=299705543; % Speed of light in the air
na=1.00029;    % Index of refraction of the air
nw=1.33;       % Index of refraction of the water



% INTRODUCTION OF PARAMETERS---------------------------------------

L1=input('The first limit you want to scan (meters), L1=');
L2=input('The last limit you want to scan (meters), L2=');
h1=input('Throwing height(meters)=');
Res=input('The resolution in meters=');
y_max_water=input('Maximum in water(meters)=');
A_1=0.1;
lambda=5;
BW=(18*10^(-6))*180/pi;
P=10^6;

% Finding the angles to cover the whole area

theta_in=atand(h1/L1);
theta_fin=atand(h1/L2);

% We have to ensure the resolution at the farthest point

alfa=atand(h1/(L2-Res));

% Angular resolution: we will send pulses each inc_theta degrees
% Lower values give us better resolution

inc_theta_k=alfa-theta_fin;
display(sprintf('We will shoot from %f° to %f°. One shot each %f
degrees\n', theta_in, theta_fin, inc_theta_k));
y_max_water=input('Maximum in water(meters):');


% DEFINITION OF MATRIX

% We are using matrix to store the information of each point.
% 3-Storing the sea description with the object
% 1-Storing the data received
```

```
% Values to know our limits of the matrix

% Round trip time. With this value we can follow the pulse along its
whole
% way, higher rtt means that we are measuring the backscattering in a
% deeper part of the sea.
% To know the maximum rtt we have that

R_air_max_max=h1/sind(theta_fin); %Maximum distance covered in the air
rtt_min_airmax_airmax=2*R_air_max_max/c_a; %Rtt to cover it
theta_t_k=asind(na*sind(90-theta_fin)/nw);
R_max_water=y_max_water/cosd(theta_t_k); %Distance covered in water at
                                          farthest point
rtt_max_w=2*R_max_water/c_w; %Rtt to cover the maximum distance in
                             water
rtt_max=rtt_min_airmax_airmax+rtt_max_w; %Maximum rtt

% To know the x and y values of the matrix

R_air_max_min=h1/sind(theta_in); %Minimum distance covered in the air.
rtt_min_airmax_airmin=2*R_air_max_min/c_a; %Rtt needed to cover it
rtt_wat_airmin=rtt_max-rtt_min_airmax_airmin;%Maximum time in water
R_wat_max=rtt_wat_airmin*c_w/2;%Maximum distance covered in water
theta_t_min=asind(na*sind(90-theta_in)/nw);
y_max_wat=R_wat_max*cosd(theta_t_min); %Maximum depth
x_mat_max=L2+y_max_water/tand(theta_t_k);%Maximum distance in
                                          horizontal

% Our matrix in going to be defined in dm, this one will be our
resolution.

error_margin=5;
x_max_mat=(round(x_mat_max)+error_margin)*10;
y_max_mat=(round(y_max_wat)+error_margin)*10;
y_max_water_r=y_max_water*10;


% ATTENUATION IN THE AIR
% We call the function Attenuation where the user choose the
climatology and it will determine a value for attenuation in the air

alpha_dB=Attenuation;

%ATTENUATION IN THE WATER

a=zeros(y_max_mat,x_max_mat); %Creation of a matrix for the absorption
b=zeros(y_max_mat,x_max_mat); %Creation of a matrix for the scattering
a=absorption_w(y_max_mat,x_max_mat);
b=scattering_w(y_max_mat,x_max_mat);
Backscat=zeros(y_max_mat,x_max_mat);%Creation of a matrix for the
backscattering
[Backscat,b_1]=Target_type(y_max_mat,x_max_mat,L1,L2,y_max_water_r,b);

% Total attenuation in water.
```

```
c=zeros(y_max_mat,x_max_mat); %Creation of the attenuation matrix
c=a+b_1; %Sum of scattering and absorption


% GENERATE A SWEEP

%To know the maximum rtt value
rtt_max=round(rtt_max*10^9)+1; % Convert to nanoseconds
t_max=round((theta_in-theta_fin)/inc_theta_k)+1; % Number of samples

% The noise that our receiver will have
Noise=10^-10;

% This one will be where we are going to collect our data
A=zeros(rtt_max,t_max);
A=ones(rtt_max,t_max)*Noise;

% Our beam is going to have a footprint, with this parameter we will
try to
% take in care all point of the footprint

incr_theta_ini=BW/25;
theta_k=theta_in;
t=1;
Po=P/25;

% The sweep will start in the first point of the range and will arrive
% until the last point. From L1 to L2
% All time values we have, they are in nanoseconds.
while theta_k>theta_fin
  theta_ini=theta_k+(BW/2);
  theta_fini=theta_k-(BW/2);
  Pr_i=0; % Will be the sum of the different aperture width

  while theta_ini>theta_fini
      x=point(A_1,h1,lambda,theta_ini);
      theta_wave=angle_wav(A_1,lambda,x);
      theta_ini_1=theta_ini+theta_wave;
      R_min=x/cosd(theta_ini);
      rtt_min_airmax_1=2*R_min/c_a;
      rtt_min_airmax=rtt_min_airmax_1*10^9;

    % We have to know where our pulse is, if it is in the air or in
    % both of them.
    rtt=10;

    % SNELL
    % Angle of incidice over the normal direction (°)
    theta_i=90-theta_ini_1;
    % Transmitted angle
    theta_t_1=asind(na*sind(theta_i)/nw);
    theta_t=theta_t_1+theta_wave;

    % FRESNEL
    %Reflectance
```

```
Rs=((tand(theta_t_1-theta_i))/(tand(theta_t_1+theta_i)))^2;
gamma=1-Rs; % Transmittance

    while rtt < rtt_max

        if (rtt<round(rtt_min_airmax))
            Po=P/25;
            Pr_t=Pulse_air_1(rtt,Po,alpha_dB);
        else
           % Once the ligth hits the water surface one part of it
           % is going to be transmitted to the water and the other
           % is going to be reflected to the air
            if rtt==round(rtt_min_airmax)
             Surface=Backscat(1,round(x*10));
             Pr_t=Pulse_air_3(rtt_min_airmax,Po,alpha_dB,Surface);
            else



           % BACKSCATTER MEASUREMENT

           % Distance covered by the light in the air (m)
            rtt_1=rtt*10^(-9);%To convert in nanoseconds
            R1=R_min;    %The distance done in the air

           % Horizontal distance to the crossing point
            R2=(rtt_1-2*R1/c_a)*c_w/2;
           % Distance done behind the water in x axis
            L2_sub=R2*sind(theta_t);
           %The exact point in x axis
            x_1=(x+L2_sub)*10;
           %The distance done behind the water in y axis
            h2=sqrt(R2^2-L2_sub^2);
            y=h2*10;
            x_t=round(x_1)+1;
            y_t=round(y)+1;
           % The backscatter value from x_t,y_t
            sigma=Backscat(y_t,x_t); %Backscattering matrix.

           %ATTENUATION IN THE WATER

            rtt_min_1=rtt_min_airmax+0.1;
            alpha_wat=0;

                while rtt_min_1<rtt
                    rtt_water=rtt_min_1-rtt_min_airmax;
                    R_wat=(c_w/2)*rtt_water*10^-9;
                    x_wat_at_1=(x+R_wat*sind(theta_t))*10;
                    y_wat_at_1=R_wat*cosd(theta_t)*10;
                    x_wat_at=round(x_wat_at_1)+1;
                    y_wat_at=round(y_wat_at_1)+1;
                    alpha_wat_1=c(y_wat_at,x_wat_at);
                    R_wat_2=0.1*10^-9*c_w/2;
                    alpha_wat_2=alpha_wat_1*R_wat_2;
                    alpha_wat=alpha_wat+alpha_wat_2;
```

```
                    rtt_min_1=rtt_min_1+0.1;
                end
          Pr_t_1=Pulse_water(Po,R1,R2,alpha_dB,alpha_wat,gamma,sigma);
          Pr_t_2=Pulse_air_2(rtt,Po,alpha_dB,Rs);
                Pr_t=(Pr_t_1+Pr_t_2);
            end
            end

            Pr_i=(Pr_t+Noise); %We add the different received powers
                               from different aperture angles
            A(rtt,t)=A(rtt,t)+Pr_i;
            rtt=rtt+1;

        end
        theta_ini=theta_ini-incr_theta_ini %To cover the whole
                                           aperture range


  end

  theta_k=theta_k-inc_theta_k;
  t=t+1
end
contour(A)
title(sprintf('Between %f and %f contour',L1,L2));
xlabel('Different scanning moment')
ylabel('Rtt time in ns')
figure

mesh(A)
title(sprintf('Between %f and %f mesh',L1,L2));
xlabel('Different scanning moment')
ylabel('Rtt time in ns')
figure

Image_1=A;
maxi=max(max(Image_1));
Image=Image_1*(255/maxi);
image(Image)
colormap(gray(100))
title(sprintf('Between %f and %f image in gray',L1,L2));
xlabel('Different scanning moment')
ylabel('Rtt time in ns')
figure
save('matrix','A')
```

APPENDIX D.1: *Attenuation.m*

```
function alpha_1= Attenuation

%-------------------------------------------------------------------
%Name: Attenuation.m
%Authors: Unai Ayala and Luis Hernández
%
%Description: The user will decide which kind of weather wants to
simulate
%-------------------------------------------------------------------

choice=0;

while choice~=9

    choice=menu('Choose the type of meterology','Extremely
clear','Standard clear','Clear','Ligth Haze','Medium
Haze','Haze','Medium rain','Fog','Exit');


    %The attenuation value is given in dBs
    %It is possible to see that while the meteorological condition are
    %making worse, the attenuation coeficient will be higher, so the
signal
    %is going to dissapear faster

    %Attenuation with a Extremely clear atmosphere

    if choice==1;
        alpha_1=0.1;
        choice=9;
    end

    %Attenuation with a Standard Clear atmosphere

    if choice==2;
        alpha_1=0.5;
        choice=9;
    end

    %Attenuation with a Clear atmosphere

    if choice==3;
        alpha_1=1;
        choice=9;
    end

    %Attenuation with a Ligth Haze

    if choice==4;
        alpha_1=1.7;
        choice=9;
    end
```

```
    %Attenuation with Medium Haze atmosphere

    if choice==5;
        alpha_1=2.8;
        choice=9;
    end

    %Attenuation with Haze atmosphere

    if choice==6;
        alpha_1=5.2;
        choice=9;
    end

    %Attenuation with Medium Rain atmosphere

    if choice==7;
        alpha_1=5.5;
        choice=9;
    end

    %Attenuation with Fog atmosphere

    if choice==8;
        alpha_1=9;
        choice=9;
    end
end
```

APPENDIX D.2: *absorption.m*

```
function a=absorption_w(l_ya,l_xa)
%-------------------------------------------------------------------
%Name: absorption_w.m
%Authors: Unai Ayala and Luis Hernández
%
%Description: Based on Morel equations the absoprtion of each point is
%             going to be created.
%
%-------------------------------------------------------------------
C=chlorophyll(l_ya);
a_1=0.052;
a_2=0.468;
a=zeros(l_ya,l_xa);
i=1;

while i<l_ya
 j=1;
    while j<l_xa
    a(i,j)=(a_1+0.06*a_2*C(i)^0.65)*(1+0.2*exp(-0.014*(532-440)));
    j=j+1;
    end
    i=i+1;
end
```

APPENDIX D.3: *scattering_w.m*

```
function b=scattering_w(l_ys,l_xs)

%-------------------------------------------------------------------
%Name: scattering_w.m
%Authors: Unai Ayala and Luis Hernández
%
%Description: Based on Morel equations the scattering of each point is
%             going to be created.
%
%-------------------------------------------------------------------

C=chlorophyll(l_ys);
b_1=21*10^-4;
b=zeros(l_ys,l_xs);
i=1;

while i<l_ys
 j=1;
    while j<l_xs
    b(i,j)=(550/532)*0.30*C(i)^0.62+b_1;
    j=j+1;
    end
    i=i+1;
end
```

APPENDIX D.4: *chlorophyll.m*

```
function C=chlorophyll(l_y_1)
%-------------------------------------------------------------------------
%Name: chlorophyll.m
%Authors: Unai Ayala and Luis Hernández
%
%Description: Definition of the chlorophyll profile, the values will
be
%             defined by the user
%
%-------------------------------------------------------------------------

C_0=0.5; %mg m^-3
s=9; %m
h=50; %mg m^-2
z_max=5; % m
l_y_2=round(l_y_1/10)+1;
z=0:0.1:l_y_2;

C=C_0+(h/(s*sqrt(2*pi)))*exp((-1/2)*((z-z_max)/s).^2);
```

APPENDIX D.5: *Target_type.m*

```
function [Target,b]= Target_type (l_y,l_x,L1,L2,y_max,b)

%-------------------------------------------------------------------
%Name: Target_type.m
%Authors: Unai Ayala and Luis Hernández
%
%Description: Definition of the backscattering of the sea volume, the
user
%             can choose between different targets, and he can define
the
%             position and backscattering value of the target
%
%-------------------------------------------------------------------

% DEFINITION OF THE BACKSCATTERING OF SEA WATER BASED ON MOREL
EQUATIONS

b_w=21*10^-4;
b_w2=19.24*10^-4;
B=zeros(l_y,l_x);
i=1;
C=chlorophyll(l_y);

while i<l_y
 j=1;
    while j<l_x
    B(i,j)=0.5*b_w+((0.002+0.02*(0.5-0.25*log(C(i))))*(0.30*C(i)^0.62-
b_w2));
    j=j+1;
    end
    i=i+1;
end
Target=B;

option_1=0;

lx1=L2-L1; % range over the sea surface to be scanned

% DEFINITON OF THE TARGET POSITION

x_center=1; % Center of the target in the horizontal axis
y_center=y_max-2; % Center of the target in the vertical axis

sigma_s=0.1; %Backscattering value of the target.

while option_1~=5
    option_1=menu('Choose the type of target you want','Small
Target','Large target','Flat target','Round Target','IRTEN');

    %Here we will have a small target

    if option_1==1
        length_x=6; %Length of the target in x
```

```
        length_y=1; %Length of the target in y
        lx=0;
        ly=0;
        while(lx<length_x)
            ly=0;
            while(ly<length_y)
                position_x=x_center+lx
                position_y=y_center+ly
                B(position_y,position_x)=sigma_s;
                b(position_y,position_x)=sigma_s;
                ly=ly+1;
            end
            lx=lx+1;
        end
        Target=B;
        option_1=5;
        size(Target)
        size(b)
    end

   % Large target

    if option_1==2
        length_x=20;
        length_y=1;
        lx=0;
        ly=0;
        while(lx<length_x)
            while(ly<length_y)
                position_x=x_center+lx;
                position_y=y_center+ly;
                B(position_y,position_x)=sigma_s;
                b(position_y,position_x)=sigma_s;
                ly=ly+1;
            end
            ly=0;
            lx=lx+1;
        end
        Target=B;
        option_1=5;
        size(Target)
        size(b)
    end

    % Flat target

       if option_1==3
        length_x=(L2-10)*10;
        length_y=5;
        lx=0;
        ly=0;
        while(lx<length_x)
            while(ly<length_y)
                position_x=x_center+lx;
                position_y=y_center+ly;
```

```
                B(position_y,position_x)=sigma_s;
                b(position_y,position_x)=sigma_s;
                ly=ly+1;
            end
            ly=0;
            lx=lx+1;
        end
        Target=B;
        option_1=5;
        size(Target)
        size(b)
       end

       % Round target

       if option_1==4
        radio=5;
        lx=-round(sqrt(radio));
        ly=-round(sqrt(radio));
        length_x=round(sqrt(radio))+1;
        length_y=round(sqrt(radio))+1;
        while(lx<length_x)
            while(ly<length_y)
                r=lx^2+ly^2;
                if r<=radio
                position_x=x_center+lx;
                position_y=y_center+ly;
                B(position_y,position_x)=sigma_s;
                ly=ly+1;
                else
                position_x=x_center+lx;
                position_y=y_center+ly;
                B(position_y,position_x)=0;
                b(position_y,position_x)=sigma_s;
                ly=ly+1;
                end
            end
            ly=-round(sqrt(radio));
            lx=lx+1;
        end
        Target=B;
        option_1=5;
        size(Target)
        size(b)
       end
end
```

APPENDIX D.6: *Pulse_air_1.m*

```
function Pr = Pulse_air_1(rtt,P,alpha_dB)
%-------------------------------------------------------------------
%Name: Pulse_air_1.m
%Authors: Unai Ayala and Luis Hernández
%
%Description: Calculation of the received power, from round trip rtt,
%             before hitting the sea surface
%
%-------------------------------------------------------------------

%Speed of light in the air
c_a=299705543;
% The distance that our pulse has done in the air,
R=(c_a*rtt*10^(-9))/2;

%Attenuation per km, we have to make the conversion from the dB to
real
%units
alpha_km=10^(alpha_dB/10);
%Attenuation per meter
alpha=alpha_km/1000;

%Pulse length
tau=10^-6;
%Area of our receiver
%Area=pi*(Diameter/2)^2, Diameter 6,35mm
A=pi*((6.35*10^-3)/2)^2;
%Efficiency of the system;
efi=0.95;

%System factor
K=P*c_a*tau*A*efi/2;

% Geometrical factor
G=O(R)/R^2;

%Backscattering value, it is a ramdom number. We have to put a
realistic
%value based on the chosen scattering
Back_scat_Air=1.39*(550/532)^4*100*10^-8;

%Transmision losses
T=exp(-2*alpha*R);

%Received power from distance R
Pr=K*G*Back_scat_Air*T;
```

APPENDIX D.7: *Pulse_air_2.m*

```
function Pr = Pulse_air_2(rtt,Po,alpha_dB,Rs)
%-------------------------------------------------------------------
%Name: Pulse_air_2.m
%Authors: Unai Ayala and Luis Hernández
%
%Description: Calculation of the received power, from round trip rtt,
%             after hitting the sea surface
%
%-------------------------------------------------------------------

% Speed of light in the air
c_a=299705543;
% The distance that our pulse has done in the air
R=(c_a*rtt*10^(-9))/2;

% POWER CALCULATION-----------------------------------------------------

% Attenuation per km, we have to make the conversion from the dB to
real
% units
alpha_km=10^(alpha_dB/10);
% Attenuation per meter
alpha=alpha_km/1000;

% Pulse length
tau=10^-6;
% Area of our receiver: Area=pi*(Diameter/2)^2, Diameter 6,35mm
A=pi*((6.35*10^-3)/2)^2;
% Efficiency of the system;
efi=0.95;
% System factor
K=Po*c_a*tau*A*efi/2;

% Geometrical factor
G=O(R)/R^2;

% Backscattering value, it is a ramdom number. We have to put a
realistic
% value based on the chosen scattering
Back_scat_Air=1.39*(550/532)^4*100*10^-8;

% Transmision losses
T=exp(-2*alpha*R);

% Received power from distance R
Pr=K*G*Back_scat_Air*T*Rs;
```

APPENDIX D.8: *Pulse_air_3.m*

```
function Pr = Pulse_air_3(rtt,P,alpha_dB,sigma)
%-------------------------------------------------------------------------
%Name: Pulse_air_3.m
%Authors: Unai Ayala and Luis Hernández
%
%Description: Calculation of the received power from the sea surface
%
%-------------------------------------------------------------------------

%Speed of light in the air
c_a=299705543;
% The distance that our pulse has done in the air,
% 10^-9 factor, it is used to convert rtt to its real value in
nanoseconds
R=(c_a*rtt*10^(-9))/2;

%Attenuation per km, we have to make the conversion from the dB to
real
%units
alpha_km=10^(alpha_dB/10);
%Attenuation per meter
alpha=alpha_km/1000;

%Pulse length
tau=10^-6;
%Area of our receiver
%Area=pi*(Diameter/2)^2, Diameter 6,35mm
A=pi*((6.35*10^-3)/2)^2;
%Efficiency of the system;
efi=0.95;
%System factor
K=P*c_a*tau*A*efi/2;

% Geometrical factor
G=O(R)/R^2;

%Backscattering value, it is a ramdom number. We have to put a
realistic
%value based on the chosen scattering
Back_scat_Air=sigma;

%Transmision losses
T=exp(-2*alpha*R);

%Received power from distance R
Pr=K*G*Back_scat_Air*T;
```

APPENDIX D.9: *Pulse_water.m*

```
function Pr=
Pulse_water(Po,R_air_wat,R_wat_wat,alpha_dB,alpha_wat,gamma,sigma)

%--------------------------------------------------------------------
%Name: Pulse_water.m
%Authors: Unai Ayala and Luis Hernández
%
%Description: Calculation of the received power from the submerged
target
%
%--------------------------------------------------------------------
%Power calculation
%Distance, it is the sum of the distance done in air and water
R=R_wat_wat+R_air_wat;
c_a=299705543;
% Attenuation per km, we have to make the conversion from the dB to
real
% units
alpha_km=10^(alpha_dB/10);
% Attenuation per meter
alpha=alpha_km/1000;

% Pulse length
tau=10^-6;
% Area of our receiver: Area=pi*(Diameter/2)^2, Diameter 6,35mm
A=pi*((6.35*10^-3)/2)^2;
% Efficiency of the system;
efi=0.95;
% System factor
K=Po*c_a*tau*A*efi/2;

% Geometrical factor
G=O(R)/R^2;

% Backscattering value
Back_scat_wat=sigma;

%Transmision losses, from the air and the water
T=exp(-2*alpha*R_air_wat-2*alpha_wat);

%Received power from distance R=R1+R2
Pr=K*G*Back_scat_wat*T*gamma^2;
```

APPENDIX D.10: *point.m*

```
function z=point(A_1,h1,lambda,theta_t)

%-------------------------------------------------------------------
%Name: point.m
%Authors: Unai Ayala and Luis Hernández
%
%Description: Calculation of the crossing point between the wavy sea
and
%             the laser beam
%-------------------------------------------------------------------

format long
A_2=A_1;
theta_tx=theta_t;
h=h1;
yo=h-A_2;
x=yo/tand(theta_tx);
error=h-tand(theta_tx)*x-A_2*sin(2*pi*x/lambda);
i=50/lambda;
while abs(error)> 0.001
    while error > 0.001
    yo=yo+(A_2/i);
    x=yo/tand(theta_tx);
    error=(h-x*tand(theta_tx))-A_2*sin(2*pi*x/lambda);
    end
    i=i+7;

    if abs(error)>0.001
        while error < 0
        yo=yo-(A_2/i);
        x=yo/tand(theta_tx);
        error=(h-x*tand(theta_tx))-A_2*sin(2*pi*x/lambda);
        end
    end
    i=i+7;
end
z=x;
```

APPENDIX D.11: *angle_wav.m*

```
function theta_wave=angle_wav(A,lambda,x)

%-------------------------------------------------------------------
%Name: angle_wav.m
%Authors: Unai Ayala and Luis Hernández
%
%Description: Calculation of the angle of the wave at point x.
%
%-------------------------------------------------------------------

theta_wave_1=atan(A*2*pi/lambda*cos(2*pi/lambda*x));
```

```
theta_wave=theta_wave_1*360/(2*pi);
```

APPENDIX D.12: *angle_wav.m*

```
function O=O(R)

%-------------------------------------------------------------------------
%Name: o.m
%Authors: Unai Ayala and Luis Hernández
%
%Description: Simulation of the geometric factor.
%
%-------------------------------------------------------------------------

if R<1
    O=R;
else
    O=1;
end
```